University of Alberta

Detection and Diagnosis of Poor Control Performance

by

Hailei Jiang 

A thesis submitted to the Faculty of Graduate Studies and Research in partial fulfillment of the requirements for the degree of **Doctor of Philosophy**.

in

Process Control

Department of Chemical and Materials Engineering

Edmonton, Alberta
Fall 2008

Your file Votre référence
ISBN: 978-0-494-46340-6
Our file Notre référence
ISBN: 978-0-494-46340-6

To

my parents and my wife Jia

Abstract

A typical process or power plant operates with hundreds if not thousands of control loops. For efficiency, all critical loops must operate at optimum levels. With such a large number of important loops, it is difficult for engineers to monitor and maintain these loops so that they are operating under optimum conditions at all times. Therefore process and performance monitoring systems are increasingly becoming necessary for early detection of abnormal operating conditions, or events/faults, safety violations and performance degradation before they lead to unexpected disruptions or even catastrophic failures. The monitoring of the performance of chemical processes has received much attention in the engineering research literature over the past few decades (Harris, 1989; Huang and Shah, 1999).

A challenging task after detection of poor control performance is to diagnose and locate the root cause in order to rectify the situation. There are many reasons that can cause poor control performance, such as poor controller tuning, process nonlinearity, oscillatory disturbance and inaccurate process model for processes under model-based control, etc. How to effectively diagnosis these problems, such as what is the root cause of the oscillations in a plant, is an extremely important task for ensuring efficient and safe production. Unfortunately, the diagnosis of poor control performance has received little attention and remains an open research area (Qin, 1998).

This thesis is concerned with developing new techniques for diagnosis of poor control performance. The main focus of this thesis is on the following two challenging topics in the area of performance diagnosis:

- Detection and diagnosis of plant-wide oscillations. Oscillations are a common type of plant-wide disturbances whose effects propagate to many units and thus may impact overall process performance. It is important to detect and diagnose

such oscillations early in order to rectify the situation. Several new methods based on the concept of spectral envelope and adjacency matrix are proposed to detect oscillations and isolate the root cause of oscillations.

- Detection and diagnosis of model-plant mismatch. Inaccurate process model often causes poor performance of model-based control system. Effective detection of model-plant mismatch can provide useful information for diagnosing control performance. Multiplicative and additive modelling error are analyzed. New algorithms are proposed for model validation under closed-loop conditions.

The proposed methods and techniques are evaluated by application to pilot-scale and industrial processes to demonstrate the practicality and utility of this new class of performance monitoring and diagnosis systems.

Acknowledgements

I would like to express my sincere gratitude to my supervisor, Prof. Sirish L. Shah, for his patient guidance and constant encouragement through all the years of my PhD study. Dr. Shah gave me all the support and freedom that any graduate student would crave for. He was always ready to discuss research ideas and give useful suggestions. He always spent significant amount of time to give a careful review and detailed corrections of my writings. Without all these, it would not have been possible to finish this thesis. Beside having vast knowledge and experience, Dr. Shah also has a number of great qualities that I would like to emulate. He has always been sincere, true hearted, optimistic and respectful.

I am also grateful to Prof. Mani Bhushan and Prof. Biao Huang. Prof. Bhushan was my co-supervisor in the first two years of my study. He helped me a lot with my course studies and initial literature review. Prof. Huang has been my co-supervisor for the last two years. He provided wonderful guidance on my research related to model validation and diagnosis of model-plant mismatch. He is another important person that deserves credit for making this thesis possible.

I would also like to thank Dr. Rohit Patwardhan from Matrikon Inc., Edmonton. I have learnt a lot about practical performance assessment, model identification and oscillation diagnosis techniques from him. He always made me feel welcome to ask him questions, no matter how busy he was. I am very thankful to him for the amount of time he spent with me discussing various research problems.

I was fortune to have worked with Dr. Shoukat Choudhury and Dr. Weihua Li. Dr. Choudhury taught me about valve stiction and we spent a lot of time discussing issues related to plant-wide oscillations. Dr. Li introduced me to the area of fault detection and isolation, especially the parity space approach.

In evaluating the methods that have been proposed in this thesis, I was fortunate to have interacted with Mr. Bruce Wilson, Ms. Foon Szeto, Mr. Barry Ledrew, Mr. Ramesh Kadali and Mr.Trevor Hrycay of Suncor Energy, Fort McMurray. The project of MPC monitoring at Suncor was truly rewarding and it led me to understand the needs and challenges in industrial process control.

The computer process control (CPC) group at the University of Alberta is an exciting place to learn and study process control. I really appreciate all the help I have received from my colleagues. I am thankful to following people for giving me their time in sharing, discussing and debating many interesting ideas during my time as a graduate student at the University of Alberta: Arun Tangirala, Harigopal Raghavan, Zhengang Han, Salim Ahmed, Syed Imtiaz, Ian Alleyne, Rumana Sharmin, Hangcong Liu, Liqian Zhang, Enayet Halim, Mridul Jain, Adrian Fuxman, Natalia Marcos, Yutong Qi, Fangwei Xu and Sien Lu. I will always cherish my friendship with them.

I would like to acknowledge the Department of Chemical and Materials Engineering, University of Alberta, for providing me the opportunity to pursue my doctoral degree. I also gratefully acknowledge the financial support from the Natural Sciences and Engineering Research Council of Canada (NSERC), Matrikon Inc., Suncor Energy Inc. and the Informatics Circle of Research Excellence (iCORE), through the NSERC-Matrikon-Suncor-iCORE Senior Industrial Research Chair program.

I am indebted to Professor Torsten Söderström for a very careful and constructive review of my thesis.

Last but not the least, I am eternally grateful to my parents and my wife Jia for their constant love, support and tolerance.

Contents

List of Figures

List of Tables

1 Introduction

In most chemical plants, there are several hundred or even thousands of regulatory control loops. For efficiency, all critical loops must operate at optimum levels. To ensure optimal performance of all critical control loops, process performance monitoring systems are increasingly becoming necessary for early detection of performance degradation, faults, and safety violations before they lead to unexpected disruptions or even catastrophic failures. It is for this reason that monitoring of the control performance of chemical processes has received much attention in the engineering research literature over the past few decades (Harris, 1989; Huang and Shah, 1999). Whereas the detection of poor control performance is a relatively simple task, the diagnosis of poor control performance has received little attention and remains an open research area (Qin, 1998). Performance diagnosis requires identification of the cause(s) of poor performance; and among the many possible reasons for poor control performance, the presence of oscillations and model-plant mismatch (MPM) are two common situations (See figure 1.1).

Oscillations are a common type of plant-wide disturbance and the root causes can be poorly turned controllers, sticky valves, oscillatory disturbance, etc. The oscillation effects can propagate to many units and thus may impact overall process performance. The presence of oscillations in a plant increases the variability or fluctuations of the

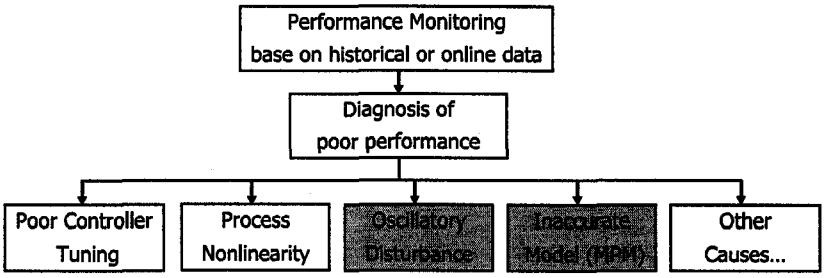

Figure 1.1: Information ow diagram for intended research area

process variables and thus naturally results in cause poor control performance, inferior quality products and larger rejection rates. Increasing emphasis on plant safety and plant profitability strongly motivates the search for techniques to detect and diagnose plant-wide oscillations.

Model-plant mismatch (MPM) is often a common reason for poor control performance, especially for model based control system, e.g. model predictive control (MPC). As the name suggests, MPC make use of a model to predict future behavior of the process given the future inputs. The precondition of good performance of model based control is usually that the MPM is negligible, or at least the model dynamics are fairly close to the plant dynamics. However, changes in plant dynamics and therefore MPM, are inevitable as operating conditions change. How to detect and diagnose the model-plant mismatch (MPM) is an open and challenging problem. A satisfactory solution to this problem would be helpful in research in both MPC design and MPC monitoring.

1.1 Scope of the Thesis

In this work, we study a wide class of techniques for detection and diagnosis of poor controller performance. As shown in figure 1.1, this thesis mainly focuses on the following two challenging topics in the area of performance diagnosis:

(1) Detection and diagnosis of plant-wide oscillations

Oscillations are a common type of plant-wide disturbances whose effects propagate to many units and thus may impact overall process performance. It is important to detect and diagnose such oscillations early in order to rectify the situation. In an industrial setting, detection and diagnosis of plant-wide oscillations requires accomplishing three challenging tasks:

- Detect the common oscillation frequency amongst many controlled variables.
- Categorize the variables that have common oscillations.
- Isolate the root cause of the plant-wide oscillations.

(2) Detection and diagnosis of model-plant mismatch.

There are several ways to represent a model. The two most frequently used representations are the state space model and a transfer function model. Although the two forms are mathematically equivalent, that is one can transfer a state space model into a transfer function model and vice verse, each presentation has its own characteristics. For example, there can be specific parameters to characterize the time delay, gain and time constant in a transfer function model, whereas there are no such parameters in a state space model; and it is easy to define sensitivity function and complimentary sensitivity function using transfer function models whereas it is not straightforward to do the same using state space model.

In process control, most of the time the purpose of model identification is for control. The role of model validation during identification is to ensure that the delivered model captures the most important dynamics of the process so that the controller design based on this model can be used to control the process. Model validation at this stage is usually in open-loop. After the designed controller is implemented, a more challenging task is: how to continuously monitor the model quality under closed-loop conditions.

1.2 Research Objectives

More specifically the research objectives of this thesis include:

1.2.1 Detection and Diagnosis of Plant-wide oscillations

1. Development of a novel method for detection of plant-wide oscillations

Thornhill and Hägglund (1997),Miao and Seborg (1999) and Thornhill *et al.* (2003*a*) have proposed methods for detection of oscillations in a loop-by-loop manner. A careful comparison of oscillation frequency in all the variables is required to identify a common oscillation frequency. These methods could be time consuming. We propose the use of the spectral envelope method to detect the common oscillation frequency. This method analyzes all the variables at the same time and automatically locate the common oscillation frequency in variables of interest. This is more efficient than looking for oscillations in a loop-by-loop manner.

2. Development of a tool to categorize variables that have oscillations

After detecting the oscillations in each variable, a traditional way to categorize variables that have common oscillation is to compare the variables one by one. To have a more efficient and accurate categorization, we propose a hypothesis test based on the spectral envelope method to test all the variables at the same time. This statistical tool gives fast and reliable categorization.

3. Development of novel methods for root cause diagnosis

Besides using the spectral envelope method to detect oscillation and categorize variables, we also use this method for root cause diagnosis. A new oscillation contribution index (OCI) is proposed to have efficient and accurate root cause diagnosis.

However, OCI is a data-based method that does not consider process information. To incorporate process knowledge and process flowsheet, we propose a novel method for oscillation diagnosis based on the concept of adjacency matrix. The method is non-data-based and it can be carried out without using any data.

1.2.2 Detection and Diagnosis of Model-plant Mismatch

1. Model-plant mismatch detection and diagnosis for multivariate dynamic systems

A state space model is particularly suitable for representing the dynamics of multivariate systems. The concept of primary residual vector (PRV) is used in our study to detect model-plant mismatch in the state space model. PRVs can be transformed into square weighted residuals for diagnosis of the mismatch.

2. Control relevant model validation under closed-loop condition

How to continuously monitor the quality of process model under closed-loop condition is a challenging problem. In our study, we propose different techniques to validate a model under-closed loop conditions. Our objective is to issue an alarm only when the process performance has been compromised due to model-plant-mismatch. A technique based on the two model divergence method is proposed to issue an alarm when the sensitivity function of the closed-loop has changed significantly. Another method is proposed to issue an alarm when the stability margin of the closed-loop system has changed significantly.

3. Diagnosis of Modelling Error

Modelling error is inevitable in practice. How modelling error will affect process performance is still an unsolved problem. In our study, we analyze the effect of modelling error on process output error (which is the difference between the true process output and the simulated output). We also explore the relationship between modelling error and robust stability and use robust stability conditions for on-line model validation.

4. Industrial case studies on model validation and performance assess-

ment

Maintenances of model-predictive controller (MPC) is an important task to ensure persistent process performance in industry. Two case studies of monitoring industrial MPC controllers are performed. New techniques are proposed for performance assessment and model quality assessment of industrial MPC systems.

1.3 Thesis Organization

This thesis begins with an introduction to provide an overview of the main areas of focus in this thesis by outlining the research scope and major objectives.

Chapter 2 proposes a new method to detect plant-wide oscillations based on the spectral envelope method. The variables that have common oscillations are identified and categorized accurately by a statistical hypothesis test. Two industrial case studies are presented to demonstrate the utility and practicality of the proposed method.

Two different methods for root cause diagnosis of plant-wide oscillations are discussed in Chapter 3. The first method is data-based and related to the spectral envelope method. A new index defined as the oscillation contribution index (OCI) is proposed to isolate the root cause. An alternative method that is a non data-based method and related the concept of adjacency matrix is proposed as it is able to take into account process flowsheet or topology to identify root causes of plant wide oscillations.

Chapter 4 deals with detection and diagnosis of model-plant mismatch (MPM) for multivariate systems. The MPM problem is formulated in the form of state space model. Three MPM detection indices (MDIs) are proposed to detect the MPM. Also a logic framework is proposed to isolate the system matrices that have MPM.

The topics of control relevant model validation under closed-loop conditions are discussed in Chapter 5. Two algorithms are proposed based on the two model divergence method. The first algorithm is sensitive to changes in both plant dynamics and disturbance dynamics. The second algorithm is only sensitive to the changes in plant dynamics, irrespective of changes in disturbance dynamics.

Chapter 6 focuses on the analysis of modelling error. The effect of modelling error

on process output error (which equals process output minus the simulated output) is first explored. Then the robust stability conditions is applied for on-line model validation. The idea is that whenever the closed-loop system violates the robust stability condition, it is a sign of significant process change.

The second last chapter (Chapter 7) presents two case studies on the performance evaluation and model validation of two industrial multivariate MPC controllers at Suncor Energy Inc., Fort McMurray, Canada. This is followed by concluding remarks on suggestions for future work in Chapter 8.

2

Detection of Plant-wide Oscillations

Plant-wide oscillations are common in many processes. Their effects propagate to many units and may impact overall process performance. It is important to detect such oscillations in order to rectify the situation. This chapter proposes a new method to detect plant-wide oscillations using routine operating data. A technique called spectral envelope is used to detect oscillations. The variables that have common oscillations are identified and categorized accurately by a statistical hypothesis test. Two industrial case studies are presented to demonstrate the utility and practicality of the proposed method. [1]

2.1 Introduction

Detection and diagnosis of plant-wide disturbances is an important issue in many process industries (Qin, 1998; Desborough and Miller, 2001). Oscillations are a common type of plant-wide disturbances. Their root causes can be poorly tuned controllers, process or actuator non-linearities, oscillatory disturbance *etc.* The effects

[1] A part of this chapter has been published as (a) Hailei Jiang, M.A.A Shoukat Choudhury and Sirish Shah, "Detection and Diagnosis of Plant-wide Oscillations using the Spectral Envelope Method", in the proceedings of *IFAC-ADCHEM 2006*, Gramado, Brazil. (b) Hailei Jiang, M.A.A Shoukat Choudhury and Sirish Shah, "Detection and Diagnosis of Plant-wide Oscillations From Industrial Data using the Spectral Envelope Method", *Journal of Process Control*, **17**(2), 143-155, 2007.

of such oscillation can propagate to many units and thus may impact overall process performance of the plant. The presence of oscillations in a plant increases the variability of the process variables and thus may cause poor control performance, inferior quality products and larger rejection rates. Increasing emphasis on plant safety and plant profitability strongly motivates the search for techniques to detect and diagnose plant-wide oscillations.

Thornhill and Hägglund (1997) used zero-crossings of the control error signal to calculate integral absolute error (IAE) in order to detect oscillations in a control loop. This method has poor performance in the cases of noisy error signals. Miao and Seborg (1999) suggested a method based on the auto-correlation function to detect excessively oscillatory feedback loop. The auto-covariance function (ACF) of a signal was utilized in Thornhill *et al.* (2003*a*) to detect oscillation(s) present in a signal. This method needs a minimum of five cycles in the auto-covariance function to detect oscillation, which is often hard to obtain, particularly in the case of a long oscillations (e.g., an oscillation with a period of 400 samples). Although the data set can be downsampled in such cases, downsampling may introduce aliasing in the data. More recently Thornhill *et al.* (2002) proposed spectral principal component analysis (SPCA) to detect oscillations and categorize the variables having similar oscillations. This method does not provide any diagnosis of the root cause of the oscillation which is generally the main objective of the exercise. In this chapter, a new procedure based on the spectral envelope method for detection of plant-wide oscillations is proposed. How to diagnose and locate the root-cause of the plant-wide oscillations will be discussed in the next chapter.

The spectral envelope method is a frequency domain technique that was first introduced by Stoffer *et al.* (1993) to explore the periodic nature of categorical time series. The idea is to assign numerical values to each of the categories followed by a spectral analysis of the resulting discrete-valued time series. In 1997, McDougall *et al.* (1997) extended the concept of spectral envelope to real-valued series. In exploring the periodic nature of a real-valued series, one can not only do spectral analysis of the original series, but also of transformed series. The key idea in McDougall *et al.* (1997) is to select optimal transformations of a real-valued series that emphasize any periodic nature in the frequency domain. This chapter extends the idea of spectral envelope

to towards the analysis of process data. The main contributions of this chapter are: (1) The concept of spectral envelope is simplified and formulated for use with process data. (2) A statistical hypothesis test is formulated to categorize the variables that have common oscillations. (3) The major advantage of the method proposed here is that it can be automated easily. This chapter is organized as follows. Section 2.2 gives an introduction of the concept of spectral envelope and how to apply it for oscillation detection. Section 2.3 presents a statistical hypothesis test for isolating variables that oscillate at a common frequency. In section 2.4, we summarize a novel procedure for detection and analysis of plant-wide oscillations. Two industrial case studies are presented in section 2.5 and 2.6 to demonstrate the utility and practicality of the proposed procedure.

2.2 Oscillation Detection using the Spectral Envelope Method

In this section, the concept of spectral envelope is introduced. A simulation example is presented to demonstrate its ability to detect multiple oscillations. The performance comparison with the SPCA method is also included.

Throughout this chapter, we use (1) bold capital letters to represent matrices; (2) bold lower case letter to represent vectors; and (3) regular letters to represent scalars.

2.2.1 Definition of the Spectral Envelope

Here we provide a simple interpretation of the concept of spectral envelope. Let

$$\mathbf{x}(t) = \begin{bmatrix} x_1(t) \\ x_2(t) \\ \vdots \\ x_m(t) \end{bmatrix} \qquad t = 0, \pm 1, \pm 2, \ldots,$$

be a multivariate, vector-valued time series on $\Re^m$. Denote matrix $\mathbf{X}$ as

$$\mathbf{X} = [\ \cdots\ \mathbf{x}(t-1)\ \mathbf{x}(t)\ \mathbf{x}(t+1)\ \cdots\ ]$$

Further, we denote the covariance matrix of $\mathbf{X}$ as $\mathbf{V_X}$ and the power spectral density (PSD) matrix of $\mathbf{X}$ as $\mathbf{P_X}(\omega)$. Here, ω represents frequency and is measured in cycles

per unit time, for $-1/2 < \omega \leq 1/2$. The definition of PSD matrix can be found in Jenkins and Watts (1968).

Let $g(t, \boldsymbol{\beta}) = \boldsymbol{\beta}^* \mathbf{x}(t)$ be a scaled series from $\Re^m$ to $\Re$, where $\boldsymbol{\beta}$ is a $m \times 1$ column vector which may be real or complex. The * represents conjugate transpose of the variable. Actually, $g(t, \boldsymbol{\beta})$ is a linear combination of the rows of $\mathbf{x}(t)$. The variance of $g(t, \boldsymbol{\beta})$ can be expressed as $V_g(\boldsymbol{\beta}) = \boldsymbol{\beta}^* \mathbf{V_X} \boldsymbol{\beta}$, and the power spectral density of $g(t, \boldsymbol{\beta})$ can be expressed as $P_g(\omega, \boldsymbol{\beta}) = \boldsymbol{\beta}^* \mathbf{P_X}(\omega) \boldsymbol{\beta}$.

The spectral envelope of $\mathbf{X}$ is defined as:

$$\lambda(\omega) \triangleq \sup_{\boldsymbol{\beta} \neq 0} \{ \frac{P_g(\omega, \boldsymbol{\beta})}{V_g(\boldsymbol{\beta})} \} = \sup_{\boldsymbol{\beta} \neq 0} \{ \frac{\boldsymbol{\beta}^* \mathbf{P_X}(\omega) \boldsymbol{\beta}}{\boldsymbol{\beta}^* \mathbf{V_X} \boldsymbol{\beta}} \} \tag{2.1}$$

where $-1/2 < \omega \leq 1/2$. It is worthwhile to note that $P_g(\omega, \boldsymbol{\beta}) = P_g(-\omega, \boldsymbol{\beta})$, and the relationship between $P_g(\omega, \boldsymbol{\beta})$ and $V_g(\boldsymbol{\beta})$ is:

$$V_g(\boldsymbol{\beta}) = \int_{-1/2}^{1/2} P_g(\omega, \boldsymbol{\beta}) d\omega = 2 \int_0^{1/2} P_g(\omega, \boldsymbol{\beta}) d\omega \tag{2.2}$$

The quantity $\lambda(\omega)$ represents the largest portion of power (or variance) that can be obtained at the frequency ω for any scaled series. The scaling vector that results in the value $\lambda(\omega)$ is called the optimal scaling vector at frequency ω, which is denoted as $\boldsymbol{\beta}(\omega)$. Accordingly, the elements of the optimal scaling vector are called the optimal scalings. The optimal scaling vector $\boldsymbol{\beta}(\omega)$ is not the same for all ω.

We prefer to limit $\boldsymbol{\beta}$ to the constraint that $\boldsymbol{\beta}^* \mathbf{V_X} \boldsymbol{\beta} = 1$. Therefore the scaled series $g(t, \boldsymbol{\beta})$ is unit variance. This will make the calculated spectral envelope more interpretable and make the magnitude of the elements of $\boldsymbol{\beta}(\omega)$ easily comparable. Accordingly, the quantity $\lambda(\omega)$ represents the largest power(variance) that can be obtained at the frequency ω for any scaled series with unit variance.

With the optimal scaling vector $\boldsymbol{\beta}(\omega)$, equation (2.1) can be rewritten as:

$$\lambda(\omega) \mathbf{V_X} \boldsymbol{\beta}(\omega) = \mathbf{P_X}(\omega) \boldsymbol{\beta}(\omega) \tag{2.3}$$

It follows that $\lambda(\omega)$ is the largest eigenvalue associated with the determinant equation:

$$|\mathbf{P_X}(\omega) - \lambda(\omega) \mathbf{V_X}| = 0 \tag{2.4}$$

$\boldsymbol{\beta}(\omega)$ is the corresponding eigenvector satisfying equation (2.3).

The viability of the spectral envelope for detecting common oscillation(s) comes from the following simple example (Stoffer, 1999). If the univariate time series $x_i(t)$, $1 \leq i \leq m$, $-\infty < t < \infty$, is in form of 'common signal plus independent white noise', say $x_i(t) = s(t) + \varepsilon_i(t)$, then in terms of power spectra, $P_{x_i}(\omega) = P_s(\omega) + {\sigma_\varepsilon}^2$, where $var(\varepsilon_i) = {\sigma_\varepsilon}^2$. A simple linear combination of $x_i(t)$, say $\bar{x}(t) = m^{-1}\sum_{i=1}^{m} x_i(t)$, will have as its power spectrum, $P_{\bar{x}}(\omega) = P_s(\omega) + m^{-1}{\sigma^2}_\varepsilon$. The signal to noise ratio of $\bar{x}(t)$ has increased by a factor of m over the individual $x_i(t)$. Therefore, this indicates that the right linear combination of the original time series will enhance the signal and attenuate the noise. The spectral envelope method actually selects the optimal linear combination that can enhance the signal spectra and dampen the noise spectra at each frequency ω for $-1/2 < \omega \leq 1/2$. This feature makes the spectral envelope particularly suitable for analyzing noise corrupted data (see simulation example in Section 2.2.4).

2.2.2 Simplified Definition of the Spectral Envelope

Denote $\mathbf{V} = diag(\mathbf{V_X})$. The diagonal elements of $\mathbf{V}$ and $\mathbf{V_X}$ are the same, but the off-diagonal elements of $\mathbf{V}$ are zero. We can use $\mathbf{V}$ instead of $\mathbf{V_X}$ in equation (2.1) and have a new expression for $\lambda(\omega)$ (Stoffer, 1999):

$$\lambda(\omega) = \sup_{\boldsymbol{\beta}\neq 0}\{\frac{\boldsymbol{\beta}^*\mathbf{P_X}(\omega)\boldsymbol{\beta}}{\boldsymbol{\beta}^*\mathbf{V}\boldsymbol{\beta}}\} \tag{2.5}$$

The resulting $\lambda(\omega)$ and $\boldsymbol{\beta}(\omega)$ are slightly different than those in the equation (2.1). Under the condition that the rows of $\mathbf{X}$ are mutually independent, $\mathbf{V}$ is equal to $\mathbf{V_X}$ and equation (2.5) is the same as equation (2.1).

We also prefer to limit $\boldsymbol{\beta}$ to the constraint such that $\boldsymbol{\beta}^*\mathbf{V}\boldsymbol{\beta} = 1$. As mentioned in Section 2.2.1, the idea in using equation (2.5) is that the right linear combination of the original time series will enhance the signal and dampen the noise.

2.2.3 Estimation of the Spectral Envelope

In practice, we can only have a finite number of samples. So here we assume $\mathbf{X} = [\mathbf{x}(0), \mathbf{x}(1), \cdots, \mathbf{x}(n-1)] \in \Re^{m\times n}$ is a $m \times n$ observed data matrix of m variables and n samples for each variable. Instead of applying the spectral envelope method to the

original data set, we prefer to work with the normalized data set which means that each variable is zero-mean with unit variance. The reasons for using normalized data are that they : (1) simplify the calculations; (2) make the calculated spectral envelope more interpretable; (3) make the calculated spectral envelope from different data sets comparable; and (4) make the magnitude of the elements of $\boldsymbol{\beta}(\omega)$ more meaningful and comparable. Here we assume $\mathbf{X}$ is already an $m \times n$ normalized data matrix.

With the normalized observed data $\mathbf{X}$, we can calculate its periodogram as:

$$\hat{\mathbf{I}}_n(\omega) = \frac{1}{n} \left[\sum_{t=0}^{n-1} \mathbf{x}(t) \exp(-2\pi i t\omega)\right] \left[\sum_{t=0}^{n-1} \mathbf{x}(t) \exp(-2\pi i t\omega)\right]^* , \quad -1/2 < \omega \leq 1/2 \tag{2.6}$$

The periodgram (equation (2.6)) provides a simple estimate of $\mathbf{P_X}(\omega)$. But, the $\hat{\mathbf{I}}_n(\omega)$ expression in equation (2.6) is still a continuous function of ω which is not feasible. In practice, if n is a large integer, the fast Fourier transformation provides for fast calculation of $\hat{\mathbf{I}}_n(k/n)$, for $k = 1, \cdots, [n/2]$, where $[n/2]$ is the greatest integer less than or equal to $n/2$. The frequencies $\omega_k = k/n$, for $k = 1, \cdots, [n/2]$, are called the Fourier frequencies. Then the $\hat{\mathbf{I}}_n(\omega_k)$ at these frequencies can be estimated as:

$$\hat{\mathbf{I}}_n(\omega_k) = \frac{1}{n} \left[\sum_{t=0}^{n-1} \mathbf{x}(t) \exp(-2\pi i t\omega_k)\right] \left[\sum_{t=0}^{n-1} \mathbf{x}(t) \exp(-2\pi i t\omega_k)\right]^* \tag{2.7}$$

The main drawbacks of using the periodogram directly is that it is not a consistent estimate of the PSD matrix. The confidence interval of the estimation is usually large (Shumway, 1988). To overcome this problem, a smoothed periodogram estimate or a consistent spectral window estimate for $\mathbf{P_X}(\omega)$ can be used. The theory for estimating the PSD matrix of a vector process is well established (Brillinger, 1981; Hannan, 1970) and we discuss this briefly. One technique for smoothing is to take a symmetric moving average of the periodogram, that is:

$$\hat{\mathbf{P}}_{\mathbf{X}}(\omega_k) = \sum_{j=-r}^{r} h_j \hat{\mathbf{I}}_n(\omega_{k+j}) \tag{2.8}$$

where $\{h_j\}$ are symmetric ($h_j = h_{-j}$) positive weights and $\sum_{j=-r}^{r} h_j = 1$. The number r is chosen to obtain a desired degree of smoothness. Larger values of r leads to smoother estimates. However, one should be careful not to smooth away significant

peaks. For $\hat{\mathbf{P}_{\mathbf{X}}}(\omega_k)$ to be a consistent estimate, the weights must satisfy $\sum h_j^2 \to 0$ as $r \to \infty$, but $r/n \to 0$ as $n \to \infty$.

Remark 2.2.1 *The optimal design of r and h_j is beyond the scope of this chapter. For more detail, readers can refer to Stoffer* et al. *(2000). Throughout this chapter, h_j is chosen as $h_j = (r - |j| + 1)/(r+1)^2$, for $|j| = 1, 2, ..., r$. In the illustrative example and the industrial case studies to follow, r was selected as an integer as 1 or 2.*

Estimation of $\lambda(\omega)$ using $\mathbf{V_X}$

Using the estimated $\hat{\mathbf{P}}_{\mathbf{X}}(\omega_k)$ and $\hat{\mathbf{V}}_{\mathbf{X}} = Cov(\mathbf{X})$, we can rewrite equation (2.1) as:

$$\hat{\lambda}(\omega_k) = \sup_{\boldsymbol{\beta} \neq 0} \{ \frac{\boldsymbol{\beta}^* \hat{\mathbf{P}}_{\mathbf{X}}(\omega_k) \boldsymbol{\beta}}{\boldsymbol{\beta}^* \hat{\mathbf{V}}_{\mathbf{X}} \boldsymbol{\beta}} \} \tag{2.9}$$

We denote the estimated $\hat{\boldsymbol{\beta}}(\omega)$ at the Fourier frequencies as $\hat{\boldsymbol{\beta}}(\omega_k)$, and limit $\hat{\boldsymbol{\beta}}(\omega_k)$ to the constraint that $\hat{\boldsymbol{\beta}}(\omega_k)^* \hat{\mathbf{V}}_{\mathbf{X}} \hat{\boldsymbol{\beta}}(\omega_k) = 1$.

For simplicity and without loss of generality, $\hat{\lambda}(\omega_k)$ is defined to be the largest eigenvalue of $\hat{\mathbf{H}}(\omega_k)$ where

$$\hat{\mathbf{H}}(\omega_k) = \hat{\mathbf{V}}_{\mathbf{X}}^{-\frac{1}{2}} \hat{\mathbf{P}}_{\mathbf{X}}(\omega_k) \hat{\mathbf{V}}_{\mathbf{X}}^{-\frac{1}{2}} \tag{2.10}$$

If we denote $\hat{\boldsymbol{\beta}}_0(\omega_k)$ as the eigenvector of $\hat{\mathbf{H}}(\omega_k)$ associated with $\hat{\lambda}(\omega_k)$, then the optimal scaling vector $\hat{\boldsymbol{\beta}}(\omega_k)$ is defined by $\hat{\boldsymbol{\beta}}(\omega_k) = \hat{\mathbf{V}}_{\mathbf{X}}^{-\frac{1}{2}} \hat{\boldsymbol{\beta}}_0(\omega_k)$.

Estimation of $\lambda(\omega)$ using $\mathbf{V}$

Using the estimated $\hat{\mathbf{P}}_{\mathbf{X}}(\omega_k)$ and $\hat{\mathbf{V}} = diag(\hat{\mathbf{V}}_{\mathbf{X}}) \in \Re^{m \times m}$, we can rewrite equation (2.5) as:

$$\hat{\lambda}(\omega_k) = \sup_{\boldsymbol{\beta} \neq 0} \{ \frac{\boldsymbol{\beta}^* \hat{\mathbf{P}}_{\mathbf{X}}(\omega_k) \boldsymbol{\beta}}{\boldsymbol{\beta}^* \hat{\mathbf{V}} \boldsymbol{\beta}} \} \tag{2.11}$$

Since the data has been normalized, we have $\hat{\mathbf{V}} = diag\{1, 1, \cdots, 1\} \in \Re^{m \times m}$. Thus the constraint $\hat{\boldsymbol{\beta}}(\omega_k)^* \hat{\mathbf{V}} \hat{\boldsymbol{\beta}}(\omega_k) = 1$ can be simplified as $\hat{\boldsymbol{\beta}}(\omega_k)^* \hat{\boldsymbol{\beta}}(\omega_k) = 1$. Then $\hat{\lambda}(\omega_k)$ is the largest eigenvalue of $\hat{\mathbf{P}}_{\mathbf{X}}(\omega_k)$, and $\hat{\boldsymbol{\beta}}(\omega_k)$ is the corresponding eigenvector.

2.2.4 Simulation Example

The following simulation example demonstrates the superiority of the performance of the spectral envelope method over the power spectrum and the SPCA method in detecting oscillation(s) and variable categorization.

Time Series Generation

This example consists of 12 time series generated with various sinusoidal oscillations. In these time series, $\varepsilon(t)$ is a white noise sequence with unit variance and $t = 1, \ldots, 512$.

The first four time series are corrupted by a moving average type colored noise terms and have base oscillation at frequency $\omega_1 = 0.1Hz$:

$$\begin{aligned} x_1(t) &= 0.8\cos(2\pi\omega_1 t) + \varepsilon(t) + 0.5\varepsilon(t-1) \\ x_2(t) &= 0.6\cos[2\pi\omega_1(t-5)] + \varepsilon(t) + 0.5\varepsilon(t-1) \\ x_3(t) &= 0.4\cos[2\pi\omega_1(t-15)] + \varepsilon(t) + 0.5\varepsilon(t-1) \\ x_4(t) &= 0.2\cos[2\pi\omega_1(t-2)] + \varepsilon(t) + 0.5\varepsilon(t-1) \end{aligned}$$

The next four time series are also corrupted by colored noise and have base oscillation at frequency $\omega_2 = 0.3Hz$:

$$\begin{aligned} x_5(t) &= 0.9\cos(2\pi\omega_2 t) + \varepsilon(t) - 0.5\varepsilon(t-1) \\ x_6(t) &= 0.7\cos[2\pi\omega_2(t-7)] + \varepsilon(t) - 0.5\varepsilon(t-1) \\ x_7(t) &= 0.5\cos[2\pi\omega_2(t-10)] + \varepsilon(t) - 0.5\varepsilon(t-1) \\ x_8(t) &= 0.3\cos[2\pi\omega_2(t-20)] + \varepsilon(t) - 0.5\varepsilon(t-1) \end{aligned}$$

The next two time series have oscillations at both frequencies $\omega_1 = 0.1Hz$ and $\omega_2 = 0.3Hz$:

$$\begin{aligned} x_9(t) &= 0.4\cos[2\pi\omega_1(t-6)] + 0.5\cos[2\pi\omega_2(t-8)] + \varepsilon(t) + 0.5\varepsilon(t-1) \\ x_{10}(t) &= 0.8\cos[2\pi\omega_1(t-16)] + 0.6\cos[2\pi\omega_2(t-4)] + \varepsilon(t) - 0.5\varepsilon(t-1) \end{aligned}$$

The last two time series consist only of moving average noise sequences:

$$\begin{aligned} x_{11}(t) &= \varepsilon(t) + 0.5\varepsilon(t-1) \\ x_{12}(t) &= \varepsilon(t) - 0.5\varepsilon(t-1) \end{aligned}$$

Before doing further analysis, all the time series are normalized to be zero-mean and unit variance. Figure 2.1 shows the time trends and the corresponding power spectra of these signals. The power spectra of the time series provide some information about the oscillations: For example, time series 1, 2 and 10 have peaks at frequency $\omega_1 = 0.1Hz$, and time series 5, 6 and 7 have peaks at frequency $\omega_1 = 0.3Hz$. However, for other time series, the power spectra do not provide clear indication of the underlying oscillations.

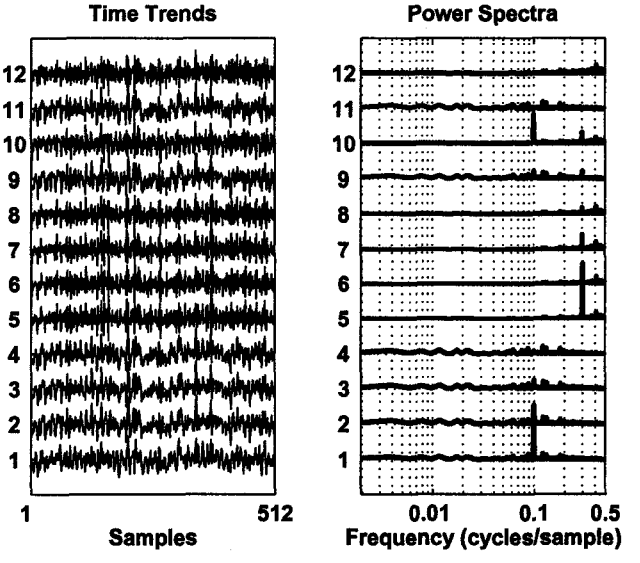

Figure 2.1: Time trends and power spectral of the 12 time series

SPCA Analysis

Description of principal components analysis (PCA) can be found in many studies, for example in Chatfield and Collins (1980) and Johnson and Wichern (1998). In spectral PCA the rows of the data matrix are the power spectra of the signals over a range of frequencies up to one-half of the sampling frequency. A full PCA decomposition reconstructs the data matrix as a sum over the orthonormal basis vectors (BVs) which are spectrum-like functions. The score plot associated with the BVs are used for clustering. Thornhill *et al.* (2002) have given a detailed description of SPCA.

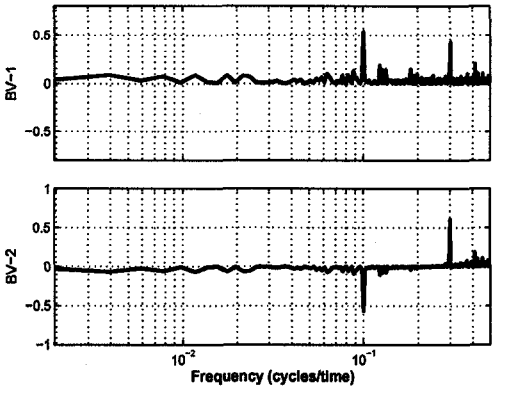

Figure 2.2: SPCA BVs plot of the 12 time series

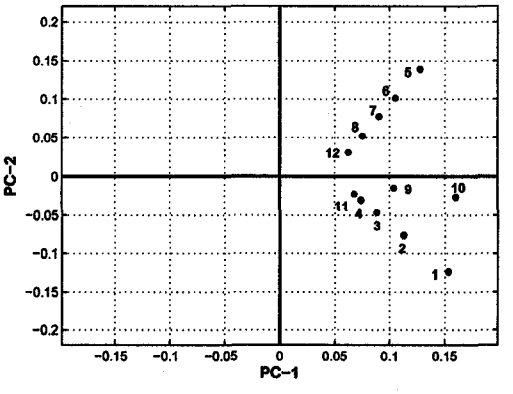

Figure 2.3: SPCA scores plot of the 12 time series

Figure 2.2 shows the plot of the first two basis vectors (BVs) of the spectral analysis of the signals. The two corresponding principal components (PCs) explain over 83% of the variability of the spectra. These two BVs give indication of the base

oscillations at $0.1Hz$ or $0.3Hz$. However, both of these BVs also indicate misleading peaks at frequencies $0.12Hz$ and $0.4Hz$, which actually are not oscillation frequencies in this example. As can be noticed in figure 2.2, part of BV2 contains a negative spectrum, which is not causal since no signal has negative power. The same problem also occurs in the industrial case studies analyzed in Section 6 and 7. Thus the physical interpretation of SPCA analysis is difficult in such cases. A modified extension of SPCA based on non-negative matrix factorization that conforms to the causality of positive power spectral has recently been published by (Tangirala *et al.*, 2007). Figure 2.3 shows the two-dimensional scores plot from SPCA analysis of the 12 time series. Each tag maps to a point in the two-dimensional space. There is no obvious cluster. From examination of figure 2.2 and 2.3 one could say: time series 1, 2 and 3 have positive PC1 value and negative PC2 value, thus they probably have oscillation at $0.1Hz$; time series 5, 6, 7 and 8 have both positive PC1 value and PC2 value, then they probably have oscillation at $0.3Hz$. But for the rest time series, it is hard to analyze their oscillation frequencies: the multiple oscillations in time series 9 and 10 are not detected; time series 11 and 12 can not be identified as not having oscillation.

Oscillation Detection via the Spectral Envelope Method

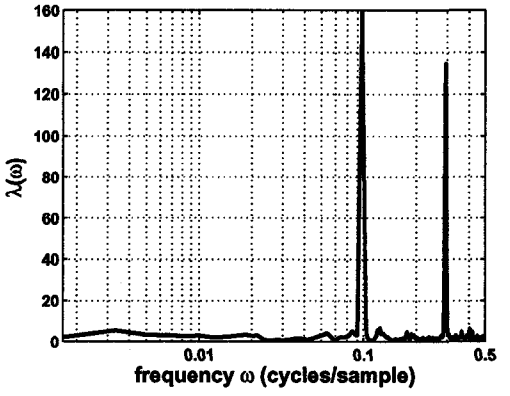

Figure 2.4: Spectral Envelope of the 12 time series

Figure 2.4 shows the spectral envelope calculated using equation (2.9). In this

analysis, we have $n = 512$, $m = 12$ with weights $\{h_0 = 3/9, h_{\pm 1} = 2/9, h_{\pm 2} = 1/9\}$. There are two significant peaks at frequencies: $51/512 \approx 0.1Hz$ and $154/512 \approx 0.3Hz$, which means that the scaled series could have significantly more power at these two frequencies than at any other frequencies. It further implies that some of (or all of) the 12 time series may have significant power at $0.1Hz$ and/or $0.3Hz$. There are no misleading peaks at other frequencies. Therefore, it can be concluded that the spectral envelope method can clearly detect the multiple oscillations present in the time series. Compared with SPCA, the spectral envelope method is frequency sensitive and thus is better in detecting multiple oscillations; also this method can attenuate the noise spectra and thus is better in analyzing noise corrupted data. Variable categorization for this simulation example is discussed in next section.

Remark 2.2.2 *Another oscillation detection technique is the auto-covariance functions (ACF) based method (Thornhill* et al., *2003a). It uses the zero crossings of filtered auto-covariance functions to detect and categorize oscillations. Compared with the spectral envelope method, this method has some limitations in application:*

- *This method is prone to false detections because the algorithm uses ideal band pass filters. If it is a narrow band pass filter, the filtered data may be oscillatory and the algorithm may provide misleading results. This difficulty can be partly overcome by using other advanced filtering technique, but this will increase the complexity of the algorithm.*

- *The presence of noise and multiple oscillations may destroy the regularity of the zero crossings of the ACF. In this case, this method may detect none or only one oscillation, though the spectrum may show multiple distinct peaks.*

- *This method needs a minimum of five cycles in the auto-covariance function to detect oscillation, which is often hard to obtain, particularly in the case of a long oscillation.*

2.3 Variable Categorization

After detecting the oscillation(s), the next task is to group the variables that oscillate at a common frequency. The ACF based method can be used to categorize similar

oscillations, but this method has some limitations in application as mentioned earlier. The SPCA can also categorize variables using the scores plot. However, there are some limitations of applying scores plot as well:

- If the selected BVs can not detect the oscillation frequencies, then the scores plot may not always deliver any useful information.
- In practice, due to noisy data, the clustering in the scores plot is not very obvious. (See the two industrial case studies in Section 6 and Section 7.)
- One variable can belong to one cluster only in the scores plot. Thus the variables that have multiple oscillations are usually hard to analyze using the scores plot. The scores plot may only capture one main oscillation and lose information at the other frequencies. Therefore it is particular difficult to categorize all variables that have common multiple oscillations.
- The visualization of the scores plot is limited by the number of PCs. A scores plot in more than 3-D is hard to analyze.

To overcome the disadvantages of ACF and SPCA methods, we utilize the optimal scaling vector $\hat{\boldsymbol{\beta}}(\omega_k)$ to categorize the variables having common oscillation(s). The magnitude of the optimal scalings (elements of the optimal scaling vector $\hat{\boldsymbol{\beta}}(\omega_k)$) is a measure of the contribution of each time series to the spectral envelope $\hat{\lambda}(\omega_k)$ at frequency ω_k. Once a certain oscillation frequency is identified, then one can investigate the magnitude of the optimal scalings at that frequency. The time series having large optimal scaling magnitude are the ones that contribute the most to the spectral envelope, and thus are the ones having oscillation at that frequency. Furthermore, statistical hypothesis test can be performed to check whether or not a particular element of $\hat{\boldsymbol{\beta}}(\omega_k)$ is zero. This will greatly help us to identify the variables that have oscillations.

In this section, we only use the optimal scaling vector $\hat{\boldsymbol{\beta}}(\omega_k)$ calculated by equation (2.11) . The reason why equation (2.11) is preferred to equation (2.9) is that equation (2.11) leads to simple calculation and one can avoid calculating equation (2.10) which involves the computation of $\hat{\mathbf{V}}_{\mathbf{X}}^{-\frac{1}{2}}$.

2.3.1 Statistical Hypothesis Test on $\hat{\boldsymbol{\beta}}(\omega)$

Details on distribution of the sample spectral envelope and the optimal scalings can be found in Stoffer *et al.* (1993) and McDougall *et al.* (1997). Here we briefly summarize the main result: if $\hat{\mathbf{P}}_{\mathbf{X}}(\omega)$ is a consistent estimator and if $\lambda(\omega)$ is a distinct eigenvalue, then $\nu_n[\hat{\boldsymbol{\beta}}(\omega) - \boldsymbol{\beta}(\omega)]$ converges $(n \to \infty)$ to a complex multivariate normal distribution. The term ν_n depends on the type of estimator being used. For example, if a weighted average as in equation (2.8) is used, $\nu_n = (\Sigma_{j=-r}^{r} h_j^2)^{1/2}$. The asymptotic $(n, r \to \infty)$ covariance matrix of the sample optimal scaling vector $\hat{\boldsymbol{\beta}}(\omega)$, say $\mathbf{V}_\beta(\omega)$, is given by:

$$\mathbf{V}_\beta(\omega) = \nu_n^{-2}\lambda_1(\omega)\Sigma_{l=2}^{m}\lambda_l(\omega)[\lambda_1(\omega) - \lambda_l(\omega)]^{-2}\boldsymbol{\beta}_l(\omega)\boldsymbol{\beta}_l^*(\omega) \tag{2.12}$$

where$\{\lambda_1(\omega) = \lambda(\omega), \lambda_2(\omega), \ldots, \lambda_m(\omega)\}$ are the eigenvalues of $\mathbf{P}_{\mathbf{X}}(\omega)$ arranged in decreasing order, and $\{\boldsymbol{\beta}_1(\omega) = \boldsymbol{\beta}(\omega), \boldsymbol{\beta}_2(\omega), \ldots, \boldsymbol{\beta}_m(\omega)\}$ are the corresponding eigenvectors.

In addition, the distribution

$$\frac{2|\hat{\beta}_{1,j}(\omega) - \beta_{1,j}(\omega)|^2}{\sigma_j(\omega)} \tag{2.13}$$

is approximately a Chi-square distribution with 2 degrees of freedom, where $\hat{\beta}_{1,j}(\omega)$, $j = 1, \ldots, m$ is the jth element of the optimal scaling vector, and $\sigma_j(\omega)$ is the jth diagonal element of $\hat{\mathbf{V}}_\beta(\omega)$, the estimate of $\mathbf{V}_\beta(\omega)$. One could use equation (2.12) and (2.13) to form confidence regions for each $\hat{\beta}_{1,j}(\omega)$. Also, one can check whether or not $\hat{\beta}_{1,j}(\omega)$ is zero by comparing $2|\hat{\beta}_{1,j}(\omega)|^2/\sigma_j(\omega)$ with $\chi_2^2(\alpha)$, the α upper tail cutoff of the Chi-square distribution. If $2|\hat{\beta}_{1,j}(\omega)|^2/\sigma_j(\omega) > \chi_2^2(\alpha)$, then the null hypothesis '$\beta_{1,j}(\omega) = 0$' is rejected with $(1 - \alpha)$ confidence. Based on this one can conclude that, with $(1 - \alpha)$ confidence, the corresponding time series does have oscillation at that frequency. If $2|\hat{\beta}_{1,j}(\omega)|^2/\sigma_j(\omega) < \chi_2^2(\alpha)$, then the null hypothesis '$\beta_{1,j}(\omega) = 0$' is accepted, the corresponding time series can be treated as not having oscillation in the statistical sense. This statistical procedure is particularly useful in automating the task of finding common oscillations in a data set.

Table 2.1 presents the optimal scalings and appropriate test statistics (based on equation. (2.13)) at the oscillation frequencies for each time series of the example in

Table 2.1: Variables categorization for simulation example

	at $0.1Hz$		at $0.3Hz$
Series	Test statistic	Series	Test statistic
1	144	1	5
2	187	2	5
3	71	3	5
4	16	4	5
5	0	5	1289
6	0	6	3920
7	0	7	1008
8	0	8	214
9	66	9	130
10	1392	10	263
11	0	11	5
12	0	12	6

Section 2.2.4. The smoothing weights used are the same $\{h_0 = 3/9, h_{\pm 1} = 2/9, h_{\pm 2} = 1/9\}$. If we choose $\chi^2_2(0.001) = 13.82$, then the conclusion reached from the hypothesis test is that the test has successfully identified the correct oscillation variables at both $0.1Hz$ and $0.3Hz$ with a 99.9% confidence, i.e. variables 1 - 4, 9 and 10 oscillate at $0.1Hz$ frequency and variables 5 - 10 oscillate at $0.3Hz$ frequency. From the intersection of these two sets, it is clear that variables 9 and 10 have oscillations at frequencies of $0.1Hz$ and $0.3Hz$.

2.4 A New Procedure for Detection of Plant-Wide Oscillations

Based on the result in previous sections, the following procedure to detect plant-wide oscillations is proposed:

1. Normalize the data matrix so that each variable has zero-mean and unit variance;

2. Calculate the spectral envelope using equation (2.1) or (2.5) to find out the main oscillation frequencies;

3. Do statistical hypothesis test to identify the variables that have oscillations at those oscillation frequencies found in step (2).

2.5 Industrial case study 1

An industrial data set was provided by the Advanced Controls Technology group of Eastman Chemical Company. Figure 2.5 shows the process schematic of the plant, which contains three distillation columns, two decanters and several recycle streams. There are 15 control loops and 15 indicators on the schematic. The Advanced Controls Technology group had identified a need for diagnosis of a common disturbance with an oscillation period of about 2 hours. In this section, the proposed procedure is applied to this data set to demonstrate its efficacy in detection of this oscillation.

2.5.1 Data Description

The provided data set contains 48 variables: 14 process variables (*pv*'s), 14 controller outputs (*op*'s), 15 indicator variables and 5 cascade loop setpoints (*sp*'s). The whole data set contains 96 hours of data with a sampling time of 20s. Thornhill *et al.* (2003*b*) used the second 48 hour data window to analyze the oscillations. Here, we use the first 48 hour data window where each variable has 8640 observations. In this case study (also for the case study in Section 7), AC, FC, LC, PC and TC represent composition, flow, level, pressure and temperature tags, respectively, that are controlled. Similarly, FI, LI, PI, TI and SI represent the flow, level, pressure, temperature and rotor speed tags, respectively, that are indicators only. We denote the set point, process value and the controller output as *sp*, *pv* and *op*, respectively.

Figure 2.6 shows the time trends and power spectra of the 14 *pv* variables. The power spectra indicate the presence of oscillation at the frequency of 0.003 cycles/sample (or about 333 samples/cycle, nearly a period of 2 hours). This oscillation had propagated through out the adjacent units and affected many variables in the process.

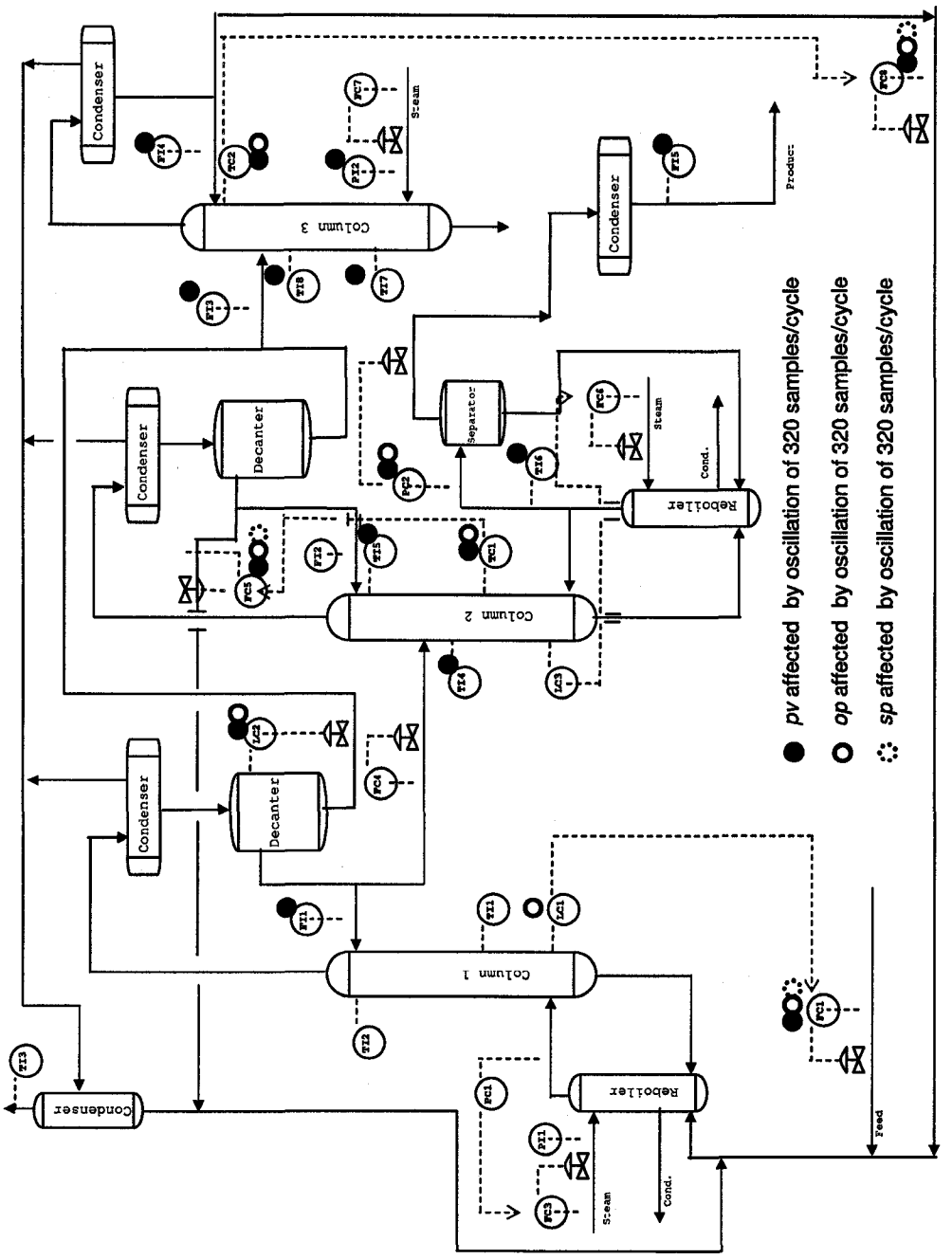

Figure 2.5: Process schematic. The oscillation variables are marked by circle symbols.

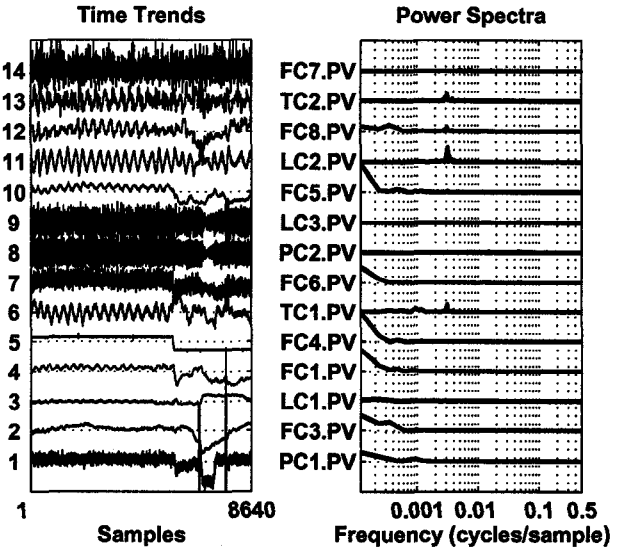

Figure 2.6: Time trend and power spectra of 14 *pv*'s

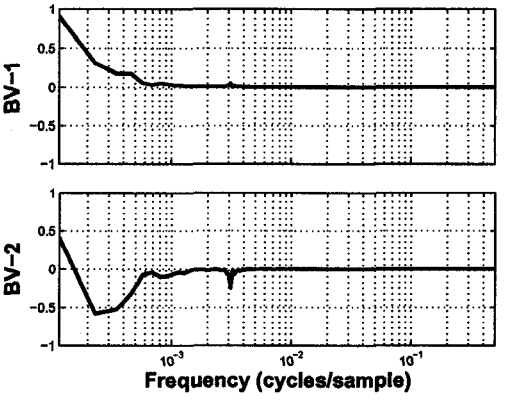

Figure 2.7: SPCA BVs plot of the 48 variables

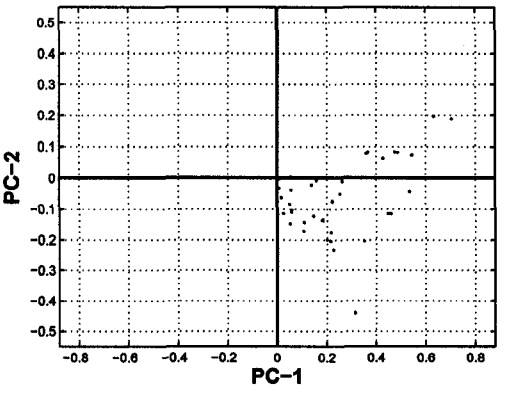

Figure 2.8: SPCA scores plot of the 48 variables

2.5.2 SPCA Analysis

Figure 2.7 shows the first two BVs. The two corresponding PCs explain 86.26% variability of the spectra. BV2 has a peak near the frequency of 0.003 cycles/sample which indicates the oscillation of interest. However, the negative spectrum in BV2 is not causal from a physical point of view. As for the categorization, the two-dimensional scores plot (figure 2.8) has no meaningful clustering. It is hard to analyze the frequency features of each variable using SPCA. Other PCs do not help the analysis either.

2.5.3 New Procedure for Detection of Oscillations

Oscillation Detection

Figure 2.9 shows the spectral envelope (from equation (2.11)) of the 48 variables. This spectral envelope is estimated using triangular smoothing with $r = 1$ and weights $\{h_0 = 1/2, h_{\pm 1} = 1/4\}$. In the spectral envelope, there are clear low frequency features. This is probably because the data is from a long term operation and there exists extremely long period influences such as diurnal weather effects that impact the process. This low frequency feature is quite common in routine operating data from industry and it is also present in the industrial case study (2) in Section 7. In addition to this low frequency feature, there is a clear peak at a frequency of $27/8640 \approx 0.0031$ cycles/sample, indicating an oscillation with a period of 320 samples/cycle. This is

exactly the oscillation that the Advanced Controls Technology group of Eastman Chemical Company wanted to detect and diagnose.

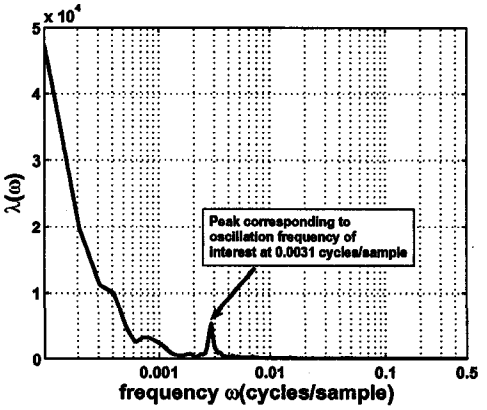

Figure 2.9: Spectral Envelope of the 48 variables

Variable Categorization

Table 2.2: Variables categorization for industrial case study (1)

Tag No.	Test statistic	Tag No.	Test statistic	Tag No.	Test statistic
LC1.op	44	PC2.pv	54	FC8.op	789
FI1.pv	39	PC2.op	52	FI4.pv	143
FC1.sp	44	FC5.sp	395	TC2.pv	254
FC1.pv	46	FC5.pv	428	TC2.op	423
FC1.op	35	FC5.op	165	TI8.pv	188
TI5.pv	78	FI5.pv	56	TI7.pv	25
TI4.pv	1156	LC2.pv	526	PI2.pv	26
TC1.pv	1285	LC2.op	583	FI3.pv	364
TC1.op	397	FC8.sp	418		
TI6.pv	91	FC8.pv	419		

Table 2.2 shows the variables that have the test statistic value bigger than $\chi^2_2(0.001)$ = 13.82 at the oscillation frequency. In other words, we can confirm with 99.9% confidence that these are the variables that have oscillations. These oscillation variables are also marked by dark circle symbols in figure 2.5.

2.6 Industrial case study 2

An industrial data set was provided by Mitsubishi Chemical Corporation (MCC), Mizushima, Japan. Figure 2.10 shows the process schematic of the plant. The plant personnel reported oscillations with a period of about $2 \sim 3$ hours in the condenser level of a distillation column. These oscillations actually propagated through out the plant, causing sub-optimal operation and large economic losses. Previous attempts for oscillation detection and root cause diagnosis by considering only the level and variables directly affecting them were not successful. In this section, the newly proposed procedure is applied to this large data set to detect the plant-wide oscillations.

2.6.1 Data Description

The provided data set consists of 58 variables: 27 process variables (*pv*'s), 15 controller outputs (*op*'s), 16 indicator variables. Each variable has 3600 observations with a sample interval of 1 minute, which corresponds to data over 2 days of operation.

2.6.2 SPCA Analysis

Figure 2.11 shows a plot of the first three BVs. The three corresponding PCs explain 94.68% variability of the spectra. BV3 has a peak near the frequency of 0.007 cycles/sample (or 143 samples/cycle) which indicates the oscillation of interest. However, the negative spectra in BV2 and BV3 is hard to interpret. As for the categorization, the three-dimensional scores plot (figure 2.12) has no meaningful clustering. It is hard to analyze the frequency features of each variable. Other PCs do not help the categorization either.

2.6.3 New Procedure for Detection of Oscillations

Oscillation Detection

Figure 2.13 shows the spectral envelope (from equation (2.11)) of the 58 variables. This spectral envelope is estimated using triangular smoothing with $r = 1$ and weights $\{h_0 = 1/2, h_{\pm 1} = 1/4\}$. Besides the low frequency features, there is a clear peak at the frequency of $25/3600 \approx 0.0069$ cycles/sample. This peak indicates a oscillation

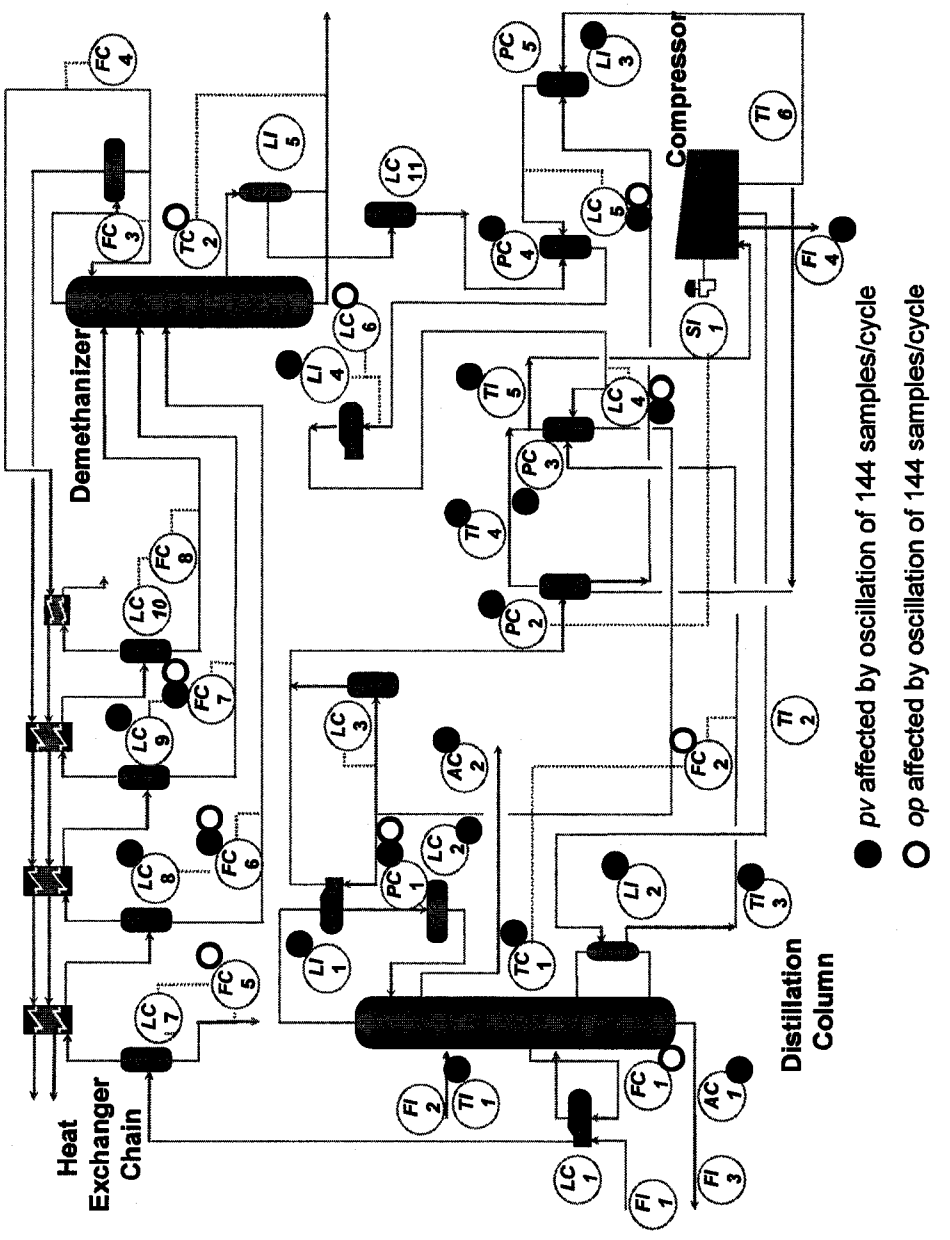

Figure 2.10: Process schematic. The oscillation variables are marked by circle symbols.

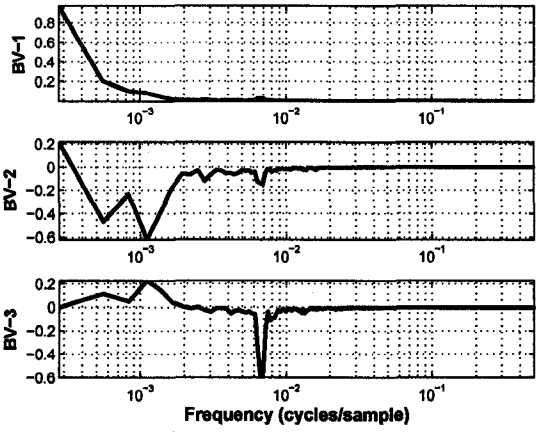

Figure 2.11: SPCA BVs plot of the 58 variables

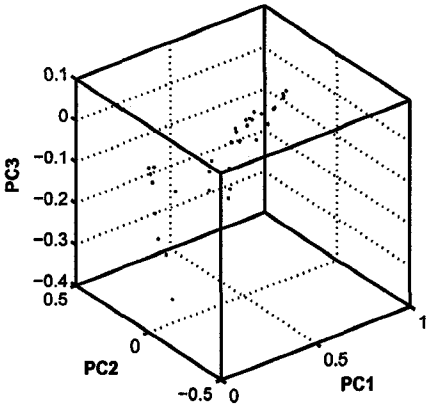

Figure 2.12: SPCA scores plot of the 58 variables

with a period of 144 samples/cycle, which is exactly the oscillation that the plant personnel wanted to detect and diagnose.

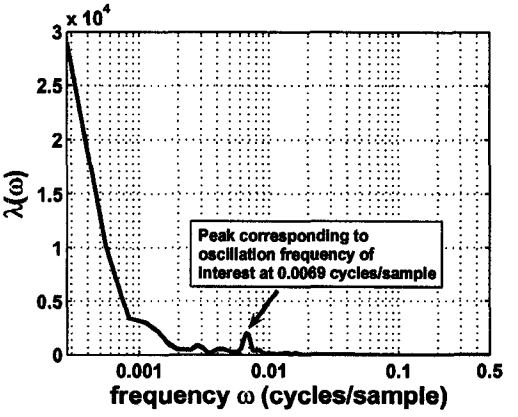

Figure 2.13: Spectral Envelope of the 58 variables

Variable Categorization

Table 2.3: Variables categorization for industrial case study (2)

Tag No.	Test statistic	Tag No.	Test statistic	Tag No.	Test statistic
TI1.pv	492	TI3.pv	96	FI4.pv	56
FC1.op	23	PC2.pv	269	LI4.pv	87
AC1.pv	33	TI4.pv	141	LC6.op	93
LI1.pv	78	PC3.pv	100	TC2.op	25
PC1.op	2867	TI5.pv	34	FC5.op	60
PC1.pv	3385	LC4.op	1310	LC8.pv	37
LC2.pv	398	LC4.pv	325	FC6.op	23
AC2.pv	120	PC4.pv	92	FC6.pv	32
TC1.pv	22	LC5.op	125	LC9.pv	36
LI2.pv	56	LC5.pv	965	FC7.op	21
FC2.op	61	LI3.pv	268	FC7.pv	40

Table 2.3 shows the variables that have the test statistic value bigger than $\chi^2_2(0.001)$ = 13.82 at the oscillation frequency. In other words, with a confidence of 99.9%, these are the variables that have oscillations. These oscillation variables are also marked by dark circle symbols in figure 2.10.

2.7 Concluding Remarks

In this chapter, the concept of spectral envelope has been modified and extended so that it is simple to apply for detecting plant-wide oscillations. This method is good at detecting single or multiple oscillations. The oscillation detection can be carried out using routine operating data and the calculation of spectral envelope is straightforward. In comparison to the ACF based method, the spectral envelope method does not suffer any limitation on the minimum number of oscillation cycles and it does not require the design of any filter. It can detect all oscillations in a single step and therefore the potential for automating this method is significant. The method can also identify variables with multiple oscillations. Furthermore, statistical hypothesis test can be performed to identify variables having common oscillation(s) accurately.

The steps required to carry out this analysis have been summarized and two industrial case studies have been conducted to demonstrate the efficacy of the new procedure.

3

Root Cause Diagnosis of Plant-wide Oscillations

Oscillations are a common type of plant-wide disturbances whose effects propagate to many units and thus may impact overall process performance. It is important to detect and diagnose such oscillations early in order to rectify the situation. Many frequency domain tools such as the power spectrum and spectrum envelope methods are capable of detecting the oscillation frequency. However, few methods are available for locating the root cause which is the main objective of oscillation diagnosis. This chapter proposes two new methods to diagnose the root cause of plant-wide oscillations. The first method is data-based and related to the spectral envelope method. A new index called the oscillation contribution index (OCI) is proposed to isolate the key variables as the potential root cause candidates of common oscillation(s). The second method is non data-based method using the concept of the adjacency matrix. A novel feature of the new method is that it utilizes the information in the process flowsheet. The method is non-data-based and it can be carried out without using any data. However this method complements the data-based methods very well and it is best used in combination with other data-based methods to provide powerful diagnosis of plant-wide oscillations. Two industrial case studies are also presented to

demonstrate the applicability of the proposed methods. [1]

3.1 Introduction

Many methods have been proposed in the literature for oscillation detection. Thornhill and Hägglund (1997) used zero-crossings of the control error signal to calculate integral absolute error (IAE) in order to detect oscillation in a control loop. Miao and Seborg (1999) suggested a method based on the auto-correlation function to detect excessively oscillatory feedback loop. The auto-covariance function (ACF) of a signal was utilized in Thornhill *et al.* (2003*a*) to detect oscillation(s) present in a signal. Thornhill *et al.* (2002) proposed spectral principal component analysis (SPCA) to detect oscillations and categorize variables having similar oscillations. However, the literature is relatively sparse on studies concerned with root cause diagnosis of plant-wide oscillations.

Root cause diagnosis is a challenging problem in the area of detection and diagnosis of plant-wide oscillations. Due to the complexity of large-scale plants and the difficulty of determining cause-effect relationship, it is difficult to conclude whether a certain variable is the root cause just simply from the analysis of plant data. Process knowledge and plant test are indispensable in determining the real root cause. The contribution of current data-based root cause diagnosis techniques (Thornhill *et al.*, 2001; Thornhill *et al.*, 2003*b*) is to isolate the few key variables as the root cause candidates, or at least identify those variables that are 'physically' close to the root cause. This will reduce the workload and cost of further plant tests to determine the real root cause. The idea in Thornhill *et al.* (2001) or Thornhill *et al.* (2003*b*) is to use distortion factor or non-linearity index as signatures to isolate the key oscillation variables as the root cause candidates.

In this section we propose two different methods for root cause diagnosis of plant-wide oscillations. One is a data-based method which only use routine operating data for diagnosis. The other one is non-data-based method which only uses process knowl-

[1] A part of this chapter has been published as (a) Hailei Jiang, M.A.A Shoukat Choudhury and Sirish Shah, "Detection and Diagnosis of Plant-wide Oscillations From Industrial Data using the Spectral Envelope Method", *Journal of Process Control*, **17**(2), 143-155, 2007. (b) Hailei Jiang, Rohit Patwardhan and Sirish Shah, "Root Cause Diagnosis of Plant-Wide Oscillations using the Adjacency Matrix", to appear in the proceedings of IFAC *World Congress 2008*, Seoul, Korea.

edge of a plant to isolate the root cause. The remainder of this chapter is organized as follows. Section 3.2 proposes a new index named, Oscillation Contribution Index (OCI) for oscillation root cause diagnosis. Result from two industrial case studies are presented. The motivation for non-data-based method for oscillation diagnosis is described in Section 3.3. Section 3.4 gives a brief introduction to the concept of the adjacency matrix and reachability matrix. In Section 3.5, through an experimental example and an industrial case study, we show how to use the adjacency matrix and reachability matrix for oscillation diagnosis. In Section 3.6, we summarize a complete procedure for oscillation detection and root cause diagnosis. This chapter ends with concluding remarks in Section 3.7.

3.2 Oscillation Contribution Index

In this section, we propose a new index called the oscillation contribution index (OCI) to serve the purpose of isolating the key oscillation variables as the root cause candidates.

The main idea of OCI is to utilize the optimal scalings of the oscillation variables that are identified by the statistical hypothesis test described in the last chapter. The root cause(s) is most likely to be within these variables that have oscillations. If $x_j(t)$ is one of the oscillation variables, then its OCI is defined to be:

$$OCI_j(\omega) = \frac{\hat{\beta}_{1,j}(\omega)}{2\sigma_{\hat{\beta}}(\omega)} \tag{3.1}$$

where $\sigma_{\hat{\beta}}(\omega)$ is the standard deviation of the optimal scalings of all the identified variables that have oscillations. The OCI is an indicator of the contribution of each oscillation variables to the spectral envelope peak at the oscillation frequency. We use the OCI to isolate the key variables as the root cause candidates. A general criteria is that the variables having $OCI(\omega) > 1$ are the likely root cause variables at frequency ω because they contribute most to the spectral envelope at the oscillation frequency. The test can be more stringent and discriminating if a three-sigma test is used. The industrial case studies in the later sections will demonstrate the efficacy of using the OCI to isolate the key variables.

Remark 3.2.1 *If there is no root cause, or the root cause variable is not included in the original data set, then of course the OCI would not be able to find it. The calculated OCI in this situation can be used to rank the variables according to their contribution to the spectral envelope at the oscillation frequency and find out the variables that have significant oscillations. In such cases the OCI for each variable can simply be interpreted as the signal strength of that variable towards the frequency of interest. In general, the purpose of the OCI is to provide a ranked list of variables that are the likely root cause variables or lie physically close to the root cause. This ranked list combined with process flowsheet, loop configuration and other pertinent information can lead to the correct diagnosis of root causes.*

3.2.1 Possible Diagnosis: Valve Stiction

Higher Order Statistical Method: The method is based on the presence of phase coupling in a non-linear time series. These phase couplings can be detected by the bicoherence of the signal defined as:

$$bic^2(f_1, f_2) \triangleq \frac{|E[X(f_1)X(f_2)X^*(f_1+f_2)]|^2}{E[|X(f_1)X(f_2)|^2]E[|X(f_1+f_2)|^2]} \tag{3.2}$$

where $X(f_1)$ is the discrete Fourier transform calculated at the frequency f_1, $X^*(f_1)$ is the complex conjugate and E is the expectation operator. The bicoherence is the normalized bispectrum and has as a value between 0 and 1, where a non-zero value results only if there is significant phase coupling in the signal between frequency components at f_1 and f_2.

In Choudhury *et al.* (2004*b*), two indices - the Non-Gaussianity Index (NGI) and the Non-Linearity Index (NLI) - have been defined based on bicoherence of a time series signal. When both NGI and NLI are greater than zero, the signal is described as non-Gaussian and nonlinear and it is inferred that the loop in question exhibits significant non-linearity. For a control loop, this test is applied to the error signal ($sp - pv$) as the error signal is often more stationary than pv or op signals. Assuming that the process is linear and no nonlinear disturbances enter the loop, the nonlinearity can be attributed to the control valve. Once a nonlinearity is detected using higher order statistical method-based NGI and NLI indices, the *pv-op* plot is used to diagnose and isolate its cause. It is well known (Hägglund, 1995; Rengaswamy

et al., 2001; Choudhury *et al.*, 2005*a*; Choudhury, 2004) that the presence of stiction in control valve in a control loop produces limit cycles in the controlled variable (*pv*) and the controller output (*op*). For such a case, the *pv-op* plot shows elliptical cyclic patterns, which are taken as a signature of valve stiction. If no such patterns are observed, it is concluded that there may be valve problems other than stiction. Note that for the cases of tightly tuned controller or a process with time delay, the *pv-op* plot may also exhibit elliptical patterns. But they do not add nonlinearity in a control loop. Therefore, these cases do not pass the nonlinearity test. The *pv-op* plot is investigated only after a successful nonlinearity detection in the loop. That is why the *pv-op* plot should not be used alone to detect stiction. This must be used in conjunction with the nonlinearity test. For a detailed discussion on these issues, refer to Choudhury *et al.* (2004*b*), Choudhury *et al.* (2006).

3.2.2 Industrial Case Study 1 using *OCI*

In section 2.5, we presented a plant at Eastman Chemical Company, USA. The schematic of the process is shown in figure 2.5. In section 2.5, we successfully isolated the variables that have common oscillation. The remaining question is: which loop is the root cause of the plant-wide oscillations? Here we use the new *OCI* index and the valve stiction technique to isolate the root cause.

Oscillation Diagnosis

Table 3.1 shows the variables that have *OCI* bigger than 1 at the oscillation frequency. They are treated as the root cause candidates. Among all the variables, the *pv* and *op* of the level control loop LC2 have the largest *OCI* at the oscillation frequency. This result indicates that the LC2 loop contributes most to the spectral envelope at the oscillation frequency and we should take this loop as the first root cause candidate.

To confirm and isolate the root cause, the *pv* and *op* data for this loop was analyzed further. Higher order statistical methods described in Choudhury *et al.* (2004*b*), Choudhury *et al.* (2004*a*) and Choudhury (2004) are used to investigate this problem.

Figure 3.1 shows the diagnostic plots for this loop. Figure 3.1(*a*) shows that there are significantly large peaks in the bicoherence plot indicating a nonlinear loop. The values of *NGI* and *NLI* for this loop are 0.15 and 0.42, respectively, which clearly

Table 3.1: Ranked list of variables having *OCI* bigger than 1 at the oscillation frequency

Tag No.	*OCI*	Tag No.	*OCI*
LC2.pv	2.09	FC8.pv	1.17
LC2.op	1.88	TC2.op	1.11
TI4.pv	1.51	FC8.sp	1.11
TC1.pv	1.48	TI5.pv	1.10
TC2.pv	1.44	TI8.pv	1.07

indicates that the loop exhibits nonlinearity. Once a loop nonlinearity is detected, it should be checked whether this is due to stiction or other process nonlinearity. Figure 3.1(*b*) shows the *pv-op* plot for this loop. The plot clearly shows an elliptic pattern indicating the presence of stiction in the control valve. The apparent stiction is quantified to be approximately 3% using the method described in Choudhury *et al.* (2006).

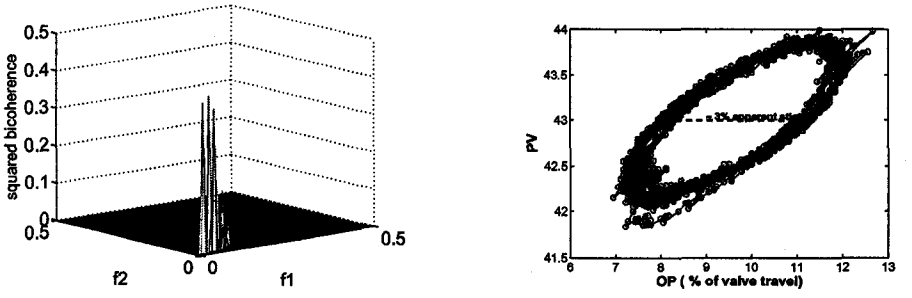

(a) Bicoherence Plot

(b) LC2.*pv* - LC2.*op* plot

Figure 3.1: Oscillation diagnosis plots for LC2 loop

Similar results of root cause diagnosis were also discussed in Thornhill *et al.* (2003*b*). It was reported that the control valve of loop LC2 suffered from a deadband problem (Thornhill *et al.*, 2003*b*). It has been confirmed that the control valve caused control variable LC2.*pv* to oscillate, and the oscillation passed through the feedback controller and made the controller output LC.*op* also to oscillate. After that, the oscillations propagated to the temperature control loop TC1 in the second distillation column and caused the temperature to oscillate. This is the reason why temperature indicator TI4.*pv* and control variable TC1.*pv* had oscillations too. For more information, refer to Thornhill *et al.* (2003*b*).

3.2.3 Industrial Case Study 2 using *OCI*

In section 2.6, we have successfully isolated the variables that have common oscillation in a plant at Mitsubishi Chemical Corporation (MCC), Mizushima, Japan. The schematic of the process is shown in figure 2.10. Here we use the new *OCI* index and the valve stiction technique to isolate the root cause.

Oscillation Diagnosis

Table 3.2 shows variables that have *OCI* bigger than 1 at the oscillation frequency. They are treated as the root cause candidates. Among all the variables, variable PC1.*pv* has the largest *OCI* value. This result indicates that this particular (PC1) loop contributes most to the spectral envelope at the oscillation frequency and we should examine this loop as the first or most likely root cause candidate.

Table 3.2: Ranked list of variables having *OCI* bigger than 1 at the oscillation frequency

Tag No.	*OCI*	Tag No.	*OCI*
PC1.pv	2.23	LI3.pv	1.36
TI4.pv	1.68	LC4.pv	1.33
LC5.pv	1.64	LC8.pv	1.18
LI1.pv	1.48	LC5.op	1.08
LC4.op	1.38		

Again, we followed the same procedure as in the earlier industrial case study (1) to diagnose the cause of the oscillations. Figure 3.2(a) shows the bicoherence plot. The values of *NGI* and *NLI* are 0.18 and 0.54 respectively, indicating a nonlinear loop. The elliptical pattern in figure 3.2(b) indicates that this control valve is suffering from stiction.

Further plant tests have confirmed that this loop with a sticky valve was indeed the leading cause of plant-wide oscillations. Before the 'plant-shutdown' for maintenance could proceed, a simple closed-loop test described in Choudhury *et al.* (2005*b*) was performed on loop PC1 to confirm the presence of valve stiction. This simple closed-loop test requires one to change the controller gain and observe whether there is a change in frequency of oscillation. If the frequency of oscillation changes, this indicates that the oscillation is generated within the loop and is not caused by an

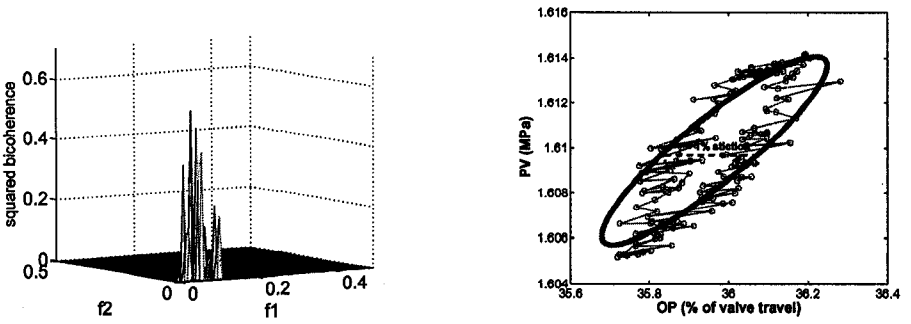

(a) bicoherence plot

(b) *pv-op* plot

Figure 3.2: Diagnostic plots for the PC1 loop

external disturbance. The results obtained from this test on loop PC1 confirmed that the oscillation was generated within the loop PC1. MCC engineers have now confirmed that the sticky valve in this loop plus interactions from other loops were the main causes of oscillations.

3.3 Motivation for Non-Data-Based Root Cause Diagnosis

Thornhill *et al.* (2001) and Thornhill *et al.* (2003*b*) proposed to calculate distortion factors and nonlinearity index of process variables and use them as an indication of possible root cause. The objective of the Oscillation Contribution Index (OCI) proposed in the last section is to evaluate the severity of oscillations in each variable and hence use the OCI as an indication of potential root cause. All these methods are data-based without using process knowledge. The main objective of these techniques is to isolate the few variables as the root cause candidates. Due to the complexity of large-scale plants and the difficulty of determining cause-effect relationship, it is difficult to conclude whether a certain variable is the root cause just simply from the analysis of plant data.

In recent years, graph-based approaches have been proposed by various researchers for safety analysis and fault diagnosis of chemical process systems (Maurya *et al.*, 2003*a*). Maurya *et al.* (2003*a*) and Maurya *et al.* (2003*b*) gave a comprehensive review of the signed digraph (SDG) and showed how to develop graph models sys-

tematically from a system of differential-algebraic equations. Yim *et al.* (2006) used process topology in plant-wide control performance assessment. They used the computer aided engineering exchange (CAEX) file to describe items of equipment in the plant, such as tanks, pipes, valves and instruments and how they are linked physically. Recently, Bauer *et al.* (2007) described a data-driven method for identifying the direction of propagation of disturbance based on the concept of transfer entropy.

The main purpose of the aforementioned sections is to incorporate process knowledge, such as process flowsheet or topology, control configuration and instrument information, into an oscillation diagnosis tool. We propose a novel way to convert a process schematic to a digraph based on the information of controllers. The new digraph is defined as the *control loop digraph.* The concept of adjacency matrix will be used to develop a process knowledge based method for oscillation diagnosis. Combination of this method with other data-based methods can provide a powerful diagnosis of root cause of plant-wide oscillations. Two industrial case studies are presented to demonstrate the applicability of the proposed method.

3.4 Digraphs and the Adjacency Matrix

A graph is a mathematical abstraction of structural relationships between discrete objects (Mah, 1989). The objects are represented by a set of *nodes*, and the existence of relationship between two objects is presented by *edges.* If a sense of direction is imparted to each edge of a graph, such a graph is called a *directed graph* or a *digraph* for short. Figure 3.3(a) shows a simple digraph where $\{a, b, c, d, e\}$ are nodes and the lines with arrow are edges. In graph theory, there are several methods to represent a digraph by a matrix. A common one is to represent a digraph by an *adjacency matrix* (Mah, 1989). In an adjacency matrix the rows and columns both represent the nodes. The (i, j)th entry is assigned a value of "1" if there is a directed edge from node i to node j, otherwise it is assigned a value of "0".

The adjacency matrix (denoted as $\mathbf{X}$) of the digraph in figure 3.3(a) is shown in figure 3.3(b). It is clear that the total number of "1"s in the adjacency matrix is given by the number of edges in the digraph. A very interesting and useful property of adjacency matrix is: the (i, j) element of $\mathbf{X}^k$ gives the number of k-step edge

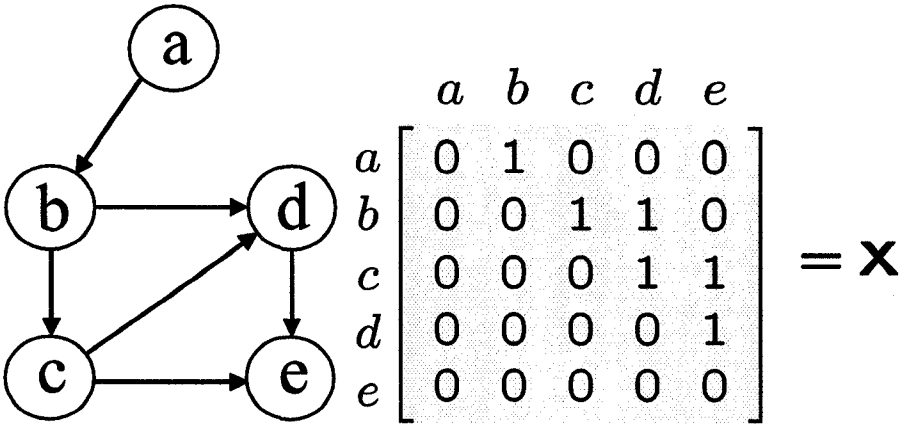

(a) A simple digraph (b) Adjacency matrix

Figure 3.3: A digraph and its adjacency matrix

sequences from node i to node j. For example, the following matrices are successive powers of the adjacency matrix in figure 3.3(b). By examining these matrices it is easy to verify the above mentioned property. For example, element $(2,5)$ in $\mathbf{X}^2$ shows that there are two 2-step edge sequences from node b to node e; and as is clear from figure 3.3(a) we can find that the two 2-step edge sequences from node b to node e as $\{b \rightarrow c \rightarrow e\}$ and $\{b \rightarrow d \rightarrow e\}$.

$$\mathbf{X}^2 = \begin{bmatrix} 0 & 0 & 1 & 1 & 0 \\ 0 & 0 & 0 & 1 & 2 \\ 0 & 0 & 0 & 0 & 1 \\ 0 & 0 & 0 & 0 & 0 \\ 0 & 0 & 0 & 0 & 0 \end{bmatrix} \qquad \mathbf{X}^3 = \begin{bmatrix} 0 & 0 & 0 & 1 & 2 \\ 0 & 0 & 0 & 0 & 1 \\ 0 & 0 & 0 & 0 & 0 \\ 0 & 0 & 0 & 0 & 0 \\ 0 & 0 & 0 & 0 & 0 \end{bmatrix}$$

$$\mathbf{X}^4 = \begin{bmatrix} 0 & 0 & 0 & 0 & 1 \\ 0 & 0 & 0 & 0 & 0 \\ 0 & 0 & 0 & 0 & 0 \\ 0 & 0 & 0 & 0 & 0 \\ 0 & 0 & 0 & 0 & 0 \end{bmatrix} \qquad \mathbf{X}^5 = \begin{bmatrix} 0 & 0 & 0 & 0 & 0 \\ 0 & 0 & 0 & 0 & 0 \\ 0 & 0 & 0 & 0 & 0 \\ 0 & 0 & 0 & 0 & 0 \\ 0 & 0 & 0 & 0 & 0 \end{bmatrix}$$

Before introducing the reachability matrix, we define the Boolean equivalent of any matrix $\mathbf{A}$ by the following relationship (Mah, 1989):

$$\mathbf{A}^{\#}(i,j) = \begin{cases} 0, & if \ \mathbf{A}(i,j) = 0 \\ 1, & if \ \mathbf{A}(i,j) \neq 0 \end{cases} \tag{3.3}$$

For a digraph with N nodes and an adjacency matrix $\mathbf{X}$, the following matrix

$$\mathbf{R} = (\mathbf{X} + \mathbf{X}^2 + \mathbf{X}^3 + ... + \mathbf{X}^N)^{\#} \tag{3.4}$$

is defined as the reachability matrix (Mah, 1989). The (i,j)th element of $\mathbf{R}$ indicates whether there exists any directed path of any length whatsoever from node i to node j. The reachability matrix for the digraph in figure 3.3(a) is

$$\mathbf{R} = \begin{bmatrix} 0 & 1 & 1 & 1 & 1 \\ 0 & 0 & 1 & 1 & 1 \\ 0 & 0 & 0 & 1 & 1 \\ 0 & 0 & 0 & 0 & 1 \\ 0 & 0 & 0 & 0 & 0 \end{bmatrix}$$

The reachability matrix provides a conceptually simple and direct method of determining the connectivity of a digraph (Mah, 1989). For instance, the entries in $\mathbf{R}$ show that node a can reach all the other nodes, but node a can not be reached from any other node. Similarly, node b can reach $\{c, d, e\}$, but not vice versa.

3.5 Control Loop Digraph based on Process Flowsheet

The idea of *process digraph* in Mah (1989) is to denote units, tanks and junctions of a process as nodes and physical connections as edges in a digraph. This process digraph is used in the design of continuous processes and in the treatment of batch plant scheduling and design. However, this equipment-based process digraph is not appropriate for oscillation diagnosis where control loops also need to be considered. In this section, we introduce the concept of a *control loop digraph* for oscillation analysis.

3.5.1 Control Loop Digraph

As mentioned earlier, because of feedback and/or feedforward control and other physical connections in a process, an oscillation often starts from a single loop and propagates to other loops. To build and analyze the digraph of a process from a control

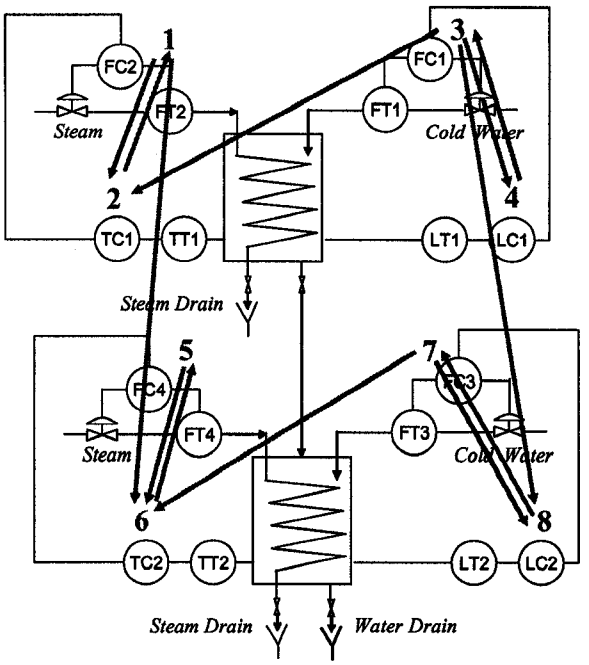

Figure 3.4: Control loop digraph of a two-tank system

plus process flowsheet perspective we denote each controller in a process schematic as a node. Next we use a concept of *direct interaction* to add edges between the nodes. We define a direct interaction from node i to node j if the output of controller i ($i.OP$) can directly affect the controlled variable of controller j ($j.PV$) without going through controller output of any other nodes; and we can add an edge from node i to node j in the process flowsheet. To achieve a complete analysis of direct interactions in a plant, we utilize all information of the control structure and process flowsheet connections. With controllers as nodes, and direct interactions as edges, we propose a new digraph that we define as a *control loop digraph*. The following example illustrates how to create a control loop digraph from a process flowsheet.

3.5.2 Example

Figure 3.4 shows a two-tank system where FT, LT, FC and LC represent flow transmitter, level transmitter, flow controller and level controller respectively. The outlet water from the upper tank flows directly into the lower tank. For each tank

		1 FC2	2 TC1	3 FC1	4 LC1	5 FC4	6 TC2	7 FC3	8 LC2
1	FC2			0	0	0		0	0
2	TC1			0	0	0	0	0	0
3	FC1	0				0	0	0	
4	LC1	0	0			0	0	0	0
5	FC4	0	0	0	0			0	0
6	TC2	0	0	0	0			0	0
7	FC3	0	0	0	0	0			
8	LC2	0	0	0	0	0	0		

Figure 3.5: Adjacency matrix of the two-tank system

		1 FC2	2 TC1	3 FC1	4 LC1	5 FC4	6 TC2	7 FC3	8 LC2
1	FC2			0	0			0	0
2	TC1			0	0			0	0
3	FC1								
4	LC1								
5	FC4	0	0	0	0			0	0
6	TC2	0	0	0	0			0	0
7	FC3	0	0	0	0				
8	LC2	0	0	0	0				

Figure 3.6: Reachability matrix of the two-tank system

there is a cascaded temperature loop and also a level cascade loop. There are total of eight controllers in this system and these controllers are assigned a number from 1 to 8 separately as shown in figure 3.4. The red lines with arrows represent the direct interactions between the controllers. For example, node 1 (FC2) has direct interactions with node 2 (TC1) and node 6 (TC2). This is because the OP of node 1 (FC2) can change the steam flowrate and therefore can affect the temperature of the upper tank (which is the PV of node 2, TC1); the temperature of the lower tank (which is the PV of node 6, TC2) can also be affected by the water from upper tank. Please note that there is no direct interaction from node 1 (FC2) to node 5 (FC4). This is because the OP of node 1 can only affect the PV of node 5 through the OP of node 6 (TC2). If node 5 (FC4) is not cascaded with node 6 (TC2), then node 1 can not affect node 5. Therefore we say there is no direct interaction from node 1 to node 5. Following the definition of direct interaction, we can obtain a complete analysis of the two-tank system and come up with the control loop digraph shown in figure 3.4.

The adjacency matrix of the control loop digraph of the two-tank system is shown in figure 3.5 which is different from the concept we introduced in Section 2. In section 2, we did not put "1" on the diagonal, but here we have assigned "1" on the diagonal

which means that the OP of a controller will affect the PV of the loop itself first. The corresponding reachability matrix is shown in figure 3.6. It is clear in figure 3.6 that node 3 (FC1) and node 4 (LC1) can reach (or affect) all the other controllers in the two-tank system. This observation is consistent with our expectation that the water flow rate to the upper tank and the level of upper tank can affect the PVs of all other controllers. Additionally, we can see in figure 3.6 that nodes 5-8 can not reach node 1-4. This means that the controllers of lower tank can not affect the controllers of upper tank which also concurs with the real situation. We can also conclude from the reachability matrix that the temperature cascade loops (nodes 1&2 and nodes 5&6) can not affect the level cascade loops (nodes 3&4 and nodes 7&8). These results do confirm that the control loop digraph (based on direct interactions) and its corresponding reachability matrix can correctly represent the interactions in a process. The row of '1's' in the reachability matrix is an indication of the reach or the influence of that controller on all other control loops.

3.5.3 Industrial Application for Oscillation Diagnosis

Figure 3.7 shows an schematic of a process at Eastman Chemical Company, USA. In this case study (and also for the case study in Section 4), AC, FC, LC, PC and TC represent composition, flow, level, pressure and temperature tags, respectively, that are controlled. Similarly, FI, LI, PI, TI and SI represent the flow, level, pressure, temperature and rotor speed tags, respectively, that are indicators only. There are 14 PID controllers in this process. To draw the control loop digraph of this process, we take the controllers as nodes and consider the direct interactions between different nodes. For example, node 1 and node 2 are the secondary and the master controllers in a cascade control loop. Either the OP of node 1 or node 2 moves, the PV of other node will be affected. Therefore, we say nodes 1 and 2 have direct interactions between them and we add edges between nodes 1 and 2. After a complete analysis of direct interactions, we can draw the control loop digraph of this process as shown in figure 3.7. The adjacency matrix of the digraph is shown in figure 3.8. The corresponding reachability matrix is shown in figure 3.9 which shows that nodes 5 and 6 have connections to all the other nodes except node 13.

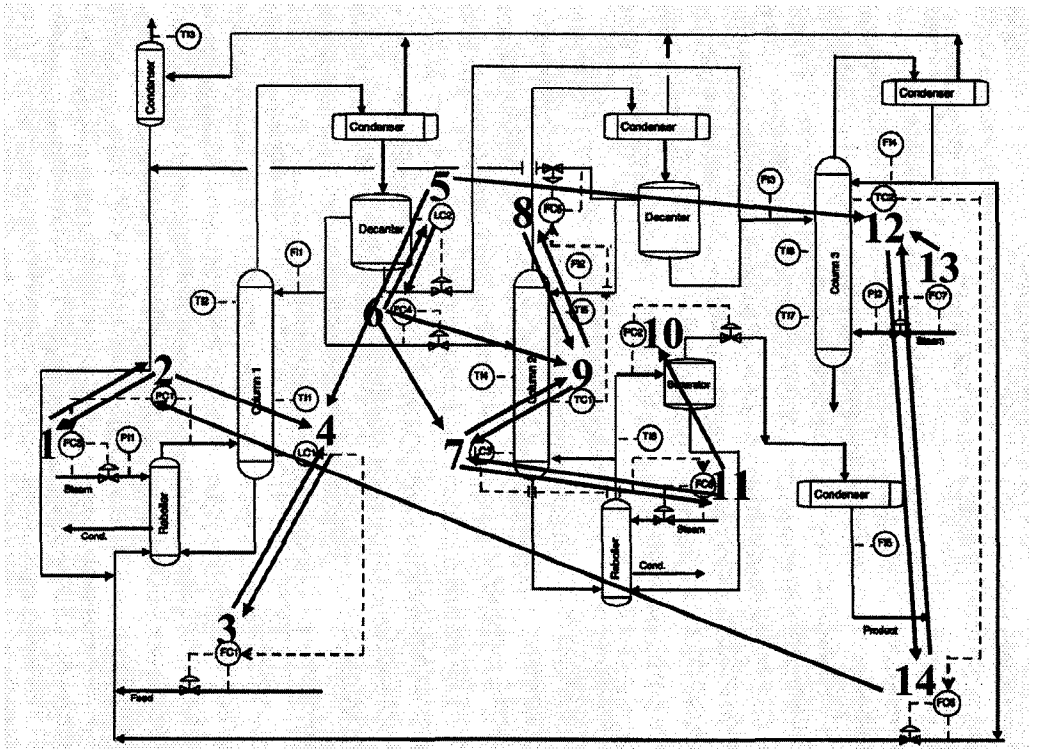

Figure 3.7: Control-based process digraph of a process from Eastman Chemical Company, USA

		1 FC3	2 PC1	3 FC1	4 LC1	5 LC2	6 FC4	7 LC3	8 FC5	9 TC1	10 PC2	11 FC6	12 TC2	13 FC7	14 FC8
1	FC3			0	0	0	0	0	0	0	0	0	0	0	0
2	PC1			0		0	0	0	0	0	0	0	0	0	0
3	FC1	0	0			0	0	0	0	0	0	0	0	0	0
4	LC1	0	0			0	0	0	0	0	0	0	0	0	0
5	LC2	0	0	0				0	0	0	0	0		0	0
6	FC4	0	0	0	0				0		0	0	0	0	0
7	LC3	0	0	0	0	0	0		0		0		0	0	0
8	FC5	0	0	0	0	0	0	0			0	0	0	0	0
9	TC1	0	0	0	0	0	0				0	0	0	0	0
10	PC2	0	0	0	0	0	0	0	0	0		0	0	0	0
11	FC6	0	0	0	0	0	0		0	0			0	0	0
12	TC2	0	0	0	0	0	0	0	0	0	0	0		0	
13	FC7	0	0	0	0	0	0	0	0	0	0	0			0
14	FC8	0		0	0	0	0	0	0	0	0	0		0	

Figure 3.8: Adjacency matrix of the Eastman Process shown in figure 3.7

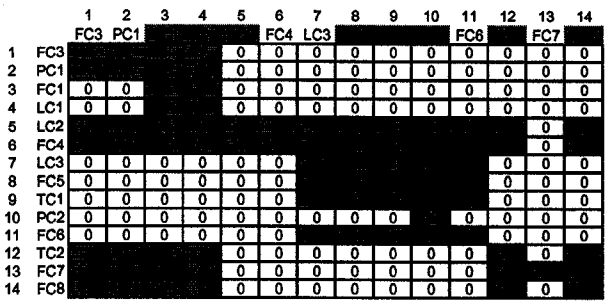

Figure 3.9: Reachability matrix of the Eastman Process shown in figure 3.7

3.5.4 Oscillation diagnosis

The Advanced Controls Technology group of Eastman Chemical Company had noticed that many of the process variables in this particular unit were oscillating and they needed to find out the root cause of these oscillations. Figure 2.6 shows the time trends and power spectra of the 14 *pv* variables. The sampling time of the time trends is 1 minute. The power spectra indicate the presence of oscillation at the frequency of 0.003 cycles/sample (or about 333 samples/cycle, nearly a period of 2 hours). This oscillation had propagated through out the adjacent units and affected many variables in the process.

In chapter 2, we have used the spectral envelope method to detect the oscillation frequencies and isolate all the variables that were oscillating at the same frequency of concern. In figure 3.9, the variables highlighted in blue are the variables oscillating at the frequency of concern (see table 2.2).

The diagnosis that we arrive at based on the reachability matrix is that: if the oscillation started from one loop in the process, then the root cause must be either loops 5 or 6 because these are the only two loops that can reach all the detected oscillatory loops. The root cause of an oscillatory signal can be many: tight tuning of the control loop, or an oscillatory disturbance or process or valve non-linearity. After further investigation it was determined that valve stiction related limit cycles was a likely source of the oscillatory signal in one of these loops. Choudhury *et al.* (2004*b*), Choudhury *et al.* (2006) used bicoherence and $pv - op$ plot to detect and diagnose valve stiction. We followed their method and figure 3.1 shows the bicoherence plot

and the $pv - op$ plot of loop 5. The presence of large bicoherence value and an ellipse in the $pv - op$ plot is a clear evidence of valve stiction in loop 5; we did not find valve stiction in loop 6. Therefore our analysis indicated loop 5 (LC2) is the root cause.

3.6 Complete Procedure for Oscillation Detection and Root Cause Diagnosis

In the previous section, we introduced the concept of control loop digraph and used its adjacency matrix and reachability matrix to diagnose the root cause of plant-wide oscillations. A novel feature of this method is that it is non-data-based. A combination of this method and other data-based methods can provide an effective detection and diagnosis tool. Next we summarize a new method for complete and comprehensive procedure for oscillation detection and diagnosis:

1. Use frequency domain methods, such as spectral envelope and power spectral to detect loops with common oscillations and their frequencies.

2. Use the method presented in the previous section for oscillation diagnosis.

3. To further confirm the diagnosis result from step (2), other methods for checking controller tuning, disturbance detection or detection of valve stiction, process nonlinearity can be used.

To show the effectiveness of the above procedure, we present one more industrial case study for the detection and diagnosis of plant-wide oscillations. An industrial data set was provided by the courtesy of Mitsubishi Chemical Corporation (MCC), Mizushima, Japan. Figure 3.10 shows the process schematic and the control loop digraph of the plant. The plant personnel reported oscillations with a period of about $2 \sim 3$ hours through out the plant, causing sub-optimal operation and large economic losses. The newly proposed procedure is applied to this large data set to detect and diagnose the cause of these plant-wide oscillations.

3.6.1 Oscillation Detection

In chapter 2, we used the spectral envelope method to detect the oscillation frequency and the oscillatory control loops. Here we give a summary of the result: among the

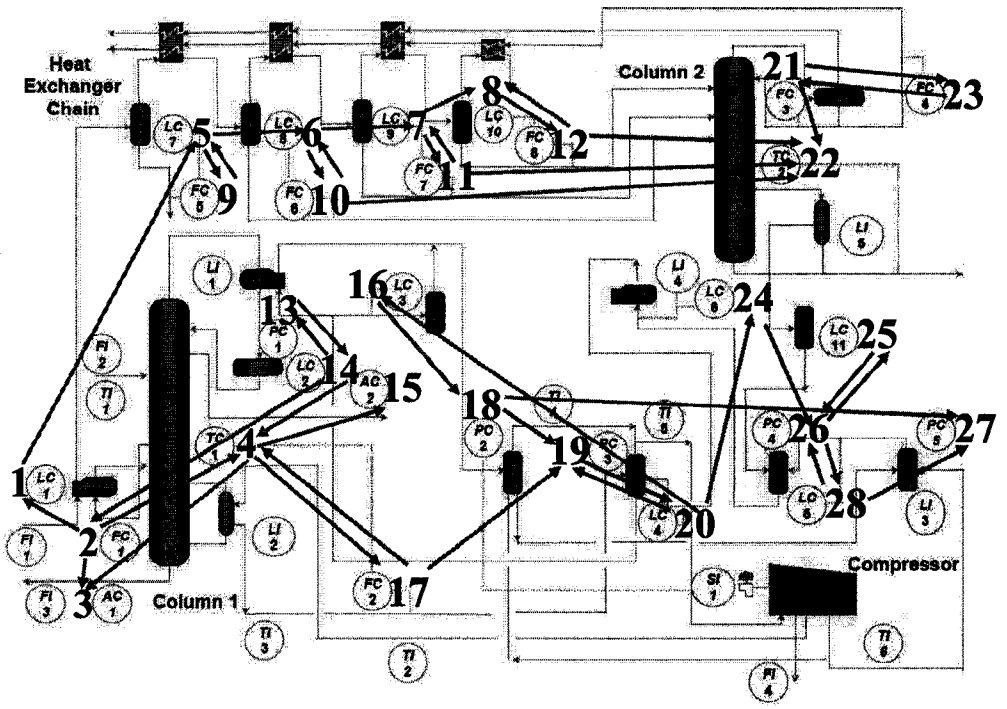

Figure 3.10: Control loop digraph of a process from Mitsubishi Chemical Corporation, Japan

total 28 loops, 19 loops were identified as having oscillations with a period of 144 mins. The variables that have oscillations are listed in the following table.

Table 3.3: The loops that have oscillations

2	3	4	6	7	9	10
FC1	AC1	TC1	LC8	LC9	FC5	FC6
11	13	14	15	17	18	19
FC7	PC1	LC2	AC2	FC2	PC2	PC3
20	22	24	26	28		
LC4	TC2	LC6	PC4	LC5		

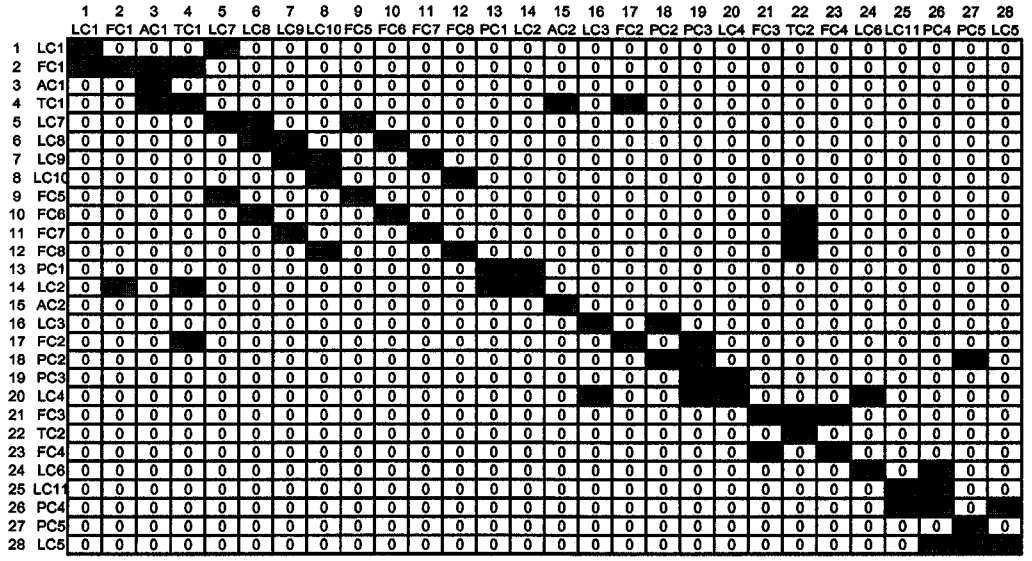

Figure 3.11: Adjacency matrix of the digraph in Fig. 3.10

3.6.2 Root Cause Diagnosis

After detecting the loops that have oscillation, the next objective was to locate the root cause in order to rectify the situation. First, considering direct interactions, we built the adjacency matrix from the control loop digraph. The adjacency matrix is shown in figure 3.11. Then we built the reachability matrix from the adjacency matrix as shown in figure 3.12. In figure 3.12, the oscillatory variables listed in table 3.3 are highlighted in blue. It is clear that, if the oscillations started from a single

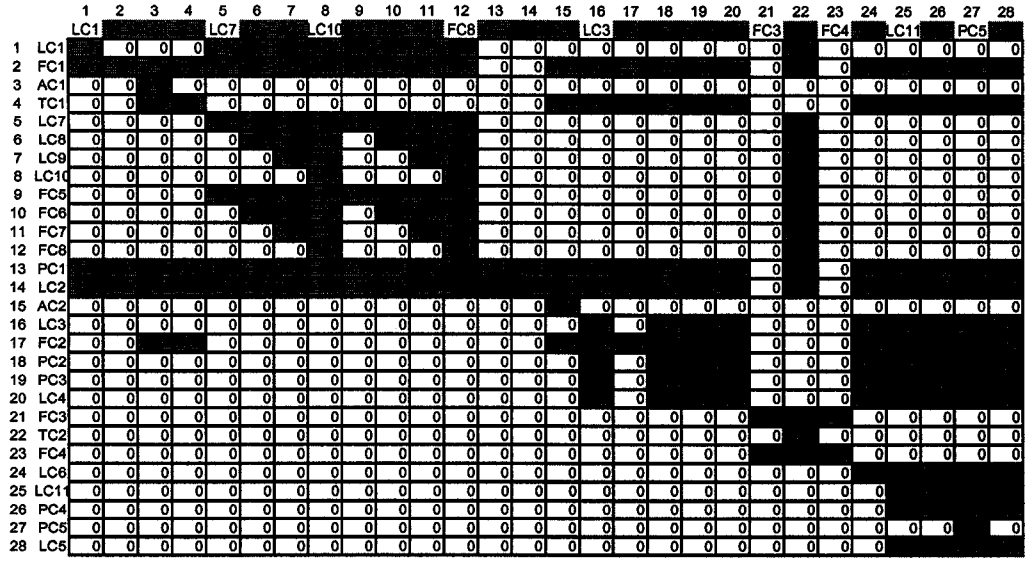

Figure 3.12: Reachability matrix of the digraph in Fig. 3.10

loops in this process, then it must be either loop 13 (PC1) or loop 14 (LC2) because these are the only two loops that can reach all the oscillatory variables. As shown in figure 3.10, these two loops are physically very close and both work for the same unit. Thus we isolate these two loops as the most likely root cause candidates.

3.6.3 Valve Stiction Detection

After narrowing down our focus to loops 13 and 14 from the total 28 loops, we use other data-based methods to support our analysis. Choudhury *et al.* (2004*b*), Choudhury *et al.* (2006) used bicoherence and $pv - op$ plot to detect and diagnose valve stiction. We followed their method to diagnose whether there is valve stiction in loop 13 or loop 14. Figure 3.2 shows the bicoherence plot and the $pv - op$ plot of loop 14 (PC1). The presence of large bicoherence value and an ellipse in the $pv - op$ plot is a clear evidence of valve stiction in loop 14.

We did not find valve stiction in loop 13. Therefore, our analysis confirmed that loop 14 (PC1) is the root cause. Further plant tests have confirmed that this loop with a sticky valve was indeed the leading cause of the plant-wide oscillations.

3.7 Concluding Remarks

In this chapter, we proposed a data-based method and non-data-based method for root cause diagnosis of plant-wide oscillations. First, a new oscillation contribution index (OCI) was proposed based on the spectral envelope method. Then, the concepts of adjacency matrix and reachability matrix were reviewed. Based on these concepts, a new method for diagnosis of root cause of plant-wide oscillations is proposed. This method is non-data-based and it can be carried out without using any data. Combination of this method and other data-based methods provides a complete procedure for detection and diagnosis of plant-wide oscillations. Two industrial case studies are presented to demonstrate the efficacy of the two methods.

4

Detection and Isolation of Model-Plant Mismatch for Multivariate Dynamic Systems

This chapter proposes a new scheme to detect and isolate model-plant mismatch (MPM) for multivariate dynamic systems. The background of our study is the increasing demands on MPM detection and isolation for performance assessment of model predictive controllers (MPCs). In this chapter, the MPM problem is formulated in terms of discrete-time state space models which are widely used in MPCs. Three MPM detection indices (MDIs) are proposed to detect the MPM. A logical framework is proposed to isolate system matrices that have MPM. A numerical example is presented to demonstrate the applicability of the proposed scheme.[1]

4.1 Introduction

Since the ground breaking work of Harris (1989), minimum variance control as a benchmark standard for controller performance assessment has been applied to many

[1]Partial results from this chapter have been published as: Hailei Jiang, Weihua Li and Sirish Shah, "Detection and Isolation of Model-Plant Mismatch for Multivariate Dynamic Systems", in the proceedings of IFAC *SafeProcess Symposium 2006*, Beijing, China.

industrial PID loops (Huang and Shah, 1999). However, it is found that minimum variance control benchmark is no longer suitable nor realistic for performance assessment of MPC systems (Huang and Tamayo, 2000), where the key component is the process model. Poor performance of the MPC is likely due to poor model, or in other words, model-plant mismatch (MPM). In order to assess and monitor the performance of systems under MPC control, industries have an increasing need to have a tool to detect MPM. The objective of this study is to focus attention on the detection and isolation of MPM. As will be shown later, the detection and diagnosis of MPM can be typically formulated as a parametric fault problem in the process under consideration. This problem can also be treated as a model validation problem (Huang and Tamayo, 2000). However the key difference between the classified model validation as carried out in the system identification literature and our work is that in our approach we attempt to detect the MPM in a closed-loop scenario.

As agreed by the fault detection and isolation (FDI) community, faults can be classified as sensor faults, actuator faults, additive process faults and parametric faults (Gertler, 1988). While tremendous research and application effort has been made on FDI for sensor and actuator faults (Gertler, 1988; Li and Shah, 2002), relatively few methods on parametric FDI have been developed. Stoustrup and Niemann (1999) proposed a detection and isolation method for parametric faults in continuous time (CT) systems represented by state space models, assuming that only the system matrix $\mathbf{A}$ can have parametric faults, while $\mathbf{B}$ and $\mathbf{C}$ matrices are fault-free. Li and Jiang (2004) also proposed a scheme for detection and isolation of parametric faults in CT systems, assuming that only one of the system matrices has parametric faults at each time.

This chapter proposes a novel scheme for detection and isolation of MPM by extending the method of Li and Jiang (2004). The chapter is organized as follows. In section 2, we formulate the MPM problem based on the discrete time state space model. Section 3 describes how to generate three different MPM detection indices (MDIs) and how to use them to isolate the faults. Section 4 presents a numerical example. The chapter ends with concluding remarks in Section 5.

4.2 Problem Formulation

Without loss of generality, we consider a multi-input multi-output(MIMO) process, which is represented by the following discrete time state space model:

$$\begin{aligned} \mathbf{x}(k+1) &= \mathbf{A}\mathbf{x}(k) + \mathbf{B}\mathbf{u}(k) + \mathbf{p}(k) \\ \mathbf{y}(k) &= \mathbf{C}\mathbf{x}(k) + \mathbf{o}(k) \end{aligned} \tag{4.1}$$

In equation (4.1), $\mathbf{x}(k) \in R^n$ is the state variable vector; $\mathbf{u}(k) \in R^l$ is the input vector to the process; $\mathbf{y}(k) \in R^m$ is the measured output vector; $\mathbf{o}(k) \in R^m$ is the relevant measurement noise; $\mathbf{p}(k) \in R^n$ is the process disturbance; and $\{\mathbf{A}, \mathbf{B}, \mathbf{C}\}$ are system matrices with appropriate dimensions. It is assumed that $\mathbf{p}(k) \in R^n$ and $\mathbf{o}(k) \in R^m$ are two independent Gaussian distributed white noise vectors with respective covariance matrices $\mathbf{R}_o$ and $\mathbf{R}_p$. Denote the nominal values of $\{\mathbf{A}, \mathbf{B}, \mathbf{C}\}$ as $\{\mathbf{A}_o, \mathbf{B}_o, \mathbf{C}_o\}$, which can be usually identified from training data using a subspace identification method. If the system matrices deviates from their nominal value, then the model can be expressed in terms of:

$$\mathbf{A} = \mathbf{A}_o + \Delta\mathbf{A}, \mathbf{B} = \mathbf{B}_o + \Delta\mathbf{B}, \mathbf{C} = \mathbf{C}_o + \Delta\mathbf{C}, \tag{4.2}$$

where $\{\Delta\mathbf{A}, \Delta\mathbf{B}, \Delta\mathbf{C}\}$ are the deviations of the system matrices, and may contain zero and non-zero elements. Using the above expression, one can rewrite the state space model as follows:

$$\begin{aligned} \mathbf{x}(k+1) &= \mathbf{A}_o\mathbf{x}(k) + \mathbf{B}_o\mathbf{u}(k) + \mathbf{p}(k) + \Delta\mathbf{A}\mathbf{x}(k) + \Delta\mathbf{B}\mathbf{u}(k) \\ \mathbf{y}(k) &= \mathbf{C}_o\mathbf{x}(k) + \mathbf{o}(k) + \Delta\mathbf{C}\mathbf{x}(k) \end{aligned} \tag{4.3}$$

Equation (4.3) can be further manipulated into

$$\begin{aligned} \mathbf{x}(k+1) = \mathbf{A}_o\mathbf{x}(k) + \mathbf{B}_o\mathbf{u}(k) + \mathbf{p}(k) + \mathbf{a}(k) + \mathbf{b}(k) \\ \mathbf{y}(k) = \mathbf{C}_o\mathbf{x}(k) + \mathbf{o}(k) + \mathbf{c}(k) \end{aligned} \tag{4.4}$$

with the following new notations:

$$\mathbf{a}(k) = \Delta\mathbf{A}\mathbf{x}(k),\ \mathbf{b}(k) = \Delta\mathbf{B}\mathbf{u}(k),\ \mathbf{c}(k) = \Delta\mathbf{C}\mathbf{x}(k),$$

In equation (4.4), $\{\mathbf{a}(k), \mathbf{b}(k), \mathbf{c}(k)\}$ account for the effects of $\{\Delta\mathbf{A},\ \Delta\mathbf{B}$ or $\Delta\mathbf{C}\}$ acting on the nominal system.

4.3 MPM Detection

With equation (4.1)-(4.3), the objective of MPM detection is to indicate if any elements in $\Delta\mathbf{A}$, $\Delta\mathbf{B}$ or $\Delta\mathbf{C}$ are non-zero, and also to indicate the time instant(s) at which MPM begins to manifest. In equation (4.4), one can verify that $a(k) \neq 0$ indicates that $\Delta\mathbf{A} \neq 0$, similarly $b(k) \neq 0$ indicates that $\Delta\mathbf{B} \neq 0$ and $c(k) \neq 0$ indicates that $\Delta\mathbf{C} \neq 0$. Therefore non-zero $a(k)$, $b(k)$ or $c(k)$ indicate MPM .

4.3.1 Preliminaries

By performing algebraic manipulation on equation (4.4), one can obtain the following stacked equation:

$$\begin{aligned} & \mathbf{y}_s(k) \\ = \; & \Gamma_s^o \mathbf{x}(k-s) + \mathbf{H}_s^o \mathbf{u}_s(k) + \mathbf{c}_s(k) + \mathbf{o}_s(k) \\ & + \mathbf{G}_s^o \mathbf{p}_{s-1}(k-1) + \mathbf{G}_s^o [\mathbf{a}_{s-1}(k-1) + \mathbf{b}_{s-1}(k-1)] \end{aligned} \tag{4.5}$$

where $\Gamma_s^o = [\mathbf{C}_o^T \;\; (\mathbf{C}_o\mathbf{A}_o)^T ... (\mathbf{C}_o\mathbf{A}_o^s)^T]^T \in R^{m_s \times n}$ is the extended observability matrix with s being the order of the parity space;

$$\mathbf{H}_s^o = \begin{bmatrix} \mathbf{0} & \cdots & \cdots & \mathbf{0} & \mathbf{0} \\ \mathbf{C}_o\mathbf{B}_o & \mathbf{0} & \cdots & \vdots & \vdots \\ \mathbf{C}_o\mathbf{A}_o\mathbf{B}_o & \mathbf{C}_o\mathbf{B}_o & \ddots & \mathbf{0} & \mathbf{0} \\ \vdots & \vdots & \ddots & \mathbf{0} & \mathbf{0} \\ \mathbf{C}_o\mathbf{A}_o^{s-1}\mathbf{B}_o & \mathbf{C}_o\mathbf{A}_o^{s-2}\mathbf{B}_o & \cdots & \mathbf{C}_o\mathbf{B}_o & \mathbf{0} \end{bmatrix} \in R^{m_s \times l_s}$$

and

$$\mathbf{G}_s^o = \begin{bmatrix} \mathbf{0} & \cdots & \cdots & \mathbf{0} \\ \mathbf{C}_o & \mathbf{0} & \cdots & \vdots \\ \mathbf{C}_o\mathbf{A}_o & \mathbf{C}_o & \ddots & \mathbf{0} \\ \vdots & \vdots & \ddots & \mathbf{0} \\ \mathbf{C}_o\mathbf{A}_o^{s-1} & \mathbf{C}_o\mathbf{A}_o^{s-2} & \cdots & \mathbf{C}_o \end{bmatrix} \in R^{m_s \times ns},$$

are two lower triangular block Toeplitz matrices.

Also in equation (4.5), $\mathbf{y}_s(k) = [\mathbf{y}^T(k-s) \; \mathbf{y}^T(k-s+1) \cdots \mathbf{y}^T(k)]^T \in R^{m_s}$ with $m_s = m(s+1)$, is the stacked output vector; $\mathbf{a}_{s-1}(k-1) \in R^{ns}$, $\mathbf{b}_{s-1}(k-1) \in R^{ns}$ $\mathbf{c}_s(k) \in R^{m_s}$, $\mathbf{o}_s(k) \in R^{m_s}$, $\mathbf{p}_{s-1}(k-1) \in R^{ns}$, $\mathbf{u}_s(k) \in R^{l_s}$ are also similarly defined stacked vectors as $\mathbf{y}_s(k)$. The choice of the order of parity space s is not unique and

the selection of s can effect the performance of the fault detection scheme according to Ding *et al.* (1999). However, the optimal determination of s is beyond the scope of this thesis, and in this chapter s is selected to be equal to n, as recommended by Chow and Willsky (1984).

Define $\mathbf{z}_s(k) = [\mathbf{y}_s^T(k)\ \mathbf{u}_s^T(k)]^T \in R^{(m_s+l_s)}$ and introduce $\tilde{\mathbf{H}}_s = [\mathbf{I}_{m_s}| - \mathbf{H}_s^o] \in R^{m_s\times(m_s+l_s)}$, with $\mathbf{I}_{m_s}$ being the m_s by m_s identity matrix. Also denote $\tilde{\mathbf{G}}_s^o = [\mathbf{G}_s^o|\mathbf{I}_{m_s}] \in R^{m_s\times(ns+m_s)}$ as the augmented fault gain matrix for $\{\mathbf{a}_{s-1}(k-1), \mathbf{b}_{s-1}(k-1), \mathbf{c}_s(k)\}$. Then equation (4.5) can be rewritten as

$$\tilde{\mathbf{H}}_s\mathbf{z}_s(k) = \Gamma_s^o\mathbf{x}(k-s) + \mathbf{G}_s^o\mathbf{p}_{s-1}(k-1) + \mathbf{o}_s(k) + \tilde{\mathbf{G}}_s^o\begin{bmatrix}\mathbf{a}_{s-1}(k-1)+\mathbf{b}_{s-1}(k-1)\\ \mathbf{c}_s(k)\end{bmatrix} \tag{4.6}$$

4.3.2 Detection of Mismatch in {A,B,C}

In this subsection, we propose a MPM detection index η_{ABC}, which can be used to detect any mismatch in matrices **A**, and/or **B**, and/or **C**.

We select a matrix $\mathbf{W}_o \in R^{(m_s-n)\times m_s}$ located in the null space of $\Gamma_s^o \in R^{(m_s\times n)}$, i.e. $\mathbf{W}_o\Gamma_s^o = 0$, and multiplying the stacked equation (4.6) by $\mathbf{W}_o$, one can obtain:

$$\mathbf{W}_o\tilde{\mathbf{H}}_s\mathbf{z}_s(k) = \mathbf{W}_o[\mathbf{G}_s^o\mathbf{p}_{s-1}(k-1) + \mathbf{o}_s(k)] + \mathbf{W}_o\tilde{\mathbf{G}}_s^o\begin{bmatrix}\mathbf{a}_{s-1}(k-1)+\mathbf{b}_{s-1}(k-1)\\ \mathbf{c}_s(k)\end{bmatrix}$$

The optimal design of $\mathbf{W}_o$ has been considered in a parallel problem in Li and Shah (2002).

Define

$$\begin{aligned}\mathbf{e}_s(k) &\equiv \mathbf{W}_o\tilde{\mathbf{H}}_s\mathbf{z}_s(k)\\ &= \mathbf{W}_o[\mathbf{G}_s^o\mathbf{p}_{s-1}(k-1) + \mathbf{o}_s(k)] + \mathbf{W}_o\tilde{\mathbf{G}}_s^o\begin{bmatrix}\mathbf{a}_{s-1}(k-1)+\mathbf{b}_{s-1}(k-1)\\ \mathbf{c}_s(k)\end{bmatrix}\end{aligned} \tag{4.7}$$

as the primary residual vector (PRV) for detecting mismatch in matrices **A**, and/or **B**, and/or **C**, and $\mathbf{W}_o\tilde{\mathbf{H}}_s\mathbf{z}_s(k)$ is the computational form. The following facts can be established for the PRV.

Remark 4.3.1 *In the mismatch-free case,* $\boldsymbol{a}_{s-1}(k-1) = 0, \boldsymbol{b}_{s-1}(k-1) = 0$ *and* $\boldsymbol{c}_s(k) = 0$, *the PRV is reduced to* $\boldsymbol{e}_s^*(k) = \boldsymbol{W}_o[\boldsymbol{G}_s^o\boldsymbol{p}_{s-1}(k-1) + \boldsymbol{o}_s(k)]$, *which is a*

moving average (MA) process of the noise vector: $\boldsymbol{p}_{s-1}(k-1)$ *and* $\boldsymbol{o}_s(k)$. *Also,* $\boldsymbol{e}_s^*(k)$ *can be proved to be a zero mean Gaussian distributed random noise vector from the assumed distributions of* $\boldsymbol{o}(k)$ *and* $\boldsymbol{p}(k)$ *with a covariance matrix* $\boldsymbol{R}_{s,e}$ *(Johnson and Wichern, 1998). The internal form of* $\boldsymbol{R}_{s,e}$ *is:*

$$\boldsymbol{R}_{s,e} = \boldsymbol{W}_o(\boldsymbol{G}_s^o \boldsymbol{R}_{s,p} \boldsymbol{G}_s^{oT} + \boldsymbol{R}_{s,o})\, \boldsymbol{W}_o^T \tag{4.8}$$

where $\boldsymbol{R}_{s,p} = \boldsymbol{I}_s \bigotimes \boldsymbol{R}_p \in R^{ns \times ns}$, $\boldsymbol{R}_{s,o} = \boldsymbol{I}_{s+1} \bigotimes \boldsymbol{R}_o \in R^{m_s \times m_s}$, *and* $\bigotimes$ *stands for the kronecker tensor product.*

Remark 4.3.2 *In the presence of any MPM, i.e., either* $\boldsymbol{a}(k) \neq 0$, $\boldsymbol{b}(k) \neq 0$ *or* $\boldsymbol{c}(k) \neq 0$,

$$\boldsymbol{e}_s(k) \equiv \boldsymbol{e}_s^*(k) + \boldsymbol{e}_s^f(k) \tag{4.9}$$

where $\boldsymbol{e}_s^f(k) = \boldsymbol{W}_o \tilde{\boldsymbol{G}}_s^o \begin{bmatrix} \boldsymbol{a}_{s-1}(k-1) + \boldsymbol{b}_{s-1}(k-1) \\ \boldsymbol{c}_s(k) \end{bmatrix}$ *is the mismatch-contribution term in the PRV. In this case, the mean of* $\boldsymbol{e}_s(k)$ *is no longer zero (but the covariance is the same as in the mismatch-free case). Instead, the mean of* $\boldsymbol{e}_s(k)$ *is* $\boldsymbol{e}_s^f(k)$. *Therefore, mismatch detection can be done by checking if the mean of the PRV is non-zero. Clearly,* $\boldsymbol{e}_s(k)$ *follows a multivariate Gaussian distribution with mean* $\boldsymbol{e}_s^f(k)$ *and covariance* $\boldsymbol{R}_{s,e}$, *i.e.* $\boldsymbol{e}_s(k) \sim \aleph(\boldsymbol{e}_s^f(k), \boldsymbol{R}_{s,e})$.

Instead of using the PRV, one can also use the square weighted residual (SWR) as the MPM detection index. The SWR is defined as:

$$\eta_{ABC}(k) = (\mathbf{e}_s(k))^T \mathbf{R}_{s,e}^{-1} \mathbf{e}_s(k) \tag{4.10}$$

η_{ABC} follows a chi-square distribution with $(m_s - n)$ degrees of freedom (Johnson and Wichern, 1998). Then given a confidence limit $\chi^2_{m_s-n}(\alpha)$, e.g. $\alpha = 1\%$, $\eta_{ABC}(k) \geq \chi^2_{m_s-n}(\alpha)$ indicates that matrix **A**, and/or matrix **B**, and/or matrix **C** have deviated from the nominal value, while $\eta_{ABC}(k) \leq \chi^2_{m_s-n}(\alpha)$ implies there is no mismatch in matrix **A**, matrix **B** and matrix **C**. To reduce the effect of transient and noise in the measured data, an exponentially weighted moving average (EWMA) filter can be applied to the PRV $\mathbf{e}s(k)$ first. Then the filtered PRV can be used to calculate the MPM detection index η_{ABC}.

4.3.3 Detection of Mismatch in {A,C}

In this subsection, we propose an MPM detection index η_{AC}, which can be used to detect any mismatch in matrices **A**, and/or **C**. Rewrite (4.4) as:

$$\begin{aligned} \mathbf{x}(k+1) &= \mathbf{A}_o\mathbf{x}(k) + \mathbf{B}\mathbf{u}(k) + \mathbf{p}(k) + \mathbf{a}(k) \\ \mathbf{y}(k) &= \mathbf{C}_o\mathbf{x}(k) + \mathbf{o}(k) + \mathbf{c}(k) \end{aligned} \tag{4.11}$$

where $\mathbf{B} = \mathbf{B}_o + \Delta\mathbf{B}$. Doing the same derivation as for (4.5), one can obtain:

$$\mathbf{y}_s(k) = \Gamma_s^o\mathbf{x}(k-s) + \mathbf{H}_s\mathbf{u}_s(k) + \mathbf{c}_s(k) + \mathbf{o}_s(k) + \mathbf{G}_s^o\mathbf{p}_{s-1}(k-1) + \mathbf{G}_s^o\mathbf{a}_{s-1}(k-1) \tag{4.12}$$

where $\mathbf{H}_s = \mathbf{H}_s^o|_{\mathbf{B}_o=\mathbf{B}}$ is unknown since **B** is an unknown matrix. Pre-multiplying $\mathbf{W}_o$ on the both side of equation (4.12), where $\mathbf{W}_o\Gamma_s^o = 0$ is defined before, one can obtain:

$$\mathbf{W}_o\mathbf{y}_s(k) = \mathbf{W}_o\mathbf{H}_s\mathbf{u}_s(k) + \mathbf{W}_o[\mathbf{G}_s^o\mathbf{p}_{s-1}(k-1) + \mathbf{o}_s(k)] + \mathbf{W}_o[\mathbf{G}_s^o\mathbf{a}_{s-1}(k-1) + \mathbf{c}_s(k)] \tag{4.13}$$

With N samples of data, we assume that faults occur at the n_fth sample which actually can be detected by η_{ABC}. Then one can select an integer k_f from the range $[(n_f + s + 1) \;\; N]$ and construct the Hankel data matrices

$$\begin{aligned} \mathbf{Y}_{s,k_f,N} &= [y_s(k_f) \;\; y_s(k_f+1) \;\; \cdots \;\; y_s(N)] \\ \mathbf{U}_{s,k_f,N} &= [u_s(k_f) \;\; u_s(k_f+1) \;\; \cdots \;\; u_s(N)] \end{aligned} \tag{4.14}$$

based on $N - k_f + 1$ samples collected after the occurrence of the faults. In the same way, one can obtain:

$$\begin{aligned} \mathbf{P}_{s-1,k_f-1,N-1} &= [p_{s-1}(k_f-1) \;\; p_{s-1}(k_f) \;\; \cdots \;\; p_{s-1}(N-1)] \\ \mathbf{A}_{s-1,k_f-1,N-1} &= [a_{s-1}(k_f-1) \;\; a_{s-1}(k_f) \;\; \cdots \;\; a_{s-1}(N-1)] \\ \mathbf{C}_{s,k_f,N} &= [c_s(k_f) \;\; c_s(k_f+1) \;\; \cdots \;\; c_s(N)] \\ \mathbf{O}_{s,k_f,N} &= [o_s(k_f) \;\; o_s(k_f+1) \;\; \cdots \;\; o_s(N)] \end{aligned}$$

Then equation (4.13) can be transformed into:

$$\begin{aligned} \mathbf{W}_o\mathbf{Y}_{s,k_f,N} = \mathbf{W}_o\mathbf{H}_s\mathbf{U}_{s,k_f,N} + \mathbf{W}_o\mathbf{C}_{s,k_f,N} + \mathbf{W}_o\mathbf{G}_s^o\mathbf{A}_{s-1,k_f-1,N-1} + \mathbf{W}_o\mathbf{O}_{s,k_f,N} \\ + \mathbf{W}_o\mathbf{G}_s^o\mathbf{P}_{s-1,k_f-1,N-1} \end{aligned} \tag{4.15}$$

Define $\mathbf{U}^{\perp}_{s,k_f,N} = \mathbf{I}_{N-k_f+1} - \mathbf{U}^{T}_{s,k_f,N}(\mathbf{U}_{s,k_f,N} \times \mathbf{U}^{T}_{s,k_f,N})^{-1}\mathbf{U}_{s,k_f,N}$, where $\mathbf{I}_{N-k_f+1}$ is an $(N-k_f+1) \times (N-k_f+1)$ identity matrix. Note that $\mathbf{U}^{\perp}_{s,k_f,N}$ is located in the right null space of $\mathbf{U}_{s,k_f,N}$, i.e. $\mathbf{U}_{s,k_f,N} \times \mathbf{U}^{\perp}_{s,k_f,N} = \mathbf{0}$. It is assumed that $\mathbf{U}_{s,k_f,N}\mathbf{U}^{T}_{s,k_f,N}$ is non-singular. This assumption is true when the input signals are persistent exciting. Post-multiplying $\mathbf{U}^{\perp}_{s,k_f,N}$ on both sides of equation (4.15) gives:

$$\begin{aligned}\mathbf{W}_o\mathbf{Y}_{s,k_f,N}\mathbf{U}^{\perp}_{s,k_f,N} = \mathbf{W}_o\mathbf{C}_{s,k_f,N}\mathbf{U}^{\perp}_{s,k_f,N} + \mathbf{W}_o\mathbf{G}^{o}_{s}\mathbf{A}_{s-1,k_f-1,N-1}\mathbf{U}^{\perp}_{s,k_f,N} \\ +\mathbf{W}_o\mathbf{G}^{o}_{s}\mathbf{P}_{s-1,k_f-1,N-1}\mathbf{U}^{\perp}_{s,k_f,N} + \mathbf{W}_o\mathbf{O}_{s,k_f,N}\mathbf{U}^{\perp}_{s,k_f,N}\end{aligned} \tag{4.16}$$

where the faults introduced by matrix $\mathbf{B}$ have been entirely removed. As $(N-k_f-1) \longrightarrow \infty$, asymptotically,

$$\begin{aligned}\mathbf{P}_{s-1,k_f-1,N-1}\mathbf{U}^{\perp}_{s,k_f,N} = \mathbf{P}_{s-1,k_f-1,N-1} - \mathbf{P}_{s-1,k_f-1,N-1}\mathbf{U}^{T}_{s,k_f,N} \times (\mathbf{U}_{s,k_f,N} \times \mathbf{U}^{T}_{s,k_f,N})^{-1} \\ \times \mathbf{U}_{s,k_f,N} \longrightarrow \mathbf{P}_{s-1,k_f-1,N-1}\end{aligned} \tag{4.17}$$

$$\mathbf{O}_{s,k_f,N}\mathbf{U}^{\perp}_{s,k_f,N} = \mathbf{O}_{s,k_f,N} - \mathbf{O}_{s,k_f,N}\mathbf{U}^{T}_{s,k_f,N} \times (\mathbf{U}_{s,k_f,N} \times \mathbf{U}^{T}_{s,k_f,N})^{-1}\mathbf{U}_{s,k_f,N} \longrightarrow \mathbf{O}_{s,k_f,N} \tag{4.18}$$

because $\mathbf{P}_{s-1,k_f-1,N-1}\mathbf{U}^{T}_{s,k_f,N} \longrightarrow \mathbf{0}$ and $\mathbf{O}_{s,k_f,N}\mathbf{U}^{T}_{s,k_f,N} \longrightarrow \mathbf{0}$ under open loop condition. This is because the input $\mathbf{u}(k)$ is independent of the white noise term $\mathbf{p}(k)$ and $\mathbf{o}(k)$. Therefore, equation (4.16) can be written as:

$$\begin{aligned}\mathbf{W}_o\mathbf{Y}_{s,k_f,N}\mathbf{U}^{\perp}_{s,k_f,N} = \mathbf{W}_o\mathbf{C}_{s,k_f,N}\mathbf{U}^{\perp}_{s,k_f,N} + \mathbf{W}_o\mathbf{G}^{o}_{s}\mathbf{A}_{s-1,k_f-1,N-1}\mathbf{U}^{\perp}_{s,k_f,N} + \mathbf{W}_o\mathbf{O}_{s,k_f,N} \\ +\mathbf{W}_o\mathbf{G}^{o}_{s}\mathbf{P}_{s-1,k_f-1,N-1}\end{aligned} \tag{4.19}$$

Define $\mathbf{E}_{\mathbf{A},\mathbf{C}} \equiv \mathbf{W}_o\mathbf{Y}_{s,k_f,N}\mathbf{U}^{\perp}_{s,k_f,N}$ as the primary residual matrix (PRM) for detecting mismatch in matrices $\mathbf{A}$ and/or $\mathbf{C}$. We denote $e_{s,ac}(k)$, $k \in [k_f, N]$, as the PRV at the kth sampling instant for detecting mismatch in matrices $\mathbf{A}$ and/or $\mathbf{C}$, where $e_{s,ac}(k)$ is the $(k-k_f+1)$th column of $\mathbf{E}_{\mathbf{A},\mathbf{C}}$.

Remark 4.3.3

If there is no mismatch in matrix $\boldsymbol{A}$ *and matrix* $\boldsymbol{C}$, *i.e.* $\boldsymbol{W}_o\boldsymbol{C}_{s,k_f,N}\boldsymbol{U}^{\perp}_{s,k_f,N} = \boldsymbol{0}$ *and* $\boldsymbol{W}_o\boldsymbol{G}^{o}_{s}\boldsymbol{A}_{s-1,k_f-1,N-1}\boldsymbol{U}^{\perp}_{s,k_f,N} = \boldsymbol{0}$, *then* $\boldsymbol{E}_{\boldsymbol{A},\boldsymbol{C}} = \boldsymbol{W}_o\boldsymbol{G}^{o}_{s}\boldsymbol{P}_{s-1,k_f-1,N-1} + \boldsymbol{W}_o\boldsymbol{O}_{s,k_f,N}$. *In this case, it can be easily verified that* $e_{s,ac}(k)$ *is a zero mean Gaussian distributed random vector with covariance* $\boldsymbol{R}_{s,e,ac}$, *i.e.* $e_{s,ac}(k) \sim \aleph(\boldsymbol{0}, \boldsymbol{R}_{s,e,ac})$, *where* $\boldsymbol{R}_{s,e,ac} = \boldsymbol{R}_{s,e}$ *which is derived in equation* (4.8).

Remark 4.3.4 *If there is mismatch in matrix* $\boldsymbol{A}$ *and/or matrix* $\boldsymbol{C}$*, then the mean of* $e_{s,ac}(k)$ *will be non-zero, while the covariance remains the same. Therefore, mismatch detection can be done by checking if the mean of the PRV is non-zero.*

Again, PRV ($e_{s,ac}(k)$) is transformed into SWR ($\eta_{AC}(k)$) as the MPM detection index, which is calculated as:

$$\eta_{AC}(k) = (e_{s,ac}(k))^T \mathbf{R}_{s,e,ac}^{-1} e_{s,ac}(k)$$

$\eta_{AC}(k)$ follows a chi-square distribution with $(m_s - n)$ degrees of freedom. Then given a confidence limit $\chi^2_{m_s-n}(\alpha)$, $\eta_{AC}(k) \geq \chi^2_{m_s-n}(\alpha)$ indicates that matrices $\mathbf{A}$ and/or $\mathbf{C}$ have faults, while $\eta_{AC}(k) \leq \chi^2_{m_s-n}(\alpha)$ implies that there is no fault in matrices $\mathbf{A}$ and $\mathbf{C}$.

4.3.4 Detection of Mismatch in {C}

In this subsection, we propose an MPM detection index η_C, which can be used to detect any mismatch in matrix $\mathbf{C}$.

Select a transformation matrix $\mathbf{W}^o \in R^{(m_s-n_s)\times m_s}$ from the null space of $\Psi_s^o = [\Gamma_s^o | \mathbf{G}_s^o]$, and pre-multiply it on the both sides of equation (4.6), to obtain:

$$\mathbf{W}^o \tilde{\mathbf{H}}_s \mathbf{z}_s(k) = \mathbf{W}^o \mathbf{c}_s(k) + \mathbf{W}^o \mathbf{o}_s(k) \tag{4.20}$$

Define

$$\mathbf{e}_{s,c}(k) \equiv \mathbf{W}^o \tilde{\mathbf{H}}_s \mathbf{z}_s(k) = \mathbf{W}^o \mathbf{c}_s(k) + \mathbf{W}^o \mathbf{o}_s(k) \tag{4.21}$$

as the PRV for detecting mismatch in matrix $\mathbf{C}$, where the right hand side (RHS) of the equation is the computational form, while the left hand side (LHS)is the internal form.

Remark 4.3.5 *If there is no mismatch in matrix* $\boldsymbol{C}$*, i.e.* $\boldsymbol{c}_s(k) = 0$*, the PRV is reduced to* $\boldsymbol{e}^*_{s,c}(k) = \boldsymbol{W}^o \boldsymbol{o}_s(k)$*, which is a moving average (MA) process of the noise vector:* $\boldsymbol{o}_s(k)$*. Also,* $\boldsymbol{e}^*_{s,c}(k)$ *can be proved to be a zero mean Gaussian distributed random noise vector from the distributions of* $\boldsymbol{o}(k)$ *with a covariance matrix* $\boldsymbol{R}_{s,e,c}$*. The internal form of* $\boldsymbol{R}_{s,e,c}$ *is:*

$$\boldsymbol{R}_{s,e,c} = \boldsymbol{W}^o \boldsymbol{R}_{s,o} \boldsymbol{W}^{oT} \tag{4.22}$$

Remark 4.3.6 *In the presence of any mismatch in matrix C, the mean of* $\mathbf{e}_{s,c}(k)$ *is no longer zero, but the covariance remains the same. Therefore, mismatch detection can be done by checking is the mean of the PRV is non-zero.*

Again, PRV ($e_{s,c}(k)$) is transformed into SWR ($\eta_C(k)$) as the MPM detection index, which is calculated as:

$$\eta_C(k) = (e_{s,c}(k))^T \mathbf{R}^{-1}_{s,e,c} e_{s,c}(k)$$

$\eta_C(k)$ follows a chi-square distribution with $(m_s - n_s)$ degrees of freedom. Then given a confidence limit $\chi^2_{m_s-n_s}(\alpha)$, $\eta_C(k) \geq \chi^2_{m_s-n_s}(\alpha)$ indicates that matrix matrix **C** has faults, while $\eta_C(k) \leq \chi^2_{m_s-n_s}(\alpha)$ implies there is no fault in matrix **C**.

4.3.5 Mismatch Isolation Logic

In last three subsections, three MPM detection indices (MDI) - η_{ABC}, η_{AC} and η_C have been proposed which can be used to detect the mismatch in the system matrices. Beside simply detecting the mismatch in the system matrices, it is desirable to tell which matrices have faults. In this subsection, we would like to propose a logic framework to isolate faults using the three MDIs. First, denote $\eta_{ABC}(k) = 1$ if there is mismatch in matrices **A**, and/or **B**, and/or **C**, and $\eta_{ABC}(k) = 0$ if there is no mismatch in these three matrices. Similarly, denote $\eta_{AC}(k) = 1$ if there is mismatch in matrices **A**, and/or **C**, and $\eta_{AC}(k) = 0$ if there is no mismatch; denote $\eta_C(k) = 1$ if there is mismatch in matrix **C**, and $\eta_C(k) = 0$ if there is no mismatch. The fault isolation logic framework can now be summarized in the following table.

Table 4.1: Fault isolation logic using $\eta_{ABC}(k)$, $\eta_{AC}(k)$, and $\eta_C(k)$

$\eta_{ABC}(k)$	$\eta_{AC}(k)$	$\eta_C(k)$	Fault Matrix
1	0	0	**B**
1	1	0	**A** or **AB**
1	1	1	**C** or **AC** or **BC** or **ABC**

4.4 Numerical Example

In this section, a numerical example is provided to demonstrates and verify the utility of the proposed scheme. The simulated process is a second order dynamic system. The system matrices in the discrete time domain are:

$$\mathbf{A}_0 = \begin{bmatrix} 0.6082 & -0.0100 \\ 2.2668 & 0.0364 \end{bmatrix}$$

$$\mathbf{B}_0 = \begin{bmatrix} 0.5602 & 0.0008 \\ 1.3760 & 0.3026 \end{bmatrix}$$

$$\mathbf{C}_0 = \begin{bmatrix} 1 & 0 \\ 0 & 1 \\ 1 & 0 \\ 0 & 1 \end{bmatrix}$$

For this process, $\mathbf{C}_0$ is only the sensor gain matrix which typically is unlikely to deviate. So in this example we assume there is no mismatch in $\mathbf{C}_0$ and we only consider three different mismatch cases: (1) mismatch in $\mathbf{A}$; (2) mismatch in $\mathbf{B}$ and (3) mismatch in both $\mathbf{A}$ and $\mathbf{B}$.

For each case, a set of 3000 samples of training data of $\{\mathbf{u}(k), \mathbf{y}(k)\}$ are collected and the fault is introduced at the 500th sample. The inputs $\mathbf{u}(k)$ are simulated by pseudo random binary signals with small magnitudes, and are assumed to be noise-free. However, the outputs $\mathbf{y}(k)$ for each case are corrupted by Gaussian distributed white noise $\mathbf{o}(k)$. If we denote the noise-free part of the outputs as $\mathbf{y}_0(k)$, then the measured outputs are expressed as $\mathbf{y}(k) = \mathbf{y}_0(k) + \mathbf{o}(k)$. Therefore, for each case, the noise-to-signal ratio (NSR) for each output variable can be expressed as:

$NSR_i = [STD\ of\ \mathbf{o}_i(k)]/[STD\ of\ \mathbf{y}_{0i}(k)],\ for\ \forall i = 1, 2,$

where STD refers to the standard deviation; $\mathbf{y}_{0i}(k)$ is the ith noise-free output sequence and $\mathbf{o}_i(k)$ is the corresponding white noise sequence.

Case (1): We introduce 10% mismatch in $\mathbf{A}_0(k)$ for this process. The NSR for the two outputs are $NSR_1 = 11.19\%$ and $NSR_2 = 2.73\%$. In figure 4.1, the mismatch detection indices $\eta_{ABC}(k)$ and $\eta_{AC}(k)$ have been scaled (or divided) by $\chi^2_{m_s-n_s}(\alpha)$, where $\alpha = 0.01$ and $\chi^2_6(0.01) = 16.812$ (same for the other two cases). The dashed line in the plot is the scaled confidence limit whose value is 1. The $\eta_{ABC}(k)$ index clearly shows that the mismatch occurs after the 500th sample. Then starting from

kf=600th sample, we begin to plot $\eta_{AC}(k)$ and it clearly shows that there is mismatch in **A** (since we have assumed no mismatch in **C**). Thus we have confirmed that there is mismatch in **A**.

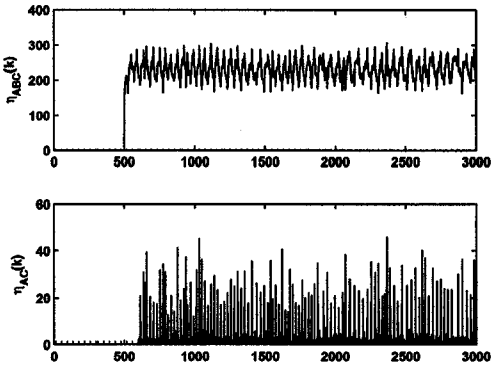

Figure 4.1: Mismatch detection indices for case 1

Case (2): We introduce a 10% mismatch in $\mathbf{B}_0(k)$ for this process. The NSR for the two outputs are $NSR_1 = 14.81\%$ and $NSR_2 = 4.12\%$. The scaled mismatch detection indices $\eta_{ABC}(k)$ and $\eta_{AC}(k)$ are plotted in figure 4.2. The $\eta_{ABC}(k)$ index clearly shows that the mismatch occurs after the 500th sample. Then starting from kf=600th sample, we begin to plot $\eta_{AC}(k)$ and it clearly shows that there is no mismatch in **A**. Thus the conclusion is that the mismatch is only in **B**.

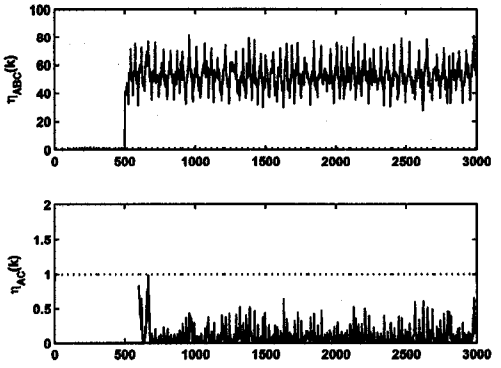

Figure 4.2: Mismatch detection indices for case 2

Case (3): We introduce 10% mismatch in both $\mathbf{A}_0(k)$ and $\mathbf{B}_0(k)$. The NSR for the two outputs are $NSR_1 = 6.94\%$ and $NSR_2 = 1.74\%$. The scaled mismatch detection indices $\eta_{ABC}(k)$ and $\eta_{AC}(k)$ are plotted in figure 4.3. The $\eta_{ABC}(k)$ index clearly shows that the mismatch occurs after the 500th sample. Then starting from kf=600th sample, we begin to plot $\eta_{AC}(k)$ and it clearly shows that there is mismatch in **A** (since we have assumed no mismatch in **C**).

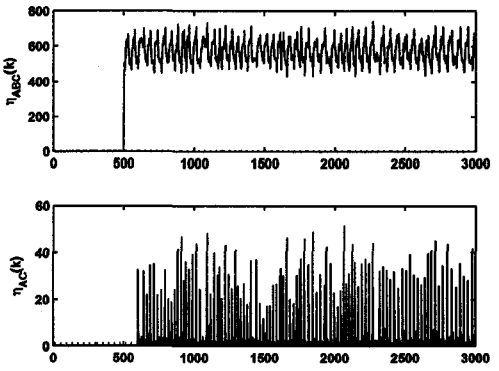

Figure 4.3: Mismatch detection indices for case 3

Comparison of Case (1) and Case (3): In case (3), there is an extra 10% mismatch in **B** compared to case (1). Thus the magnitude of $\eta_{ABC}(k)$ after the 500th sample in figure 4.3 is bigger than the one in figure 4.1. This is because $\eta_{ABC}(k)$ measures the mismatch both in **A** and **B**. However, the magnitudes of $\eta_{AC}(k)$ for both cases after the 600th sample are quite close. This is because in both cases there is the same 10% mismatch of **A** and $\eta_{AC}(k)$ only considers the mismatch in **A**.

4.5 Conclusion

A new scheme for detection and isolation of model-plant-mismatch (MPM) in multivariate dynamic process has been developed. The MPM problem has been formulated in terms of discrete time state space models. Three different mismatch detection indices (MDI) have been proposed to detect the MPM. Also the MDIs can be used to isolate the system matrices that have mismatch. The whole approach is completely data driven. Unmeasured disturbances may affect the performance of this approach.

From a theoretical point of view, analyzing the residual errors and attributing this strictly to MPM is difficult in the presence of unmeasured disturbance. However in practice, process knowledge and inferential schemes may be used to determine the presence or absence of such disturbances.

A numerical example is presented to demonstrate the efficacy of the the new scheme. Three different mismatch fault scenarios, including (1) mismatch in system matrix $\mathbf{A}$, (2) mismatch in system matrix $\mathbf{B}$ and (3) mismatch in both $\mathbf{A}$ and $\mathbf{B}$, have been simulated. The simulation results validates that the new scheme can be used effectively to detect and isolate the mismatch under different situations.

5

Control Relevant Closed-loop Model Validation

This chapter is concerned with model validation and detection of parameter changes under closed-loop conditions in the discrete time domain. Two control relevant validation algorithms are developed based on the two-model divergence method. The algorithms are only sensitive to the plant changes that affect closed-loop performance. The first algorithm is sensitive to changes in both plant and disturbance dynamics. The second algorithm is only sensitive to the changes in plant dynamics, irrespective of changes in disturbance dynamics. For the situation where the changes in plant dynamics are not a concern, then both algorithms can also be applied to detect process faults, e.g. sensor decalibration and valve stiction. The developed algorithms are evaluated by simulations as well as experimental application on a pilot scale process.[1]

5.1 Introduction

Model validation or maintenance of model quality is an important subject for process identification and control. In the identification stage, model validation plays a major

[1]A part of this chapter has been published as: Hailei Jiang, Biao Huang and Sirish Shah, "Closed-loop model validation based on the two-model divergence method", in the proceedings of *46th IEEE Conference on Decision and Control*, New Orleans, USA, 2007.

role as the last "quality control" station before a model is delivered to the user (Ljung, 1998). For example, if the identification is for model based control, then the role of model validation is to ensure that the delivered model captures the most important dynamics of the process so that the controller design based on this model can be used to control the process. There are a large number of papers concerned with model validation in the identification stage, e.g. Söderström and Stoica (1989), Ljung and Guo (1997), Ljung (1998).

In the real world, most processes are time-variant in nature. Either the process or the disturbance dynamics can change from time to time. The changes can be because of a new operating point which is different from the original identification condition, or because of quality changes of the input materials. Due to these reasons, it is common knowledge that performance of model predictive based control (MPC) degrades with time, unless MPC performance and model quality are regularly monitored. Therefore model validation performed during the identification stage alone can not ensure consistent MPC performance. So it is important to continuously validate the model even after the model is delivered to the users and thus "maintain" model quality by detecting changes in model parameters. However, the literature is relatively sparse on studies concerned with *on-line model validation* using *closed-loop data.*

It is has been shown that a "good" open-loop model (here, "good" is in the sense of model validation) is not necessarily a good model for controller design (Gevers and Ljung, 1986; Van den Hof and Schrama, 1995). On the other hand, it is also known that many models in existing model based control system may not pass the "rigorous" model validation test and yet the control system works well. In other words, mismatch in some parameters or frequencies are not critical and can be tolerated; while even a small mismatch in a critical parameter or over a critical frequency range can affect closed-loop performance. This naturally leads to the following question on closed-loop model validation: How can one avoid issuing unnecessary alarms when parameter changes or model-plant mismatches do not "significantly" affect closed-loop performance? One of the purposes of this study is to address this issue by developing control relevant validation scheme to effectively detect mismatches that affect control performance.

Another issue in model validation is the changes in disturbance dynamics. Varying disturbances are often observed in chemical processes, due to, for example, a temporary grade change of raw materials. The change of disturbances is reflected in the disturbance model parameters, which can be significantly different from their previous values. How to differentiate plant changes from disturbance changes is a challenging problem. The second objective of this study is to explore this problem under closed-loop conditions and develop an algorithm that is only sensitive to plant changes.

One area that is naturally related to on-line model validation is detection of abrupt change. Over the last two decades, research on the on-line detection of abrupt changes has emerged as an important area in the control community (Basseville and Nikiforov, 1993; Zhang *et al.*, 1994). The major concerns of this subject are fault detection and diagnosis, data segmentation, gain updating for adaptive algorithms, and process quality control. Basseville and Benveniste (1983) proposed a two-model divergence method for sequential segmentation of nonstationary digital signals. Basseville and Nikiforov (1993) extended the idea for detection of abrupt changes of time series models. In this chapter, we extend this method so that it can be applied to general process models and can be used to achieve the objectives stated in previous two paragraphs.

Huang and Tamayo (2000) have developed an algorithm to detect plant model changes under open-loop conditions. Huang (2001) extended the algorithm so that it can be applied to detect model changes under closed-loop conditions. The main contribution of the this chapter is to explore three issues that have not been discussed in the previous work: 1) Develop *control relevant* model validation algorithms that will work under closed-loop conditions; 2) How to validate plant models regardless of how disturbance dynamics change *under closed-loop conditions*; and 3) Extend the proposed algorithms for *fault detection*(e.g. detection of actuator or sensor fault, etc) under closed-loop conditions.

The remainder of this chapter is organized as follows. Section 5.2 gives a brief overview of the existing two-model divergence method. In Section 5.3, we develop an algorithm for control relevant model validation and detection of parameter changes under closed-loop conditions. The key result of this chapter is presented in Section 5.4,

where we develop an algorithm that is only sensitive to changes in plant dynamics regardless of time varying disturbances. How to apply the proposed algorithm for fault detection is discussed in Section 5.5. Simulation examples in Section 5.6 and experiment results in Section 5.7 show the effectiveness of the proposed algorithms and complement the technical presentation followed by concluding remarks in Section 5.8.

5.2 Overview of the Existing Two-model Divergence Method

Huang and Tamayo (2000) and Huang (2001) provided detailed survey of the two-model divergence method. In this section, we give a brief summary of the these and more recent results.

Basseville and Benveniste (1983) have considered sequential segmentation of non-stationary digital signals through detection of changes in an AR model with unknown model switching time t_0

$$\begin{aligned} y_t &= \sum_{i=1}^{p} \alpha_i^{(t)} y_{i-1} + a_t \\ Var(a_t) &= \sigma_t^2 \end{aligned} \tag{5.1}$$

where

$$M_0 : \begin{cases} \alpha_i^t = \alpha_i^0 (1 \le i \le p), \\ \sigma_t^2 = \sigma_0^2 \end{cases} \quad for \;\; t < t_0 \tag{5.2}$$

and

$$M_1 : \begin{cases} \alpha_i^t = \alpha_i^1 (1 \le i \le p), \\ \sigma_t^2 = \sigma_1^2 \end{cases} \quad for \;\; t \ge t_0 \tag{5.3}$$

Here M_0 and M_1 depict two different AR models. Let $Y^{t-1} = (y_{t-1}, y_{t-2}, ..., y_1)$ be the vector of past observations, $p^0(y_t \mid Y^{t-1})$ describe the conditional densities of signal y_t before change, and $p^1(y_t \mid Y^{t-1})$ describe the conditional densities of signal y_t after change. Basseville and Benveniste (1983) proposed a statistic

$$\eta_t = \int p^0(y_t \mid Y^{t-1}) log \frac{p^1(y_t \mid Y^{t-1})}{p^0(y_t \mid Y^{t-1})} dy - log \frac{p^1(y_t \mid Y^{t-1})}{p^0(y_t \mid Y^{t-1})} \tag{5.4}$$

The second term in Eq.(5.4) is the likelihood ratio between the two models, while the first term is the conditional mean of the likelihood ratio.

Basseville and Nikiforov (1993) have shown that, for a parametric time series model, this statistic can be written as

$$\eta_t = \frac{1}{2}\left[2\frac{e_t^0 e_t^1}{\sigma_1^2} - \left(1 + \frac{\sigma_0^2}{\sigma_1^2}\right)\frac{(e_t^0)^2}{\sigma_0^2} - \left(\frac{\sigma_0^2}{\sigma_1^2} - 1\right)\right] \tag{5.5}$$

where e_t^0 and e_t^1 are the innovation sequences of the model M_0 and M_1 respectively. Eq.(5.5) can be also written as (Basseville and Nikiforov, 1993)

$$\eta_t = -\frac{(e_t^0)^2}{2\sigma_0^2} + \frac{(e_t^1)^2}{2\sigma_1^2} + \frac{1}{2} - \frac{\sigma_0^2 + (e_t^0 - e_t^1)^2}{2\sigma_1^2} \tag{5.6}$$

The hypothesis test can be stated as H_0: "the observations y_t follow the model M_0" against H_1: "the observations y_t follow the model M_1".

Basseville and Benveniste (1983) have shown that the statistic η_t defined in equation (5.5) or equation (5.6) has the following properties

$$E_{H_0}(\eta_t) = 0 \tag{5.7}$$

$$E_{H_1}(\eta_t) < 0 \tag{5.8}$$

where the operator $E_{H_0}(\eta_t)$ reads as "expected value of η_t if the observations follow the model M_0"; and the operator $E_{H_1}(\eta_t)$ reads as "expected value of η_t if the observations follow the model M_1". Equation(5.7) implies that if there is no model change, then the statistic η_t will be zero mean, and equation (5.8) implies that if there is change, then the statistic η_t will have a negative mean value. These properties of η_t can be used to detect model changes by using, e.g. the CUSUM test, Shewhart control chart or EWMA test of η_t.

5.3 Closed-loop Model Validation and Detection of Model Change

In this section, we develop control relevant algorithm for closed-loop model validation and change detection .

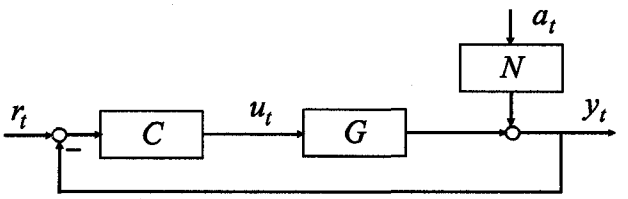

Figure 5.1: Closed-loop process

Consider a time-variant closed-loop process in figure 5.1 where G and N are time-variant plant and disturbance models respectively, and C is a linear time invariant controller. The time-variant process has the descriptions as expressed in equation (5.10) and equation (5.11).

$$y_t = \frac{CG}{1+CG} r_t + \frac{N}{1+CG} a_t \tag{5.9}$$

where

$$M_0 : \begin{cases} G = G_0, \\ N = N_0 \\ a_t = a_t^0 \\ Var(a_t) = \sigma_0^2 \end{cases} \quad for \;\; t < t_0 \tag{5.10}$$

and

$$M_1 : \begin{cases} G = G_1, \\ N = N_1 \\ a_t = a_t^1 \\ Var(a_t) = \sigma_1^2 \end{cases} \quad for \;\; t \geq t_0 \tag{5.11}$$

and a_t is a white noise sequence. In practice, the exact model M_0 and M_1 are unknown, and they are replaced by their estimates $\hat{M}_0 = \{\hat{G}_0, \hat{N}_0, \hat{\sigma}_0^2\}$ and $\hat{M}_1 = \{\hat{G}_1, \hat{N}_1, \hat{\sigma}_1^2\}$ for implementation of the detection algorithm.

The counterparts of equation (5.5) and (5.6) are therefore written as

$$\eta_t = \frac{1}{2}\left[2\frac{e_t^0 e_t^1}{\hat{\sigma}_1^2} - \left(1+\frac{\hat{\sigma}_0^2}{\hat{\sigma}_1^2}\right)\frac{(e_t^0)^2}{\hat{\sigma}_0^2} - \left(\frac{\hat{\sigma}_0^2}{\hat{\sigma}_1^2}-1\right)\right] \tag{5.12}$$

and

$$\eta_t = -\frac{(e_t^0)^2}{2\hat{\sigma}_0^2} + \frac{(e_t^1)^2}{2\hat{\sigma}_1^2} + \frac{1}{2} - \frac{\hat{\sigma}_0^2 + (e_t^0 - e_t^1)^2}{2\hat{\sigma}_1^2} \tag{5.13}$$

where e_t^0, e_t^1, $\hat{\sigma}_0^2$ and $\hat{\sigma}_1^2$ are calculated from the models $\hat{M}_0$ and $\hat{M}_1$, respectively.

5.3.1 Validate "$E_{H_0}(\eta_t) = 0$" for Closed-loop Process

To show that $E_{H_0}(\eta_t) = 0$ is valid for the Box-Jenkins model under closed-loop, consider $t < t_0$. The innovation sequence of model $\hat{M}_0$ is given by

$$\begin{aligned} e_t^0 &= \frac{1}{\hat{S}_0\hat{N}_0}\left(y_t - (1-\hat{S}_0)r_t\right) \\ &= \frac{1}{\hat{S}_0\hat{N}_0}\left[(\hat{S}_0 - S_0)r_t + S_0N_0a_t\right] = \frac{1}{\hat{S}_0\hat{N}_0}\left[-\tilde{S}_{00}r_t + S_0N_0a_t\right] \end{aligned} \tag{5.14}$$

where $S_0 = \frac{1}{1+CG_0}$ is sensitivity function; $\hat{S}_0$ is an estimate of S_0; $\tilde{S}_{00} = S_0 - \hat{S}_0$.

Similarly, for $t < t_0$, the innovation sequence of model $\hat{M}_1$ is given by

$$e_t^1 = \frac{1}{\hat{S}_1\hat{N}_1}\left[(\hat{S}_1 - S_0)r_t + S_0N_0a_t\right] = \frac{1}{\hat{S}_1\hat{N}_1}\left[-\tilde{S}_{01}r_t + S_0N_0a_t\right] \tag{5.15}$$

where $S_1 = \frac{1}{1+CG_1}$; $\hat{S}_1$ is an estimate of S_1; $\tilde{S}_{01} = S_0 - \hat{S}_1$.

For $t < t_0$, the difference of the two innovation sequences is given by

$$e_t^0 - e_t^1 = \left(\frac{\tilde{S}_{01}}{\hat{S}_1\hat{N}_1} - \frac{\tilde{S}_{00}}{\hat{S}_0\hat{N}_0}\right)r_t + \left(\frac{S_0N_0}{\hat{S}_0\hat{N}_0} - \frac{S_0N_0}{\hat{S}_1\hat{N}_1}\right)a_t^0 \tag{5.16}$$

Using Parseval's Theorem and following the same line of arguments as in Huang and Tamayo (2000), we have

$$
\begin{aligned}
& E_{H_0}(\eta_t) \\
= & -\frac{1}{4\pi\hat{\sigma}_0^2}\int_{-\pi}^{\pi}\frac{1}{|\hat{S}_0(e^{-j\omega})\hat{N}_0(e^{-j\omega})|^2}\left[|\tilde{S}_{00}(e^{-j\omega})|^2\Phi_r(\omega)+|S_0(e^{-j\omega})N_0(e^{-j\omega})|^2\sigma_0^2\right]d\omega \\
& +\frac{1}{4\pi\hat{\sigma}_1^2}\int_{-\pi}^{\pi}\frac{1}{|\hat{S}_1(e^{-j\omega})\hat{N}_1(e^{-j\omega})|^2}\left[|\tilde{S}_{01}(e^{-j\omega})|^2\Phi_r(\omega)+|S_0(e^{-j\omega})N_0(e^{-j\omega})|^2\sigma_0^2\right]d\omega \\
& +\frac{1}{2}-\frac{\hat{\sigma}_0^2}{2\hat{\sigma}_1^2} \\
& -\frac{1}{4\pi\hat{\sigma}_1^2}\int_{-\pi}^{\pi}\left[\left|\frac{\tilde{S}_{00}(e^{-j\omega})}{\hat{S}_0(e^{-j\omega})\hat{N}_0(e^{-j\omega})}-\frac{\tilde{S}_{01}(e^{-j\omega})}{\hat{S}_1(e^{-j\omega})\hat{N}_1(e^{-j\omega})}\right|^2\Phi_r(\omega)\right. \\
& \left.+\left|\frac{S_0(e^{-j\omega})N_0(e^{-j\omega})}{\hat{S}_0(e^{-j\omega})\hat{N}_0(e^{-j\omega})}-\frac{S_0(e^{-j\omega})N_0(e^{-j\omega})}{\hat{S}_1(e^{-j\omega})\hat{N}_1(e^{-j\omega})}\right|^2\sigma_0^2\right]d\omega \qquad (5.17)
\end{aligned}
$$

Lemma 5.1 *If the models before the change are correctly estimated, i.e.* $\hat{S}_0 = S_0$, $\hat{N}_0 = N_0$ *and* $\hat{\sigma}_0^2 = \sigma_0^2$, *then* $E_{H_0}(\eta_t) = 0$.

Proof. Substituting $\hat{S}_0 = S_0$, $\hat{N}_0 = N_0$ and $\hat{\sigma}_0^2 = \sigma_0^2$ into equation (5.17) yields

$$
\begin{aligned}
& E_{H_0}(\eta_t) \\
= & -\frac{1}{2} \\
& +\frac{1}{4\pi\hat{\sigma}_1^2}\int_{-\pi}^{\pi}\frac{1}{|\hat{S}_1(e^{-j\omega})\hat{N}_1(e^{-j\omega})|^2}\left[|\tilde{S}_{01}(e^{-j\omega})|^2\Phi_r(\omega)+|S_0(e^{-j\omega})N_0(e^{-j\omega})|^2\sigma_0^2\right]d\omega \\
& +\frac{1}{2}-\frac{\sigma_0^2}{2\hat{\sigma}_1^2} \\
& -\frac{1}{4\pi\hat{\sigma}_1^2}\int_{-\pi}^{\pi}\left[\left|\frac{\tilde{S}_{01}(e^{-j\omega})}{\hat{S}_1(e^{-j\omega})\hat{N}_1(e^{-j\omega})}\right|^2\Phi_r(\omega)+\left|1-\frac{S_0(e^{-j\omega})N_0(e^{-j\omega})}{\hat{S}_1(e^{-j\omega})\hat{N}_1(e^{-j\omega})}\right|^2\sigma_0^2\right]d\omega \\
= & \frac{1}{4\pi\hat{\sigma}_1^2}\int_{-\pi}^{\pi}\left|\frac{S_0(e^{-j\omega})N_0(e^{-j\omega})}{\hat{S}_1(e^{-j\omega})\hat{N}_1(e^{-j\omega})}\right|^2\sigma_0^2 d\omega-\frac{\sigma_0^2}{2\hat{\sigma}_1^2} \\
& -\frac{1}{4\pi\hat{\sigma}_1^2}\int_{-\pi}^{\pi}\left|1-\frac{S_0(e^{-j\omega})N_0(e^{-j\omega})}{\hat{S}_1(e^{-j\omega})\hat{N}_1(e^{-j\omega})}\right|^2\sigma_0^2 d\omega \qquad (5.18)
\end{aligned}
$$

Since sensitivity function $S = \frac{1}{1+CG}$ is monic, and also both N_0 and $\hat{N}_1$ are monic (Ljung, 1998), we may write

$$\frac{S_0(e^{-j\omega})N_0(e^{-j\omega})}{\hat{S}_1(e^{-j\omega})\hat{N}_1(e^{-j\omega})} = 1 + e^{-j\omega}R(e^{-j\omega}) \tag{5.19}$$

where $R(q^{-1})$ is a proper rational transfer function. Substituting equation (5.19) into equation (5.18) yields

$$\begin{aligned} E_{H_0}(\eta_t) &= \frac{1}{4\pi\hat{\sigma}_1^2}\int_{-\pi}^{\pi}|1+e^{-j\omega}R(e^{-j\omega})|^2\sigma_0^2 d\omega - \frac{\sigma_0^2}{2\hat{\sigma}_1^2} \\ &\quad -\frac{1}{4\pi\hat{\sigma}_1^2}\int_{-\pi}^{\pi}|e^{-j\omega}R(e^{-j\omega})|^2\sigma_0^2 d\omega \end{aligned} \tag{5.20}$$

Using Parseval's Theorem, we have

$$\begin{aligned} &\frac{1}{2\pi}\int_{-\pi}^{\pi}|1+e^{-j\omega}R(e^{-j\omega})|^2\sigma_0^2 d\omega \\ &= E_{H_0}[(1+q^{-1}R(q^{-1}))a_t]^2 \\ &= E_{H_0}[a_t + R(q^{-1})a_{t-1}]^2 \\ &= E_{H_0}(a_t)^2 + E_{H_0}[R(q^{-1})a_{t-1}]^2 \\ &= \sigma_0^2 + \frac{1}{2\pi}\int_{-\pi}^{\pi}|e^{-j\omega}R(e^{-j\omega})|^2\sigma_0^2 d\omega \end{aligned} \tag{5.21}$$

Substituting equation (5.21) into equation (5.20) yields $E_{H_0}(\eta_t) = 0$. □

Lemma 5.1 indicates that if the estimated models are correct or close to the true models, then the statistic η_t should have mean zero regardless how we choose the second set of models ($\hat{S}_1$, $\hat{N}_1$ and $\hat{\sigma}_1^2$). With the assumption that the controller is linear time invariant, changes in S indicate changes in G (plant model). Therefore, this lemma can be used for model validation using, for example, the CUSUM or Shewhart chart of η_t.

Remark 5.3.1 *The estimation of $\hat{S}_0$ can be obtained by two methods. One method is to estimate $\hat{S}_0$ directly, e.g. using the method proposed in Huang and Shah (1997). Alternately, if the information of controller C is known, then with the identified model, $\hat{G}$, one can calculate $\hat{S}$.*

Remark 5.3.2 *In general, there are two types of model validation problem. One is the traditional off-line model validation where the model is identified from a set of test data and the same test data or some other test data is used to verify the model*

(Ljung, 1998). The other is on-line model validation (we call the latter validation problem as the 'detection of model change') where the initial model is adequate but it may change later (Basseville et al., *1987). Mathematically, if the changing point* $t_0 = 0$, *then we are dealing with the first type of problem. If the changing point is* $t_0 > 0$, *then it is second type problem. The algorithms developed in this chapter are applicable to both problems.*

5.3.2 Validate "$E_{H_1}(\eta_t) < 0$" for Closed-loop Process

To show that $E_{H_1}(\eta_t) < 0$ is valid for the Box-Jenkins model under closed-loop, consider $t \geq t_0$. The following relationships can be derived following a similar approach presented in last sub-section:

$$e_t^0 = \frac{1}{\hat{S}_0\hat{N}_0}\left[(\hat{S}_0 - S_1)r_t + S_1N_1a_t\right] = \frac{1}{\hat{S}_0\hat{N}_0}\left[-\tilde{S}_{10}r_t + S_1N_1a_t\right] \quad (5.22)$$

$$e_t^1 = \frac{1}{\hat{S}_1\hat{N}_1}\left[(\hat{S}_1 - S_1)r_t + S_1N_1a_t\right] = \frac{1}{\hat{S}_1\hat{N}_1}\left[-\tilde{S}_{11}r_t + S_1N_1a_t\right] \quad (5.23)$$

$$e_t^0 - e_t^1 = \left(\frac{\tilde{S}_{11}}{\hat{S}_1\hat{N}_1} - \frac{\tilde{S}_{10}}{\hat{S}_0\hat{N}_0}\right)r_t + \left(\frac{S_1N_1}{\hat{S}_0\hat{N}_0} - \frac{S_1N_1}{\hat{S}_1\hat{N}_1}\right)a_t^0 \quad (5.24)$$

where $\tilde{S}_{10} = S_1 - \hat{S}_0$ and $\tilde{S}_{11} = S_1 - \hat{S}_1$.

Expectation of equation (5.13) subject to that model (5.11) is given by

$$\begin{aligned}
& E_{H_1}(\eta_t) \\
= & -\frac{1}{4\pi\hat{\sigma}_0^2}\int_{-\pi}^{\pi}\frac{1}{|\hat{S}_0(e^{-j\omega})\hat{N}_0(e^{-j\omega})|^2}\left[|\tilde{S}_{10}(e^{-j\omega})|^2\Phi_r(\omega) + |S_1(e^{-j\omega})N_1(e^{-j\omega})|^2\sigma_1^2\right]d\omega \\
& + \frac{1}{4\pi\hat{\sigma}_1^2}\int_{-\pi}^{\pi}\frac{1}{|\hat{S}_1(e^{-j\omega})\hat{N}_1(e^{-j\omega})|^2}\left[|\tilde{S}_{11}(e^{-j\omega})|^2\Phi_r(\omega) + |S_1(e^{-j\omega})N_1(e^{-j\omega})|^2\sigma_1^2\right]d\omega \\
& + \frac{1}{2} - \frac{\hat{\sigma}_0^2}{2\hat{\sigma}_1^2} \\
& - \frac{1}{4\pi\hat{\sigma}_1^2}\int_{-\pi}^{\pi}\left[\left|\frac{\tilde{S}_{10}(e^{-j\omega})}{\hat{S}_0(e^{-j\omega})\hat{N}_0(e^{-j\omega})} - \frac{\tilde{S}_{11}(e^{-j\omega})}{\hat{S}_1(e^{-j\omega})\hat{N}_1(e^{-j\omega})}\right|^2\Phi_r(\omega)\right. \\
& \left. + \left|\frac{S_1(e^{-j\omega})N_1(e^{-j\omega})}{\hat{S}_0(e^{-j\omega})\hat{N}_0(e^{-j\omega})} - \frac{S_1(e^{-j\omega})N_1(e^{-j\omega})}{\hat{S}_1(e^{-j\omega})\hat{N}_1(e^{-j\omega})}\right|^2\sigma_0^2\right]d\omega
\end{aligned} \quad (5.25)$$

Lemma 5.2 *If the models after the change are correctly estimated, i.e.* $\hat{S}_1 = S_1$, $\hat{N}_1 = N_1$ *and* $\hat{\sigma}_1^2 = \sigma_1^2$, *then* $E_{H_1}(\eta_t) < 0$.

Proof. Substituting $\hat{S}_1 = S_1$, $\hat{N}_1 = N_1$ and $\hat{\sigma}_1^2 = \sigma_1^2$ into equation (5.25) yields

$$\begin{aligned} E_{H_1}(\eta_t) &= 1 - \left(\frac{1}{2\hat{\sigma}_0^2} + \frac{1}{2\sigma_1^2}\right)\frac{1}{2\pi}\int_{-\pi}^{\pi}\left|\frac{\tilde{S}_{10}(e^{-j\omega})}{\hat{S}_0(e^{-j\omega})\hat{N}_0(e^{-j\omega})}\right|^2\Phi_r(\omega)d\omega - \frac{\hat{\sigma}_0^2}{2\sigma_1^2} \\ &\quad -\frac{1}{4\pi\hat{\sigma}_0^2}\int_{-\pi}^{\pi}\left|\frac{S_1(e^{-j\omega})N_1(e^{-j\omega})}{\hat{S}_0(e^{-j\omega})\hat{N}_0(e^{-j\omega})}\right|^2\sigma_0^2 d\omega \\ &\quad -\frac{1}{4\pi\sigma_1^2}\int_{-\pi}^{\pi}\left|1 - \frac{S_1(e^{-j\omega})N_1(e^{-j\omega})}{\hat{S}_0(e^{-j\omega})\hat{N}_0(e^{-j\omega})}\right|^2\sigma_0^2 d\omega \end{aligned}$$

We may write

$$\frac{S_1(e^{-j\omega})N_1(e^{-j\omega})}{\hat{S}_0(e^{-j\omega})\hat{N}_0(e^{-j\omega})} = 1 + e^{-j\omega}P(e^{-j\omega}) \tag{5.26}$$

where $P(q^{-1})$ is a proper rational transfer function. Following the similar approach as the derivation of equation (5.21), equation (5.26) can be written as

$$\begin{aligned} E_{H_1}(\eta_t) &= 1 - \left(\frac{1}{2\hat{\sigma}_0^2} + \frac{1}{2\sigma_1^2}\right)\frac{1}{2\pi}\int_{-\pi}^{\pi}\left|\frac{\tilde{S}_{10}(e^{-j\omega})}{\hat{S}_0(e^{-j\omega})\hat{N}_0(e^{-j\omega})}\right|^2\Phi_r(\omega)d\omega - \frac{\hat{\sigma}_0^2}{2\sigma_1^2} \\ &\quad -\frac{1}{2\hat{\sigma}_0^2}\left[\sigma_1^2 + \frac{1}{2\pi}\int_{-\pi}^{\pi}|e^{-j\omega}P(e^{-j\omega})|^2\sigma_1^2 d\omega\right] \\ &\quad -\frac{1}{4\pi\sigma_1^2}\int_{-\pi}^{\pi}|e^{-j\omega}P(e^{-j\omega})|^2\sigma_1^2 d\omega \\ &= \left[1 - \left(\frac{\sigma_1^2}{2\hat{\sigma}_0^2} + \frac{\hat{\sigma_0}^2}{2\sigma_1^2}\right)\right] \\ &\quad -\left(\frac{1}{2\hat{\sigma}_0^2} + \frac{1}{2\sigma_1^2}\right)\frac{1}{2\pi}\int_{-\pi}^{\pi}\left|\frac{\tilde{S}_{10}(e^{-j\omega})}{\hat{S}_0(e^{-j\omega})\hat{N}_0(e^{-j\omega})}\right|^2\Phi_r(\omega)d\omega \\ &\quad -\left(\frac{1}{2} + \frac{\sigma_1^2}{2\hat{\sigma}_0^2}\right)\frac{1}{2\pi}\int_{-\pi}^{\pi}|e^{-j\omega}P(e^{-j\omega})|^2\sigma_1^2 d\omega \end{aligned} \tag{5.27}$$

It is can be shown that $\left[1 - \left(\frac{\sigma_1^2}{2\hat{\sigma}_0^2} + \frac{\hat{\sigma}_0^2}{2\sigma_1^2}\right)\right] \leq 0$, so $E_{H_1}(\eta_t) < 0$. □

Lemma 5.2 indicates that if the second set of models are correct or close to the true models, then the statistic η_t should have negative mean value regardless of how

we choose the first models ($\hat{S}_0$, $\hat{N}_0$ and $\hat{\sigma}_0^2$). This lemma therefore can be used for model validation.

To summarize, Lemmas 5.1 and 5.2 use the statistic η_t for model validation or detection of model change. If the statistic η_t has a non-zero mean from the beginning, then it implies that the first model is not correct. If the statistic η_t has a zero mean at the beginning and then shifts to a negative mean, then it implies that a change of model has occurred. Since the algorithm is derived under closed-loop conditions, it can be used for on-line closed-loop model validation and detection of parameter changes. It is worthwhile to point out that the algorithm developed in this section is applicable to the MISO process or the MIMO process (by transferring the MIMO process into several MISO processes). This is because the calculation of η_t for the MISO process is similar to that for SISO process.

Huang (2001) has also used the two-model divergence method to develop an algorithm for closed-loop model validation. It is worthwhile to compare these two algorithms and analyze the differences. The major difference between two algorithms is that: we use signals $\{y_t, r_t\}$ and the relationship $y_t = (1-S)r_t + SNa_t$ to calculate the sequence $e_t = \frac{1}{\hat{S}\hat{N}_0}[y_t - (1-\hat{S})r_t]$; while Huang (2001) used signals $\{y_t, u_t\}$ and the relationship $y_t = Gu_t + Na_t$ to calculate the sequence $e_t = \frac{1}{\hat{N}_0}[y_t - \hat{G}_0 u_t]$. So in our algorithm, the η_t calculated using $e_t = \frac{1}{\hat{S}\hat{N}_0}[y_t - (1-\hat{S})r_t]$ can be used to detect changes in S and N; while the η_t calculated using $e_t = \frac{1}{\hat{N}_0}[y_t - \hat{G}_0 u_t]$ in Huang (2001) can be used to detect changes in G and N. With the assumption of a linear time invariant controller, detection of changes in S is equivalent to detection of changes in G. It is important to note that one advantage of our algorithm is that it is control relevant, meaning that it is sensitive to the changes in G that significantly affects S, but not sensitive to the changes in G that have relatively small effect on S. While controller design is implicitly an activity to shape S, as long as model changes do not affect S significantly, it will not affect the control performance much as well. So it is desirable that our algorithm can avoid issuing unnecessary alarms when model changes do not significantly affect the closed-loop behavior.

5.4 Validation and Change Detection of the Plant-model-only under Closed-loop Conditions

The algorithm proposed in last section and the one in Huang (2001) are sensitive to both plant changes and disturbance changes. In other words, they can not differentiate plant changes from disturbance changes. In practice, processes often experience frequent changes in disturbance dynamics. Therefore validation and change detection of the plant model regardless how disturbance changes is of great interest. In such cases, the algorithms we mentioned earlier are not appropriate. In this section, we will develop a new algorithm that can be used to test plant models regardless of varying disturbance dynamics. To achieve this objective, we propose use of the following statistic in this section:

$$\mu_t = -(v_t^0)^2 + (v_t^1)^2 - (v_t^0 - v_t^1)^2 \tag{5.28}$$

where v_t^0 and v_t^1 are residuals from the following equations:

$$v_t^0 = y_t - (1 - \hat{S}_0)r_t \tag{5.29}$$

$$v_t^1 = y_t - (1 - \hat{S}_1)r_t \tag{5.30}$$

Theorem 5.1 *Let the process be described by one of the two Box-Jenkins models shown in equation* (5.9)*, with the switching time of the parameters occurring at some unknown time* t_0*. All observations are sampled under closed-loop conditions. Then the following results are true:*

1. *For* $t < t_0$*, if the sensitivity function before the change is correctly estimated, i.e.* $\hat{S}_0 = S_0$*, then* $E_{H_0}(\mu_t) = 0$*, regardless how we choose* $\{\hat{N}_0, \hat{S}_1, \hat{N}_1\}$.

2. *For* $t \geq t_0$*, if the sensitivity function after the change is correctly estimated, i.e.* $\hat{S}_1 = S_1$*, then* $E_{H_1}(\mu_t) < 0$*, regardless how we choose* $\{\hat{N}_1, \hat{S}_0, \hat{N}_0\}$.

Proof. (1). For $t < t_0$, we have

$$
\begin{aligned}
& E_{H_0}(\mu_t) \\
= \; & -E_{H_0}(v_t^0)^2 + E_{H_0}(v_t^1)^2 - E_{H_0}(v_t^0 - v_t^1)^2 \\
= \; & -E_{H_0}\left(y_t - (1-\hat{S}_0)r_t\right)^2 + E_{H_0}\left(y_t - (1-\hat{S}_1)r_t\right)^2 \\
& -E_{H_0}\left(y_t - (1-\hat{S}_0)r_t - y_t + (1-\hat{S}_1)r_t\right)^2 \\
= \; & -E_{H_0}(-\tilde{S}_{00}r_t + S_0N_0a_t)^2 + E_{H_0}(-\tilde{S}_{01}r_t + S_0N_0a_t)^2 \\
& -E_{H_0}(\hat{S}_0r_t - \hat{S}_1r_t)^2 \\
= \; & -\frac{1}{2\pi}\int_{-\pi}^{\pi}\left[|\tilde{S}_{00}(e^{-j\omega})|^2\Phi_r(\omega) + |S_0(e^{-j\omega})N_0(e^{-j\omega})|^2\sigma_0^2\right]d\omega \\
& +\frac{1}{2\pi}\int_{-\pi}^{\pi}\left[|\tilde{S}_{01}(e^{-j\omega})|^2\Phi_r(\omega) + |S_0(e^{-j\omega})N_0(e^{-j\omega})|^2\sigma_0^2\right]d\omega \\
& -\frac{1}{2\pi}\int_{-\pi}^{\pi}|\hat{S}_0(e^{-j\omega}) - \hat{S}_1(e^{-j\omega})|^2\Phi_r(\omega)d\omega \\
= \; & -\frac{1}{2\pi}\int_{-\pi}^{\pi}\left[|\tilde{S}_{00}(e^{-j\omega})|^2 - |\tilde{S}_{01}(e^{-j\omega})|^2 + |\hat{S}_0(e^{-j\omega}) - \hat{S}_1(e^{-j\omega})|^2\right]\Phi_r(\omega)d\omega
\end{aligned}
\tag{5.31}
$$

Note that

$$
\hat{S}_0(e^{-j\omega}) - \hat{S}_1(e^{-j\omega}) = \tilde{S}_{01}(e^{-j\omega}) - \tilde{S}_{00}(e^{-j\omega}) \tag{5.32}
$$

Substituting equation (5.32) into equation (5.31) yields

$$
\begin{aligned}
& E_{H_0}(\mu_t) \\
= \; & -\frac{1}{2\pi}\int_{-\pi}^{\pi}\left[|\tilde{S}_{00}(e^{-j\omega})|^2 - |\tilde{S}_{01}(e^{-j\omega})|^2 + |\tilde{S}_{00}(e^{-j\omega}) - \tilde{S}_{01}(e^{-j\omega})|^2\right]\Phi_r(\omega)d\omega
\end{aligned}
\tag{5.33}
$$

Substituting $\hat{S}_0 = S_0$ or $\tilde{S}_{00} = 0$ into equation (5.33), we have $E_{H_0}(\mu_t) = 0$.

(2). Similarly, for $t \geq t_0$, we have

$$
\begin{aligned}
& E_{H_1}(\mu_t) \\
= \; & -E_{H_1}(v_t^0)^2 + E_{H_1}(v_t^1)^2 - E_{H_1}(v_t^0 - v_t^1)^2 \\
= \; & -\frac{1}{2\pi}\int_{-\pi}^{\pi}\left[|\tilde{S}_{10}(e^{-j\omega})|^2 - |\tilde{S}_{11}(e^{-j\omega})|^2 + |\tilde{S}_{10}(e^{-j\omega}) - \tilde{S}_{11}(e^{-j\omega})|^2\right]\Phi_r(\omega)d\omega
\end{aligned}
\tag{5.34}
$$

Substituting $\hat{S}_1 = S_1$ or $\tilde{S}_{11} = 0$ into equation (5.34), we have

$$
E_{H_1}(\mu_t) = -\frac{1}{\pi}\int_{-\pi}^{\pi}|\tilde{S}_{10}(e^{-j\omega})|^2\Phi_r(\omega)d\omega < 0. \qquad \square
$$

Theorem 5.1 is useful for detecting changes in the sensitivity function S. With the assumption of a linear time invariant controller, it is equivalent to detecting changes in the plant model G. The time varying disturbance dynamics does not affect the algorithm. The algorithm developed here is also control relevant, meaning that it is sensitive to the changes in G that significantly affects S, and not sensitive to the changes in G that have relatively small effect on S. Therefore this algorithm can avoid issuing unnecessary alarms when model changes do not notably affect the closed-loop behavior. The advantage of this algorithm over the one proposed in Section 5.3 is that this algorithm is not sensitive to disturbance changes; thus it can effectively reduce false alarms due to disturbance changes. Theorem 5.1 can also apply to MIMO processes.

5.4.1 Detectability of the Plant Model Change

In practice, it is rare to have an exact knowledge of the models before and after change, and there will inevitably always be some model-plant mismatch. If the first plant sensitivity function is not correct before the change, i.e. $\hat{S}_0 \neq S_0$, or if the second plant sensitivity function is not correct after the change, i.e. $\hat{S}_1 \neq S_1$, then it is important to know how the model-plant mismatch affects the algorithm.

Corollary 5.1 *If $\hat{S}_0 \neq S_0$, then $E_{H_0}(\mu_t)$ has a lower bound expressed by the following inequality:*

$$E_{H_0}(\mu_t) \geq -\frac{1}{\pi}\int_{-\pi}^{\pi}\left[|\tilde{S}_{00}(e^{-j\omega})|^2 + |\tilde{S}_{00}(e^{-j\omega})\tilde{S}_{01}(e^{-j\omega})|\right]\Phi_r(\omega)d\omega \tag{5.35}$$

and if $\hat{S}_1 \neq S_1$,, *then* $E_{H_1}(\mu_t)$ *has an upper bound given by the following inequality:*

$$E_{H_1}(\mu_t) \leq -\frac{1}{\pi}\int_{-\pi}^{\pi}\left[|\tilde{S}_{10}(e^{-j\omega})|^2 - |\tilde{S}_{10}(e^{-j\omega})\tilde{S}_{11}(e^{-j\omega})|\right]\Phi_r(\omega)d\omega \tag{5.36}$$

Proof. Using the following triangular inequalities

$$|\tilde{S}_{00}(e^{-j\omega}) - \tilde{S}_{01}(e^{-j\omega})|^2 \leq \left(|\tilde{S}_{00}(e^{-j\omega})| + |\tilde{S}_{01}(e^{-j\omega})|\right)^2$$

and

$$|\tilde{S}_{10}(e^{-j\omega}) - \tilde{S}_{11}(e^{-j\omega})|^2 \geq \left(|\tilde{S}_{10}(e^{-j\omega})| - |\tilde{S}_{11}(e^{-j\omega})|\right)^2,$$

we have

$$\begin{aligned}
& E_{H_0}(\mu_t) \\
= & -\frac{1}{2\pi}\int_{-\pi}^{\pi}\left[|\tilde{S}_{00}(e^{-j\omega})|^2 - |\tilde{S}_{01}(e^{-j\omega})|^2 + |\tilde{S}_{00}(e^{-j\omega}) - \tilde{S}_{01}(e^{-j\omega})|^2\right]\Phi_r(\omega)d\omega \\
\geq & -\frac{1}{2\pi}\int_{-\pi}^{\pi}\left[|\tilde{S}_{00}(e^{-j\omega})|^2 - |\tilde{S}_{01}(e^{-j\omega})|^2 + \left(|\tilde{S}_{00}(e^{-j\omega})| + |\tilde{S}_{01}(e^{-j\omega})|\right)^2\right]\Phi_r(\omega)d\omega \\
= & -\frac{1}{\pi}\int_{-\pi}^{\pi}\left[|\tilde{S}_{00}(e^{-j\omega})|^2 + |\tilde{S}_{00}(e^{-j\omega})\tilde{S}_{01}(e^{-j\omega})|\right]\Phi_r(\omega)d\omega
\end{aligned}$$

and

$$E_{H_1}(\mu_t) \leq -\frac{1}{\pi}\int_{-\pi}^{\pi}\left[|\tilde{S}_{10}(e^{-j\omega})|^2 - |\tilde{S}_{10}(e^{-j\omega})\tilde{S}_{11}(e^{-j\omega})|\right]\Phi_r(\omega)d\omega \qquad \square$$

In order to improve detectability of the change, one would like that the lower bound in inequality (5.35) to be as large as possible (with a maximum value zero). Similarly, the upper bound in inequality (5.36) should be as small as possible.

Inequality (5.35) states that the model-plant mismatch $\tilde{S}_{00}$ affects $E_{H_0}(\mu_t)$ by reducing its lower bound. In addition, the term $\tilde{S}_{01}$, which is the difference between the sensitivity function S_0 (before change) and the model $\hat{S}_1$ (after change), also

reduces the lower bound of $E_{H_0}(\mu_t)$ through the interacting term with $\tilde{S}_{00}$. Since $\tilde{S}_{01}$ can be arbitrarily large, it is important to keep $\tilde{S}_{00}$ small or at least to keep it small in the frequency range where $\tilde{S}_{01}$ is large.

The term $\tilde{S}_{10}$ in inequality (5.36) is the difference between the changed sensitivity S_1 and the model $\hat{S}_0$ (before change). This term represents the model change that we want to detect. From inequality (5.36), it can be observed that the change of sensitivity function $\tilde{S}_{10}$ directly contributes to the decrease of the upper bound of $E_{H_1}(\mu_t)$. Thus, the larger the change is, better the detectability. However, this term $\tilde{S}_{10}$ also increases the upper bound through the interacting term with model-plant mismatch $\tilde{S}_{11}$. So again, it is important to keep $\tilde{S}_{11}$ small or at least to keep it small in the frequency range where $\tilde{S}_{10}$ is large.

Corollary 5.2 *If the sensitivity function before a change is correctly estimated, i.e.* $\hat{S}_0 = S_0$, *then a sufficient condition for detectability of the model change is that the model-plant mismatch of the second process* $\tilde{S}_{11}$ *satisfies the following inequality:*

$$\frac{1}{2\pi}\int_{-\pi}^{\pi} |\tilde{S}_{11}(e^{-j\omega})|^2 \Phi_r(\omega) d\omega < \frac{1}{2\pi}\int_{-\pi}^{\pi} |\tilde{S}_{10}(e^{-j\omega})|^2 \Phi_r(\omega) d\omega \tag{5.37}$$

Proof. For detectability of the model change, we must have $E_{H_1}(\mu_t) < 0$. Following equation (5.36), we have

$$\frac{1}{\pi}\int_{-\pi}^{\pi} \left[|\tilde{S}_{10}(e^{-j\omega})|^2 - |\tilde{S}_{10}(e^{-j\omega})\tilde{S}_{11}(e^{-j\omega})| \right] \Phi_r(\omega) d\omega > 0 \tag{5.38}$$

Using the following inequality

$$2|\tilde{S}_{10}(e^{-j\omega})\tilde{S}_{11}(e^{-j\omega})| \leq |\tilde{S}_{10}(e^{-j\omega})|^2 + |\tilde{S}_{11}(e^{-j\omega})|^2 \tag{5.39}$$

in equation (5.38), the corollary can be proved. □

Corollary 5.2 implies that if the norm of the mismatch of the changed sensitivity function $\hat{S}_1$ is less than the norm of the sensitivity function difference before and after the change, then the change is detectable. The norm is weighted by the spectrum of the signal r_t.

5.5 Detection of Multiplicative Fault under Closed-loop Conditions

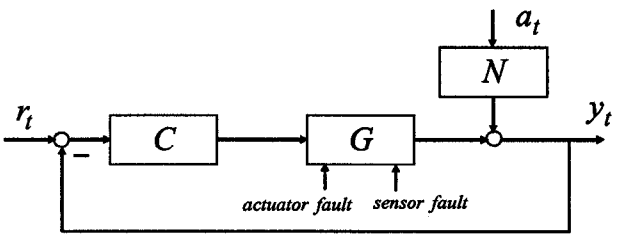

Figure 5.2: Closed-loop process with possible faults

The proposed two model validation algorithms can be extended to solve multiplicative fault detection problems in straightforward manner. In this section, we elaborate two type of FDI problems concerned with instrument faults.

Faults (e.g. sensor or actuator fault) in process can result in inferior products, increased operating costs and even possibility of catastrophic accidents. Therefore, it is important to detect (incipient) fault before it becomes serious. Frequently, actuator and sensor problems do not just affect the process in an additive manner. These equipment problems can also change the process dynamics, e.g introduce extra process nonlinearity (Choudhury *et al.*, 2004*b*). In Gertler (1998), most of sensor faults (e.g. sticking, sensor decalibration) and actuator faults (e.g. valve stiction or valve failure) are categorized as multiplicative faults, meaning that their effects on process outputs also depend on the magnitude of inputs. How to detect multiplicative fault *under closed-loop condition* is a challenge problem.

On-line model validation is closely related to the area of fault detection. Generally speaking, the objectives of these two areas are both to detect changes in a process: on-line model validation is to detect model changes; while fault detection is to detect undesirable process changes due to faults in process components, such as actuator or sensor faults. Figure 5.2 shows a closed-loop process with possible actuator and/or sensor faults. If we assume there is no actuator or sensor fault, then detecting changes in the process is a model validation problem. If we assume that there is no plant

change, then detecting changes in the process is a fault detection problem. In the previous sections, an implicit assumption is that there are no actuator or sensor faults, which is a common assumption in model validation. In this section, we show that the two algorithms can be used for detection of multiplicative faults *under closed-loop conditions* if there is no plant change.

5.5.1 Detection of Actuator Faults

In process control, a valve is typically the actuating device. Presence of valve problems, e.g., stiction, hysteresis and deadband in a control valve limits the control performances. Bialkowski (1992) reported that approximately 30% of the loops are oscillatory due to control valve problems. Desborough and Miller (2001) reported that control valve problems account for about one-third of the controllers that are classified as 'poor' or 'fair' in industry. A lot of valve problems arise not because of changes or degradation during plant operations, but rather because of valves being over or under-specified (generally over-sized) during the design phase of a project. i.e. many poorly performing valves are ones that operate near their fully open or fully closed position where non-linearity, stiction, hysteresis, etc. effects are most likely to occur. Choudhury *et al.* (2004*b*) and Choudhury *et al.* (2005*a*) have shown that valve problems typically introduce nonlinearity in the process and therefore affect control performance. In this subsection, we view the effect of valve problem from the perspective of control system: changes of nonlinearity in a process indicate changes of the process sensitivity function, and therefore indicate changes in control performance. If we can detect the changes in the sensitivity function due to valve stiction, then we can detect the valve problem.

Figure 5.3 shows a closed-loop process with a valve problem. F_a represents dynamics of the valve problem and the relationship between y_t and r_t can be expressed as:

$$y_t = \frac{CF_aG}{1+CF_aG}r_t + \frac{N}{1+CF_aG}a_t \tag{5.40}$$

Strictly speaking, equation (5.40) is only valid if F_a is linear functions, e.g. if there is no fault. With slight abuse of notation, we will use this equation to represent

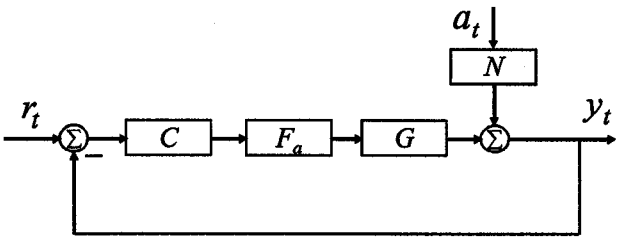

Figure 5.3: Closed-loop process with valve stiction

F_a to signify the logic relationship, even if F_a is a nonlinear function. It is clear from equation (5.40) that a valve problem will affect the sensitivity function and therefore will affect the control performance. As proved earlier, both algorithms are sensitive to changes in the sensitivity function. Therefore these two algorithms can be used to detect valve problems in the control loop. Simulation examples of detection of valve stiction will be shown in Section 5.6.

5.5.2 Detection of Sensor Faults

Sensors are important elements in process control and automation. A sensor giving incorrect information can have a deleterious effect on a process as undesired and unnecessary control moves may be implemented based on the wrong sensor readings. For example, a common problem in process industry is sensor decalibration where the sensor gain is not correct. Both O'Reilly (1998) and Malhotra and Huang (2002) model the sensor dynamics as an ARIMA structure and then use the local approach to detect the gain changes of the ARIMA model. In this subsection, we will show that multiplicative sensor faults will affect the process sensitivity function and therefore can be detected using the proposed two algorithms without modelling any sensor dynamics.

Figure 5.4 shows a closed-loop process with the multiplicative sensor fault. F_s represents dynamics of multiplicative sensor fault (it can be just a constant value) and the relationship between y_t and r_t can be expressed:

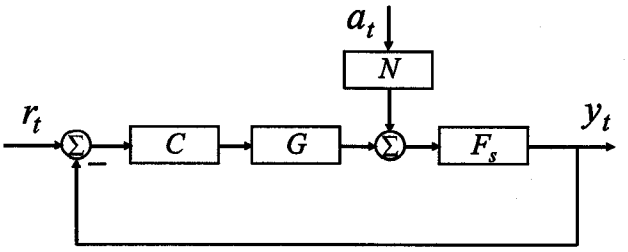

Figure 5.4: Closed-loop process with sensor decalibration

$$y_t = \frac{CGF_s}{1+CGF_s} r_t + \frac{N}{1+CGF_s} a_t \tag{5.41}$$

It is clear from equation (5.41) that multiplicative sensor fault shall affect the sensitivity function and therefore will affect the control performance. As proved earlier, both algorithms are sensitive to changes in sensitivity function. Therefore these two algorithms can be used to detect multiplicative sensor fault in the process. Experiment results of a successful detection of sensor decalibration in a pilot scale process will be shown in Section 5.7.

Remark 5.5.1 *In addition to actuator and sensor faults, process faults (or component faults) are also discussed in literature. Process faults are changes in some plant parameters caused by faults. For instance, changes of electrical resistance, mechanical friction coefficients and heat exchanger coefficients. Process faults can be treated as process changes and can be detected by the two developed algorithms.*

Remark 5.5.2 *Compared to the first algorithm developed in Section 5.3 , a clear advantage of the second algorithm developed in Section 5.4 is that it is not sensitive to time varying disturbances. This will reduce the effect of disturbances and therefore increase the reliability of fault detection.*

5.6 Simulation Examples

In this section, we will show examples to illustrate the application of the two algorithms for on-line closed-loop model validation. From now on, we denote the algo-

rithm developed in Section 5.3 as algorithm 1 and the one developed in Section 5.4 as algorithm 2.

To detect mean shift of η_t or μ_t, we use the recommended *tabular CUSUM (Cumulative SUM) test* (Montgomery and Runger, 1994). To apply the developed algorithms, we are only concerned about the mean drift in negative direction. So the lower one-sided CUSUM test is considered. It is briefly discussed here using our notation.

Let $s_L(t)$ be a lower one-sided CUSUM threshold and it is calculated from

$$s_L(t) = max[0, (\eta_{tar} - K) - \eta_t + s_L(t-1)] \quad for \quad algorithm \quad 1; \tag{5.42}$$

$$s_L(t) = max[0, (\mu_{tar} - K) - \mu_t + s_L(t-1)] \quad for \quad algorithm \quad 2; \tag{5.43}$$

where $s_L(0) = 0$.

K is called the reference value. η_{tar} and μ_{tar} are target values of η_t and μ_t respectively. $s_L(t)$ accumulates deviations from the target value that are greater than K, and resets to zero upon becoming negative. The target values η_{tar} and μ_{tar} are both zero for our application. If $-s_L(t)$ exceeds a constant $-H$ which is defined as decision interval, then a negative mean shift is detected. The selection of K and H has been recommended according to the average run length (ARL) property (Montgomery and Runger, 1994). Using $H = 4\sigma_\eta$ or $H = 5\sigma_\eta$, and $K = 0.5\sigma_\eta$ will generally provide CUSUM test that has good ARL properties against a shift of about $1\sigma_\eta$ in the mean of η_t, where σ_η is the standard deviation of η_t. Similarly, we can use $H = 4\sigma_\mu$ or $H = 5\sigma_\mu$, and $K = 0.5\sigma_\mu$ for test mean shift of μ_t, where σ_μ is the standard deviation of μ_t.

5.6.1 Model Validation using the Two Algorithms

Consider a process given by

$$y_t = q^{-4}\frac{K_p}{1 - 0.67q^{-1}}u_t + \frac{1 - 0.4q^{-1}}{1 - \lambda q^{-1}}a_t \tag{5.44}$$

a feedback controller with the transfer function

$$C(q^{-1}) = \frac{0.7 - 0.47q^{-1}}{0.33 - 0.10q^{-1} - 0.23q^{-4}} \tag{5.45}$$

is used to control the process. In this example, we shall consider detection of model changes using algorithms 1 and 2 under closed-loop conditions. Four scenarios are considered: (1) no plant dynamics change ("plant dynamics" means the $q^{-4}\frac{K_p}{1-0.67q^{-1}}$ part) and no disturbance dynamics change ("disturbance dynamics" means the $\frac{1-0.4q^{-1}}{1-\lambda q^{-1}}$ part); (2) changes in the plant dynamics only (3) changes in the disturbance dynamics only; (4) changes in both the plant and disturbance dynamics.

For all the cases, the process initial parameters are $K_p = 0.33$ and $\lambda = 0.17$. A total of 4000 data points are simulated. The input r_t is a series of random binary signal with magnitude ± 2. The variance of a_t is $\sigma_a^2 = 1$ for the purpose of showing the performance of the algorithms under low signal to noise ratio situation. The first 1000 data points of y_t and r_t are used to identify an initial model of $\{\hat{S}_0, \hat{N}_0, \hat{\sigma}_0^2\}$. The second model $\{\hat{S}_1, \hat{N}_1, \hat{\sigma}_1^2\}$ is estimated on-line using the recursive identification algorithm with a forgetting factor of 0.97 (from MATLAB/System Identification Toolbox®). The statistic η_t can be calculated from equation (5.13) and μ_t can be calculated from equation (5.28).

The CUSUM for algorithm 1 is calculated from equation (5.42) where $\eta_{tar} = 0$, $K = 0.5\sigma_\eta$, $H = 5\sigma_\eta$; σ_η is estimated from 1001st-1900th data points. Similarly, the CUSUM for algorithm 2 is calculated from equation (5.43) where $\mu_{tar} = 0$, $K = 0.5\sigma_\mu$, $H = 5\sigma_\mu$; σ_μ is estimated from 1001st-1900th data points. Therefore, the CUSUM tests for η and μ start from $t = 1901$.

Case 1. There is no change in the plant or disturbance dynamics in this case. Figure 5.5(a) shows the result from algorithm 1 and figure 5.5(b) shows the result from algorithm 2. Both pass the test, i.e. no persistent violation of the decision level or violation of the decision level over a significant time period is identified. Therefore, no change has been detected.

Case 2. To illustrate that the two algorithms are control relevant, we introduce changes of different magnitudes to the process.

(1) There is an abrupt change at the 3001st data point and $K_p = 0.40$ after the change, i.e. there is a gain change in the plant dynamics. The result from algorithm

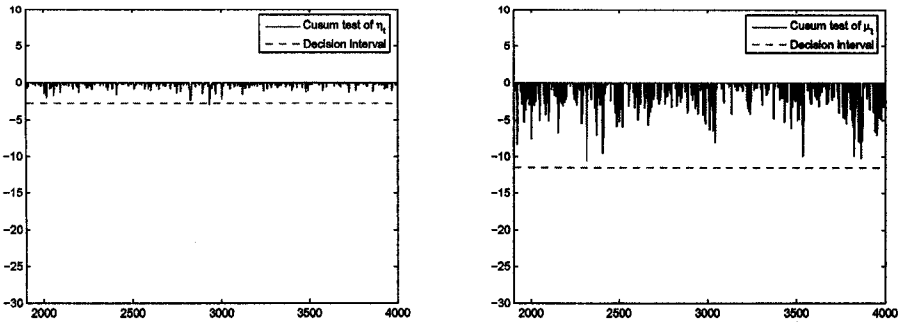

(a) CUSUM test of η_t (algorithm 1) (b) CUSUM test of μ_t (algorithm 2)

Figure 5.5: Case 1: No change in the plant or disturbance dynamics

1 is shown in figure 5.6(a); and the result from algorithm 2 is shown in figure 5.6(b). It is clear that figure 5.6(a) and 5.6(b) do not show any violation of the decision level. This indicates that the process gain change does not affect the sensitivity function much, and the two algorithms do not issue a warning.

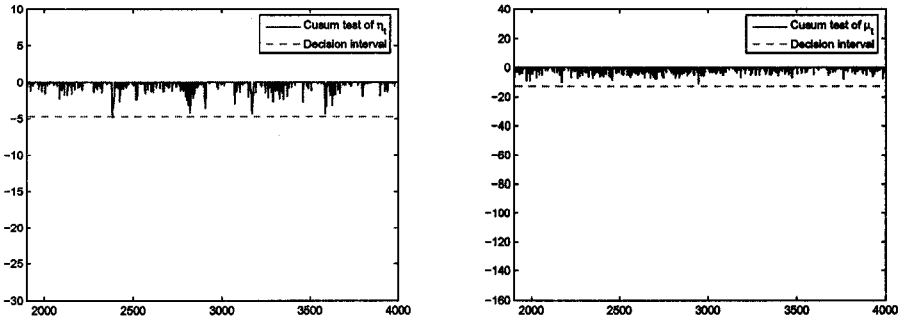

(a) CUSUM test of η_t (algorithm 1) (b) CUSUM test of η_t (algorithm 2)

Figure 5.6: Case 2: (1) Process gain is changed to 0.4

(2) We introduce larger gain change to the process. There is now an abrupt change at the 3001st data point when $K_p = 0.56$ after the change. The result from algorithm 1 is shown in figure 5.7(a); and the result from algorithm 2 is shown in figure 5.7(b). It is clear from figure 5.7(a) and 5.7(b) that there is persistent violation of the decision level after the plant changes. Both algorithms are correctly able to indicate that a process change has occurred.

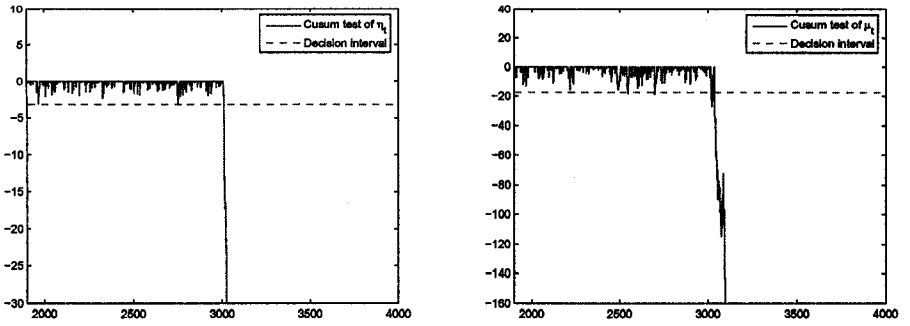

(a) CUSUM test of η_t (algorithm 1) (b) CUSUM test of η_t (algorithm 2)

Figure 5.7: Case 2: (2) Process gain is changed to 0.56

To investigate why the algorithms do not respond to gain changes to 0.4, but do respond to gain change to 0.56, we draw the bode plot of sensitivity functions of the original process and the changed processes. Figure 5.8 shows bode plots of the sensitivity functions. It is clear that the frequency response of the sensitivity function of the process with gain 0.4 is very close to the original process; but the frequency response of the sensitivity function of the process with gain 0.56 is farther away from the original process. These bode plots and results from the two simulations demonstrate that the two algorithms are control relevant and they are only sensitive to the process changes that significantly affect the process.

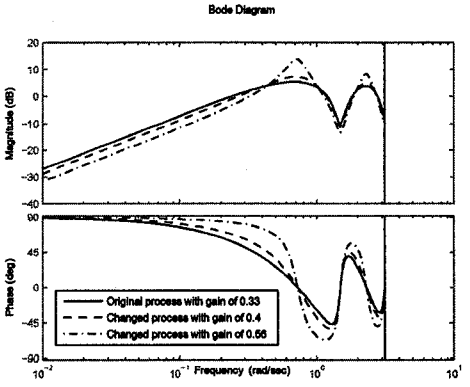

Figure 5.8: Bode plot of the sensitivity functions

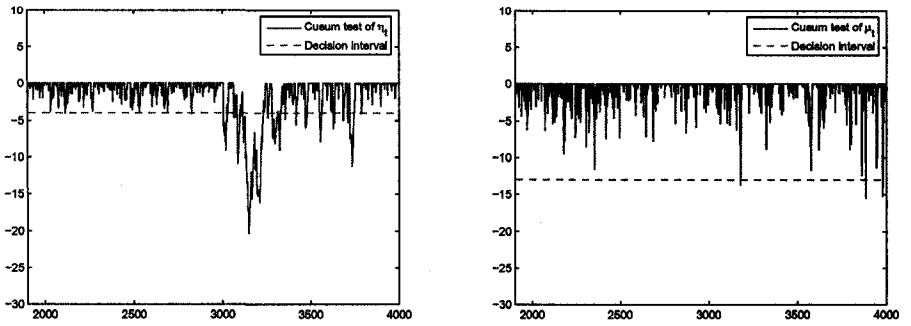

(a) CUSUM test of η_t (algorithm 1) (b) CUSUM test of η_t (algorithm 2)

Figure 5.9: Case 3: Changes in the disturbance dynamics

Case 3. There is an abrupt change at the 3001st data point and $\lambda = 0.97$ after the change, i.e. there is a change in the disturbance dynamics. The result from algorithm 1 is shown in figure 5.9(a) and the result from algorithm 2 is shown in figure 5.9(b). Figure 5.9(a) shows violation of the decision level over a significant time period. This indicates that the process has changed. However, figure 5.9(a) does not tell whether the change is in the plant dynamics or disturbance dynamics. As we explained in Section 5.3, algorithm 1 is sensitive to changes in both plant and disturbance dynamics. Figure 5.9(b) shows that the CUSUM test of μ_t does not indicate any mean shift of μ_t. This means that no change in the plant dynamics has been detected. This is the result that we have expected, because algorithm 2 is only sensitive to changes in plant dynamics and not to changes in disturbance dynamics.

Case 4. There is an abrupt change at the 3001st data point and $K_p = 0.56$, $\lambda = 0.97$ after the change, i.e. there is a change in both plant and disturbance dynamics. The result for this case is very similar to case 2-(2), so we do not show the plots of CUSUM test for brevity.

5.6.2 Fault Detection using the Two Algorithms

This simulation case is to demonstrate the effectiveness of the two algorithms for fault detection. A stiction model from Choudhury *et al.* (2005a) is used to simulate valve stiction. The valve stiction is introduced after the 3001st sample. The procedures of simulation and CUSUM test are the same as previous cases.

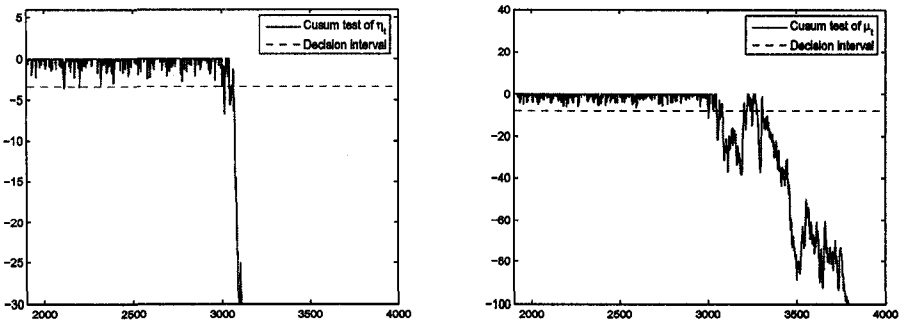

(a) CUSUM test of η_t (algorithm 1) (b) CUSUM test of η_t (algorithm 2)

Figure 5.10: Presence of valve stiction in the process

The result from algorithm 1 is shown in figure 5.10(a) and the result from algorithm 2 is shown in figure 5.10(b). Both figures show persistent violation of the decision level in the presence of valve stiction. Therefore both algorithms are able to successfully detect faults in the valve.

5.7 Pilot Scale Experiment Evaluation

To further evaluate the effectiveness of the proposed algorithms, closed-loop experiments were conducted on a pilot scale tank system shown in figure 5.11. Tank 1 has a constant cross sectional area. Tank 2 has a conical cross section and thus has nonlinear dynamics. The levels of the tanks can be controlled by controllers in the computer through manipulating the pump speed. The liquid flows out of the tanks due to gravity. The sampling interval of the system is 1 second.

5.7.1 Model Validation using the Two Algorithms

Experiment 1. This experiment is designed to demonstrate the effectiveness of the two algorithms for on-line model validation. The level range of tank 2 is 0∼0.3m. A model around level 0.1m is identified:

$$G_{tank2} = \frac{1.0043}{1+59s}e^{-11s} \tag{5.46}$$

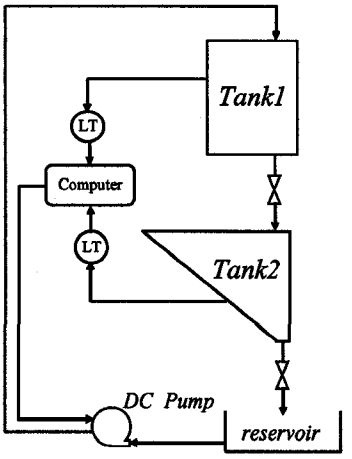

Figure 5.11: Schematic of the tank system

The following model-based PI controller is designed for this process:

$$C_{tank2} = 2 + \frac{0.034}{s} \tag{5.47}$$

There is no control of tank 1 level. The level of tank 2 is controlled at 0.1m at the beginning, then we introduce some step changes of magnitude ±0.02m at the level setpoint (0.1m). At 3001st data point, we change the level setpoint to 0.2m and introduce an extra 4 seconds process delay. A total of 4000 data points are collected. The procedure of CUSUM test is similar as in Section 5.6.

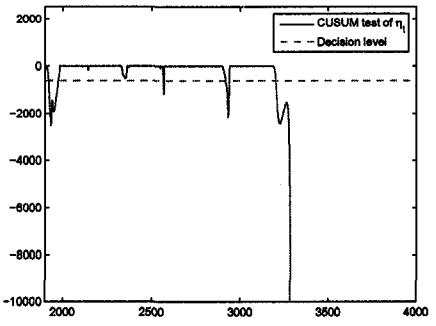

(a) CUSUM test of η_t (algorithm 1)

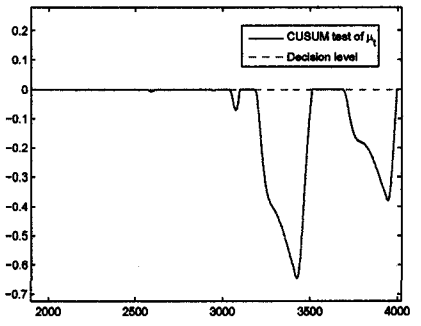

(b) CUSUM test of η_t (algorithm 2)

Figure 5.12: Operating point change in the tank system

As mentioned earlier, tank 2 has a conical cross section. Therefore, changing its operating level will change the process dynamics due to the nonlinearity in the process. We expect that both algorithms will detect the process change. The result from algorithm 1 is shown in figure 5.12(a) and the result from algorithm 2 is shown in figure 5.12(b). Both figures show persistent violation of the decision level after the process change. In other words, both algorithms are able to detect the process change successfully. However, figure 5.12(a) shows false alarms before 3001st data points, while figure 5.12(b) does not. Since algorithm 1 is sensitive to disturbance change, it is quite possible that some unmeasured disturbance during the experiment caused the false alarms in figure 5.12(a). Therefore, in this example, algorithm 2 gives better performance because it is not sensitive to disturbance changes.

5.7.2 Fault Detection using the Two Algorithms

Experiment 2. This experiment is designed to demonstrate the effectiveness of the two algorithms for detection of sensor decalibration. The level range of tank 1 is 0$\sim$0.3m. A model around level at 0.2m has been identified:

$$G_{tank1} = \frac{0.76545}{1 + 31.306s} e^{-s} \tag{5.48}$$

A PI controller based on the above model is designed:

$$C_{tank1} = 10 + \frac{0.235}{s} \tag{5.49}$$

There is no control of tank 2 level. The level of tank 1 is controlled at 0.2m at the beginning, then we introduce some step changes of magnitude $\pm$0.02m at the setpoint (0.2m) of the PI controller in the computer. A fault in sensor decalibration (every measurement is increased by 10%) is introduced at the 3001st data point. This fault is multiplicative in nature. A total of 4000 data points are collected. The procedure for the CUSUM test is similar to the one described in Section 5.6.

The result from algorithm 1 is shown in figure 5.13(a) and the result from algorithm 2 is shown in figure 5.13(b). Both figures show persistent violation of the decision level after the fault due to sensor decalibration. In other words, both algorithms are able to detect the sensor decalibration successfully.

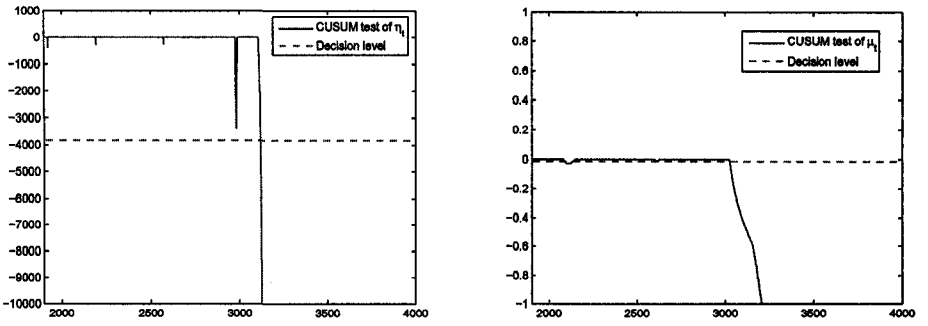

(a) CUSUM test of η_t (algorithm 1) (b) CUSUM test of η_t (algorithm 2)

Figure 5.13: Presence of sensor decalibration in the tank system

5.8 Conclusion

In this chapter, we have developed two algorithms based on the two-model divergence method for model validation and detection of abrupt parameter changes under closed-loop conditions. The frequency domain expressions of the algorithms are derived. It is shown that the algorithms are control relevant, they are sensitive only to those plant changes that significantly affect the sensitivity function under closed-loop conditions. The second algorithm has useful properties: 1) it is not sensitive to changes in disturbance dynamics; 2) it is not sensitive to additive process faults such as sensor offsets. This is helpful in reducing unnecessary alarms for model quality. When there is no plant change, the algorithms can also be applied for detection of multiplicative process faults, e.g. valve stiction and sensor decalibration. The utility of the proposed algorithms have been illustrated by both simulation and experimental applications.

6

Modelling Error Diagnosis under Closed-loop Conditions

This chapter is concerned with detection and diagnosis of modelling error under closed-loop conditions. We first analyze the effect of modelling error on process output error (which is the error between the process output and the simulated output). Then robust stability conditions for on-line model validation are applied. The main premise is that whenever the closed-loop system violates the robust stability condition, it is a sign of significant process change and a signal that the control system may become potentially unstable. We relate the process output error with robust stability conditions and introduce three propositions for on-line model validation. Any process change (or modelling error) that makes the system violate the condition specified by the robust stability theorem can be detected. Simulation examples are presented to demonstrate the applicability of the propositions. We also propose an index to quantify modelling error in frequency domain. Simulation examples and an experimental case study are presented to demonstrate the use of the new index.

6.1 Introduction

Model validation has been an active research area over the last two decades and many methods have been proposed (Söderström and Stoica, 1989; Ljung, 1998). The goal of model validation is to test whether the model is good enough for intended applications. A conventional method (Ljung, 1998), under open loop conditions, is based on residual analysis which includes whiteness tests of the residual (by examining its autocorrelation) and independence tests between residual and past inputs (by examining cross-correlation between them). Many other methods, such as model validation based on local approach (Basseville *et al.*, 1987; Zhang *et al.*, 1994; Huang, 2000) in a prediction error identification framework (Gevers *et al.*, 2003) and recursive algorithms for detection of model changes (Lai and Shan, 1999) have also been proposed.

Robust control design methods have pointed to the need for reliable modelling error bounds. For linear models, such model error bounds are preferably described in the frequency domain. A large volume of literature has been published in this area, e.g., Goodwin and Salgado (1989), Goodwin *et al.* (1992), Wahlberg and Ljung (1992), Kosut *et al.* (1992*b*) and Kosut *et al.* (1992*a*). The theoretical results therein provide techniques for designing closed-loop systems which are theoretically robust. One of the important robustness tools that examine the stability of a system in the presence of modelling error is the robust stability theorem (Goodwin *et al.*, 2001), which is also known as small-gain theorem (Zames, 1966; Doyle *et al.*, 1992). The robust stability theory provides a sufficient condition for stability of closed-loop systems.

The objectives of this chapter are: (1) analysis of the effect of modelling error on closed loop output error; (2) development of on-line model validation schemes with consideration for robust stability; and (3) quantification of modelling error in the frequency domain. The motivation is to demonstrate the impact of modelling error on robust control theory and thus provide a new perspective on the role of output error analysis. The remainder of this chapter is organized as follows: Section 6.2 outlines the preliminaries required for further analysis in this chapter. This includes introduction to conventional feedback control, internal model control (IMC), robust stability theory, and some common norms used for signals and systems. Section 6.3 focusses on analyzing the effect of modelling error on closed loop output error.

Specifically, we explore the relationship between output error and modelling error and derive bounds on output error variance. In Section 6.4, we relate output error with the robust stability theorem and propose three propositions for on-line model validation. All the propositions use the robust stability theorem as a criterion to detect significant process changes (or in other words, modelling error). A detection test is provided to alert any process change (or modelling error) that makes the system no longer satisfy the condition specified by the robust stability theorem. Simulation examples are presented to demonstrate the applicability of the propositions. Section 6.5 discusses modelling error in the frequency domain and proposes an index to quantify the extent of modelling error. Simulation and experimental examples are presented to show the effectiveness of the quantification of modelling error. This chapter ends with concluding remarks in Section 6.6.

6.2 Preliminaries

Figure 6.1 shows a standard process under feedback control, where C is the controller transfer function, G is the process transfer function, N is the disturbance transfer function, and a is a white noise sequence with zero mean ($d = Na$ is the unmeasured disturbance affecting the process). In this chapter, we assume r and d is independent. For the sake of brevity and convenience, the operator s in the transfer function is omitted.

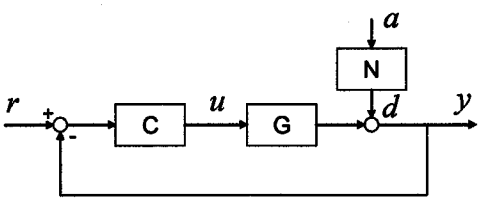

Figure 6.1: General feedback control framework

It follows from figure 6.1 that

$$y = \frac{GC}{1+GC}r + \frac{1}{1+GC}Na = Tr + SNa \tag{6.1}$$

where $S = \frac{1}{1+GC}$ is the achieved (or true) sensitivity function and $T = \frac{GC}{1+GC}$ is the

achieved complementary sensitive function. From the definitions of S and T, it is well known that

$$S + T = 1$$

Ideally, we should have S as small as possible for a control system to have good disturbance rejection performance and T close to unity to achieve good tracking performance. However this ideal property is difficult to achieve over the entire frequency range because of system limitations, such as right half plane zeros, input constraints, and process uncertainty. For process control systems, most setpoint changes and undesirable disturbances usually occur at low frequencies, and therefore controllers are often designed such that S is small at low frequencies (consequently T is close to 1) and T is small at high frequencies. A more detailed discussion on robust design issues can be found in Goodwin *et al.* (2001) and Skogestad and Postlethwaite (1996).

6.2.1 Modified Feedback Structure

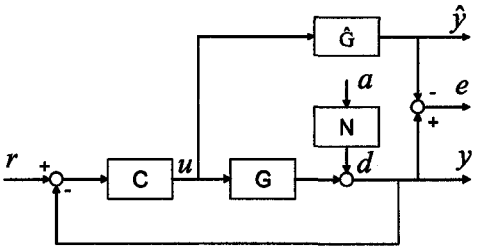

Figure 6.2: Modified feedback control framework

In practice, the true process transfer function G is generally of high order and is not exactly known. Generally a reduced complexity model is desired for which the true process, G, is represented by a low order model, $\hat{G}$, typically obtained from an identification experiment. To monitor the error between the true process and the estimated lower order model, consider the setup shown in figure 6.2, where $e = y - \hat{y}$, is the output error. In the modified feedback structure, $\hat{y} = \hat{G}u$ is the simulation output as defined in Ljung (1998).

The controller C is usually designed based on the identified model $\hat{G}$ with consideration for the shape of $\hat{S}$ and $\hat{T}$ over the frequency range of interest (Skogestad and

Postlethwaite, 1996). $\hat{G}$ is denoted as a nominal model, then the nominal sensitivity function and nominal complementary sensitively function are defined as

$$\hat{S} = \frac{1}{1+\hat{G}C} \tag{6.2}$$

$$\hat{T} = \frac{\hat{G}C}{1+\hat{G}C} \tag{6.3}$$

An useful expression for the output error e, that can be derived from figure 6.2 is

$$e = \frac{(G-\hat{G})C}{1+GC}r + \frac{1+\hat{G}C}{1+GC}Na \tag{6.4}$$

This expression reveals the relationship among the output error e, setpoint activity r and unmeasured disturbance d. For example, when there is no modelling error ($\hat{G} = G$), the output error e is equal to unmeasured disturbance d. More discussion on the output error and modelling error expressions will be presented in the later sections of this chapter.

6.2.2 IMC Feedback Structure

The modified feedback structure, shown in figure 6.2, has a close relationship with the IMC feedback structure shown in figure 6.3. The IMC framework provides a way of re-parameterizing the conventional controller (Morari and Zafiriou, 1989) and the IMC controller Q is related to the conventional controller C through the expression

$$Q = \frac{C}{1+\hat{G}C} \tag{6.5}$$

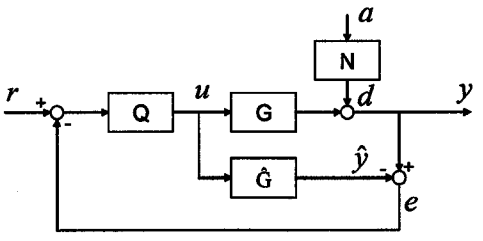

Figure 6.3: IMC feedback structure

The nominal sensitivity and complimentary sensitivity functions can also be expressed in terms of Q as

$$\hat{T} = Q\hat{G}, \quad \hat{S} = 1 - Q\hat{G}$$

6.2.3 Robust Stability Theorem

As mentioned earlier the true model of a real process is usually of high order, whereas the estimated model is usually a low order approximation of the dominant dynamics of the high order process. In other words, modelling error is inevitable in reality. There are two alternative ways of representing a modelling errors: additive modelling error and multiplicative modelling error (Goodwin *et al.*, 2001). Δ_a in Eq.(6.6) is defined as additive modelling error and Δ_m in Eq.(6.7) is defined as the multiplicative modelling error.

$$G = \hat{G} + \Delta_a \tag{6.6}$$

$$G = \hat{G}(1 + \Delta_m) \tag{6.7}$$

Since modelling error is inevitable in reality, it is important to ensure that the controller designed based on the nominal model can achieve stability when it is applied to the real process. With the presence of modelling error, a sufficient condition for a feedback loop to be robustly stable is given in the following theorem (Goodwin *et al.* (2001)):

Theorem 6.1 ***Robust stability theorem:*** Consider a plant with nominal transfer function $\hat{G}(s)$ and true transfer function given by $G(s)$. Assume that $C(s)$ is the transfer function of a controller that achieves nominal internal stability for the designed loop. Also assume that $G(s)C(s)$ and $\hat{G}(s)C(s)$ have the same number of unstable poles. Then, a sufficient condition for stability of the true feedback loop obtained by applying the controller to the true plant is that

$$|\hat{T}(j\omega)||\Delta_m(j\omega)| < 1 \qquad \forall\omega \tag{6.8}$$

where $\hat{T}(j\omega)$ and $\Delta_m(j\omega)$ are the frequency responses of $\hat{T}$ and Δ_m at frequency ω.

Remark 6.2.1 *For model validation, or model-plant mismatch detection, it is equivalent to indicating whether the magnitude of Δ_m is significantly large; or for more practical purposes, whether Δ_m is significantly different from the tolerable control range.*

6.2.4 Signal Norms and System Norms

Throughout the remainder of this chapter, the 2-norm is used as a measure of the magnitude of a signal and the H_∞ norm is used as a measure of the size of a system, such as the sensitivity function. Here we give a brief introduction of these norms.

For a signal u, the 2-norm is defined as:

$$2-norm \quad : \quad \|u\|_2 = [u(0)^2 + u(1)^2 + u(2)^2 + ...]^{1/2} \tag{6.9}$$

For a linear time invariant system G, the H_∞ norm is defined as (Skogestad and Postlethwaite, 1996):

$$H_\infty \; norm \quad : \quad \|G(s)\|_\infty = \sup_\omega |G(j\omega)|$$

6.3 Effects of Modelling Error on Output Error

As shown in Eq.(6.4), the output error expression $e = y - \hat{y}$ equals the unmeasured disturbance when there is no modelling error. However, uncertainty or modelling error always exists in practice. Patwardhan and Shah (2002) have discussed the effect of modelling error on control performance. The objective of this section is to quantify the effect of modelling error on the output error e. We will concentrate on the analysis of stable systems which satisfy the robust stability theorem. For unstable systems, the output error $e = y - \hat{y}$ will be unstable because of the instability of the system, and it is easy to detect the instability by simply plotting the output y or the output error e.

6.3.1 Effect of Multiplicative Modelling Error

First we consider the multiplicative modelling error as defined in equation (6.7). The following lemma reveals the relationship between the output error and multiplicative modelling error.

Lemma 6.1 *If $\hat{S} = \frac{1}{1+\hat{G}C}$ is denoted the nominal sensitivity, $\hat{T} = \frac{\hat{G}C}{1+\hat{G}C}$ the nominal complementary sensitivity, and Δ_m the multiplicative modelling error, such that $G = \hat{G}(1+\Delta_m)$, then the following equation holds:*

$$e = \frac{\hat{T}\Delta_m}{1+\hat{T}\Delta_m} r + \frac{1}{1+\hat{T}\Delta_m} Na \tag{6.10}$$

Proof.

$$\begin{aligned} e &= \frac{(G-\hat{G})C}{1+GC} r + \frac{1+\hat{G}C}{1+GC} Na \\ &= \frac{\hat{G}\Delta_m C}{1+GC} r + \frac{1+C(G-\hat{G}\Delta_m)}{1+GC} Na \\ &= \frac{\hat{G}C}{1+GC}\Delta_m r - \frac{\hat{G}C}{1+GC}\Delta_m Na + Na \end{aligned} \tag{6.11}$$

Denote $S_e = \frac{1}{1+\hat{T}\Delta_m}$, and it is known that $S = \hat{S}S_e$ (Goodwin *et al.*, 2001). Then we have

$$\begin{aligned} \frac{\hat{G}C}{1+GC}\Delta_m &= SC\hat{G}\Delta_m \\ &= \hat{S}S_e\hat{G}C\Delta_m \\ &= (\hat{S}\hat{G}C)\Delta_m S_e \\ &= \hat{T}\Delta_m S_e \\ &= \frac{\hat{T}\Delta_m}{1+\hat{T}\Delta_m} \end{aligned} \tag{6.12}$$

Substituting equation (6.12) into equation (6.11), we have

$$\begin{aligned} e &= \frac{\hat{T}\Delta_m}{1+\hat{T}\Delta_m} r - \frac{\hat{T}\Delta_m}{1+\hat{T}\Delta_m} Na + Na \\ &= \frac{\hat{T}\Delta_m}{1+\hat{T}\Delta_m} r + \frac{1}{1+\hat{T}\Delta_m} Na \end{aligned}$$

□

Comparing equation (6.1) and (6.10), we can observe that the structure of these two equations are very similar. We can consider equation (6.10) as the transfer function of a closed-loop system shown in figure 6.4. The signal after the $\hat{T}$ block is the actual u from the closed-loop system (figure 6.1) filtered by $\hat{G}$.

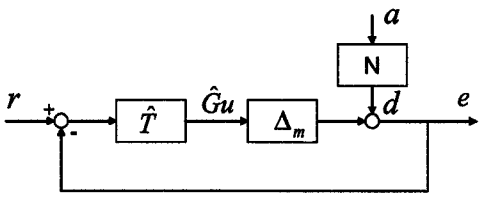

Figure 6.4: Feedback structure for output error with multiplicative modelling error

In figure 6.4, Δ_m is the unknown part and $\hat{T}$ is the designed part. Therefore, at the controller design stage, we have to ensure that the designed $\hat{T}$ will stabilize the feedback loop with output error, e, as the output. The robust stability theorem 6.1 ($|\hat{T}\Delta_m| < 1$) apparently provides a sufficient condition to achieve stability. So equation (6.10) provides another perspective for the proof and an interesting interpretation of the robust stability theorem.

Remark 6.3.1 *According to control theory, $\hat{T}$ is usually designed to have a large gain (close to 1) at low frequencies and small gain ($\ll$ 1) at high frequencies. Equation* (6.10) *shows that low frequency modelling errors will affect the process without being attenuated by $\hat{T}$, while the effect of high frequency modelling error will be attenuated because of the low gain of $\hat{T}$ at high frequency. This observation concurs with the identification and control experience in which the accuracy of the low frequency part of a model has to be emphasized as it is relatively more important than the accuracy of the high frequency part. In this respect, Lemma* 6.1 *provides a different perspective for the diagnosis of modelling error.*

When there is no setpoint activity, equation (6.10) can be simplified as:

$$e = \frac{1}{1+\hat{T}\Delta_m} Na = \frac{1}{1+\hat{T}\Delta_m} d \tag{6.13}$$

It is clear that when $\Delta_m = 0$, $e = d$. In other words, when there is no modelling error, the output error equals the unmeasured disturbance which is the part that can not be predicted by the model.

Theorem 6.2 *In the case that there is no setpoint change, i.e. for the regulatory case, the bounds on the ratio of the output error variance to the disturbance variance are given by*

$$\frac{1}{(1+\left\|\hat{T}\Delta_m\right\|_\infty)^2} \leq \frac{Var(e)}{Var(d)} \leq \frac{1}{(1-\left\|\hat{T}\Delta_m\right\|_\infty)^2} \tag{6.14}$$

Proof. Applying Parseval's Theorem to equation (6.13) we have:

$$\begin{aligned} Var(e) &= \frac{\sigma_a^2}{2\pi}\int_0^{2\pi}\left|\frac{1}{1+\hat{T}\Delta_m}\right|^2|N|^2d\omega \\ &\leq \frac{\sigma_a^2}{2\pi}\int_0^{2\pi}\left\|\frac{1}{1+\hat{T}\Delta_m}\right\|_\infty^2|N|^2d\omega \\ &= \left\|\frac{1}{1+\hat{T}\Delta_m}\right\|_\infty^2 Var(d) \end{aligned} \tag{6.15}$$

Similarly, we can get the following lower bound,

$$\begin{aligned} Var(e) &= \frac{\sigma_a^2}{2\pi}\int_0^{2\pi}\left|\frac{1}{1+\hat{T}\Delta_m}\right|^2|N|^2d\omega \\ &\geq \frac{\sigma_a^2}{2\pi}\int_0^{2\pi}\frac{1}{\left\|1+\hat{T}\Delta_m\right\|_\infty^2}|N|^2d\omega \\ &= \frac{1}{\left\|1+\hat{T}\Delta_m\right\|_\infty^2}Var(d) \end{aligned} \tag{6.16}$$

Therefore, in the time domain the ratio of prediction error variance to disturbance variance is bounded as:

$$\frac{1}{\left\|1+\hat{T}\Delta_m\right\|_\infty^2} \leq \frac{Var(e)}{Var(d)} \leq \left\|\frac{1}{1+\hat{T}\Delta_m}\right\|_\infty^2 \tag{6.17}$$

For the case when $\|\hat{T}\Delta_m\|_\infty < 1$, the bound can be further simplified and expressed in terms of $\|\hat{T}\Delta_m\|_\infty$:

$$\frac{1}{(1+\left\|\hat{T}\Delta_m\right\|_\infty)^2} \leq \frac{Var(e)}{Var(d)} \leq \frac{1}{(1-\left\|\hat{T}\Delta_m\right\|_\infty)^2} \qquad \square$$

6.3.2 Effect of Additive Modelling Error

Lemma 6.1 and Theorem 6.2 reveal the relationship between the multiplicative modelling error and the output error. Now we consider the effect of additive modelling error on the output error.

Lemma 6.2 *If we denote:* $Q = \frac{C}{1+\hat{G}C}$ *as the IMC controller, and* Δ_a *as the additive modelling error, such that* $G = \hat{G} + \Delta_a$*, then the following equation holds:*

$$e = \frac{Q\Delta_a}{1+Q\Delta_a}r + \frac{1}{1+Q\Delta_a}Na \tag{6.18}$$

Proof. The multiplicative modelling error is in the form of

$$G = \hat{G}(1+\Delta_m)$$

The additive modelling error is related to the multiplicative modelling error by

$$\Delta_a = \hat{G}\Delta_m$$

The relationship between the nominal complementary sensitivity function and the IMC controller is

$$\hat{T} = Q\hat{G}$$

Then, we have:

$$Q\Delta_a = Q\hat{G}\Delta_m = \hat{T}\Delta_m$$

Therefore $\hat{T}\Delta_m$ in equation (6.10) can be replaced by $Q\Delta_a$, and we get equation (6.18). $\square$

Again, we can see that equation (6.1) and (6.18) have the similar structure. We can consider equation (6.18) as a transfer function of a closed-loop system shown in

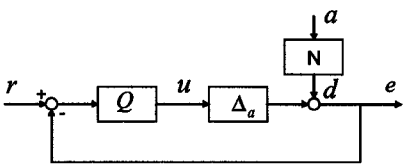

Figure 6.5: Feedback structure for output error with additive modelling error

figure 6.5. The signal after the Q block is the actual u from the closed-loop system (figure 6.1).

From equation (6.10) and (6.18), we define the output error sensitivity function S_e and the output error complementary sensitivity function T_e as follows:

$$S_e \triangleq \frac{1}{1+\hat{T}\Delta_m} = \frac{1}{1+Q\Delta_a} \tag{6.19}$$

$$T_e \triangleq \frac{\hat{T}\Delta_m}{1+\hat{T}\Delta_m} = \frac{Q\Delta_a}{1+Q\Delta_a} \tag{6.20}$$

These two functions reveal the relationship among the output error e, setpoint r and unmeasured disturbance d.

Remark 6.3.2 *Lemmas 6.1 and 6.2 allow us to express the output error as the output of a closed-loop system with appropriately designed sensitivity and complementary sensitivity functions. The main difference in handling the two classes of errors is the 'control block' ($\hat{T}$ for multiplicative modelling error in figure* 6.4 *and Q for additive modelling error in figure* 6.5*).*

Theorem 6.3 *In the case that there is no setpoint change, i.e. for the regulatory case, the bounds on the ratio of the output error variance to the disturbance variance are given by*

$$\frac{1}{(1+\|Q\Delta_a\|_\infty)^2} \leq \frac{Var(e)}{Var(d)} \leq \frac{1}{(1-\|Q\Delta_a\|_\infty)^2} \tag{6.21}$$

Proof. Replace $\hat{T}\Delta_m$ in equation (6.14) by $Q\Delta_a$, and we get equation (6.21). □

Remark 6.3.3 *It is interesting to observe from Theorems* 6.2 *and* 6.3 *that the output error variance can actually be smaller than the disturbance variance. In other words, it is possible that the modelling error will improve the control performance in terms of output error variance.*

6.3.3 Extension to the Multivariate Case

For the multivariate case, similar results can be derived based on the definition of the 2-norm. We now denote

$$\begin{aligned} \Delta_a &= G - \hat{G} \\ \Delta_m &= G\hat{G}^{-1} - I \end{aligned}$$

as additive modelling and multiplicative modelling errors respectively of multivariate systems.

Corollary 6.1 *For multivariate systems, in the case that there is no setpoint change, i.e. the regulatory case, the ratio of the output error 2-norm to the disturbance 2-norm is bounded by*

$$\frac{1}{(1+\bar{\sigma}(\Delta_a Q))^2} \leq \frac{\|e\|_2^2}{\|d\|_2^2} \leq \frac{1}{(1-\bar{\sigma}(\Delta_a Q))^2} \tag{6.22}$$

$$\frac{1}{(1+\bar{\sigma}(\Delta_m \hat{T}))^2} \leq \frac{\|e\|_2^2}{\|d\|_2^2} \leq \frac{1}{(1-\bar{\sigma}(\Delta_m \hat{T}))^2} \tag{6.23}$$

Proof. For the IMC feedback structure, we have

$$e = \Delta_a Q(I + \Delta_a Q)^{-1} r + (I + \Delta_a Q)^{-1} d \tag{6.24}$$

For the case of multiplicative modelling error with the standard feedback structure, we have

$$e = \Delta_m \hat{T}(I + \Delta_m \hat{T})^{-1} r + (I + \Delta_m \hat{T})^{-1} d \tag{6.25}$$

For the case when there are no setpoints changes,

$$\begin{aligned} e &= (I + \Delta_a Q)^{-1} d \\ &= (I + \Delta_m \hat{T})^{-1} d \end{aligned}$$

Following the proof for Theorem 6.3 and the definition of the ∞ norm, we get

$$\begin{aligned} \frac{1}{\|I + \Delta_a Q\|_\infty^2} \leq \frac{\|e\|_2^2}{\|d\|_2^2} \leq \left\| \frac{1}{I + \Delta_a Q} \right\|_\infty^2 \\ \frac{1}{\|I + \Delta_m \hat{T}\|_\infty^2} \leq \frac{\|e\|_2^2}{\|d\|_2^2} \leq \left\| \frac{1}{I + \Delta_m \hat{T}} \right\|_\infty^2 \end{aligned}$$

For stable systems with $\bar{\sigma}(\Delta_a Q) < 1$ ($\bar{\sigma}(\Delta_m \hat{T}) < 1$), we have

$$\begin{aligned} \frac{1}{(1 + \bar{\sigma}(\Delta_a Q))^2} \leq \frac{\|e\|_2^2}{\|d\|_2^2} \leq \frac{1}{(1 - \bar{\sigma}(\Delta_a Q))^2} \\ \frac{1}{(1 + \bar{\sigma}(\Delta_m \hat{T}))^2} \leq \frac{\|e\|_2^2}{\|d\|_2^2} \leq \frac{1}{(1 - \bar{\sigma}(\Delta_m \hat{T}))^2} \end{aligned}$$

6.4 Control Relevant On-line Model Validation using Robust Stability Conditions

The objective of good controller design is to optimize process performance under closed-loop conditions. Depending on the nature of the process and the control objective, one can choose different design objectives. It is possible that several controllers can satisfy the same design objective. A basic yet important requirement included in all design objectives is the stability of the closed-loop system. All designed and implemented controllers should ensure stability.

It is no longer a difficult task to design a good controller based on an accurate model. Many books and papers discuss issues of control system design (Skogestad and Postlethwaite, 1996; Goodwin *et al.*, 2001). In industry, most controllers are able to deliver satisfactory performance when initially implemented. However, it is frequently observed that control performance often degrades with time. The main reason of performance degradation is that the process dynamics change and the identified model

no longer fits the process (Qin, 1998). How to continually validate the model and give early warnings of an inadequate model to prevent unnecessary plant showdown or even catastrophic accident is important.

The objective of on-line model validation is to determine whether the process has changed significantly and therefore whether the existing controller is still suitable to control the system. An important task for on-line model validation is to choose reasonable criteria to validate the model. The model validation methods in Söderström and Stoica (1989) and Ljung (1998) are suitable for checking the adequacy of a model during the identification stage; the main objective there is to check if the model fits the collected experiment data. These methods are not suitable for on-line model validation as they need a long data set. In this work, the robust stability theorem 6.1 is used as a preferred model validation criterion for continuously monitoring model quality. Whenever the closed-loop system violates the robust stability theorem, it is a sign of significant process change and a signal that the control system could become potentially unstable. The main contribution of this section is the application of the robust stability theorem into on-line model validation criterion *without* having to estimate the model error.

Proposition 6.4.1 *A process is considered to have changed significantly and one should reject the identified model if at any frequency* ω

$$\frac{|Q(jw)|^2(\gamma\Phi_e(\omega) - \frac{\gamma}{1-\gamma}\Phi_d(\omega))}{\Phi_u(\omega)} > 1 \tag{6.26}$$

where $Q = C(1+\hat{G}C)^{-1}$, e *is the output error as shown in figures* 6.2 *and* 6.3, u *is the plant input,* d *is the disturbance affecting the process, and* $\Phi.(\omega)$ *is interpreted as the power spectrum at frequency* ω. γ *is a user defined variable which must be chosen within the range* $0 < \gamma < 1$.

Derivation. Consider the IMC feedback structure in figure 6.3, the following relationship holds:

$$\begin{aligned} e &= Gu + d - \hat{G}u \\ &= (G - \hat{G})u + d \\ &= \Delta_a u + d \end{aligned} \tag{6.27}$$

Multiplying both sides with Q and rearranging the equation, we have

$$Q(e - d) = Q\Delta_a u \tag{6.28}$$

According to the robust stability theorem, a sufficient condition for stability of a linear system is $|Q(j\omega)||\Delta_a(j\omega)| < 1$ for all ω, or equivalently, $|Q(j\omega)|^2|\Delta_a(j\omega)|^2\Phi_u(\omega) < \Phi_u(\omega)$ for all ω. Therefore, a necessary condition for instability is $|Q(j\omega)|^2|\Delta_a(j\omega)|^2\Phi_u(\omega) > \Phi_u(\omega)$ for one or some ω.

In the frequency domain, equation (6.28) implies

$$|Q(j\omega)|^2\Phi_{e-d}(\omega) = |Q(j\omega)|^2|\Delta_a(j\omega)|^2\Phi_u(\omega) \tag{6.29}$$

Thus, a necessary condition for instability is

$$|Q(j\omega)|^2\Phi_{e-d}(\omega) > \Phi_u(\omega) \quad \textit{for one or some } \omega \tag{6.30}$$

A restriction on applying equation (6.30) to detect possible instability issues is that disturbance d is unmeasured in the real world, and therefore we can not calculate $\Phi_{e-d}(\omega)$. We need to further extend this equation. Using equation (6.10), we can show that the following inequality holds for systems satisfying the robust stability theorem (proof follows this derivation)

$$\Phi_{e-d}(\omega) > \gamma\Phi_e(\omega) - \frac{\gamma}{1-\gamma}\Phi_d(\omega) \quad \textit{for } 0 < \gamma < 1 \tag{6.31}$$

Therefore, the following inequality

$$\frac{|Q(jw)|^2(\gamma\Phi_e(\omega) - \frac{\gamma}{1-\gamma}\Phi_d(\omega))}{\Phi_u(\omega)} > 1 \quad \textit{for one or some } \omega$$

is an indication of significant model change and a signal that the current feedback control system can not satisfy the robust stability theorem. □

Proof of inequality (6.31)

Based on the expression in equation (6.10), one can express $\Phi_{e-d}(\omega)$ and $\gamma\Phi_e(\omega) - \frac{\gamma}{1-\gamma}\Phi_d(\omega)$ as

$$\Phi_{e-d}(\omega) = \left|\frac{\hat{T}(j\omega)\Delta_m(j\omega)}{1+\hat{T}(j\omega)\Delta_m(j\omega)}\right|^2 \Phi_r(\omega) + \left|\frac{\hat{T}(j\omega)\Delta_m(j\omega)}{1+\hat{T}(j\omega)\Delta_m(j\omega)}\right|^2 \Phi_d(\omega)$$

$$\begin{aligned} & \gamma\Phi_e(\omega) - \frac{\gamma}{1-\gamma}\Phi_d(\omega) \\ = \; & \gamma\left|\frac{\hat{T}(j\omega)\Delta_m(j\omega)}{1+\hat{T}(j\omega)\Delta_m(j\omega)}\right|^2 \Phi_r(\omega) + \left[\gamma\left|\frac{1}{1+\hat{T}(j\omega)\Delta_m(j\omega)}\right|^2 - \frac{\gamma}{1-\gamma}\right]\Phi_d(\omega) \end{aligned}$$

Since $\hat{T}(j\omega)\Delta_m(j\omega)$ can be a complex number, we assume $\hat{T}(j\omega)\Delta_m(j\omega) = a + bi$ where a and b are real numbers. For systems satisfying the robust stability theorem ($|\hat{T}(j\omega)\Delta_m(j\omega)| < 1$), it is easy to show that $|a| < 1$ and $|b| < 1$. Denote $A = (1-\gamma)\left|\frac{\hat{T}(j\omega)\Delta_m(j\omega)}{1+\hat{T}(j\omega)\Delta_m(j\omega)}\right|^2 \Phi_r(\omega)$ and $A \geq 0$ since $0 < \gamma < 1$. Then

$$\begin{aligned} & \Phi_{e-d}(\omega) - \left[\gamma\Phi_e(\omega) - \frac{\gamma}{1-\gamma}\Phi_d(\omega)\right] \\ = \; & \left[\left|\frac{\hat{T}(j\omega)\Delta_m(j\omega)}{1+\hat{T}(j\omega)\Delta_m(j\omega)}\right|^2 - \gamma\left|\frac{1}{1+\hat{T}(j\omega)\Delta_m(j\omega)}\right|^2 + \frac{\gamma}{1-\gamma}\right]\Phi_d(\omega) + A \\ = \; & \left(|\hat{T}(j\omega)\Delta_m(j\omega)|^2 - \gamma + \frac{\gamma}{1-\gamma}|1+\hat{T}(j\omega)\Delta_m(j\omega)|^2\right)\frac{\Phi_d(\omega)}{|\hat{T}(j\omega)\Delta_m(j\omega)|^2} + A \\ = \; & \left(a^2+b^2-\gamma+\frac{\gamma}{1-\gamma}(1+a)^2+\frac{\gamma}{1-\gamma}b^2\right)\frac{\Phi_d(\omega)}{(1+a)^2+b^2} + A \\ = \; & \left(\frac{1}{1-\gamma}(a+\gamma)^2+\frac{1}{1-\gamma}b^2\right)\frac{\Phi_d(\omega)}{(1+a)^2+b^2} + A > 0 \quad \textit{for } 0<\gamma<1 \end{aligned}$$

Therefore, for systems satisfying the robust stability theorem, $\Phi_{e-d}(\omega) > \gamma\Phi_e(\omega) - \frac{\gamma}{1-\gamma}\Phi_d(\omega)$ when $0 < \gamma < 1$. □

Remark 6.4.1 *When $\gamma \to 0$, $\gamma\Phi_e(\omega) - \frac{\gamma}{1-\gamma}\Phi_d(\omega) \approx \gamma(\Phi_e(\omega) - \Phi_d(\omega)) \to 0$, it will be difficult for proposition 6.4.1 to detect the process change because the numerator is close to 0. When $\gamma \to 1$, $\gamma\Phi_e(\omega) - \frac{\gamma}{1-\gamma}\Phi_d(\omega) \approx \Phi_e(\omega) - \infty \cdot \Phi_d(\omega)$, it will also be difficult for 6.4.1 to detect the process change because the numerator may be smaller*

than 0 at all frequencies. We recommend choosing γ from a range between $0.4 \sim 0.6$. These remarks also apply to the proposition 6.4.3 which will be proposed shortly. In the simulation examples in Section 6.4.1, we choose $\gamma = 0.5$.

Remark 6.4.2 *As shown in equation* (6.10)*, when there is no modelling error, $e = d$. So a good time to estimate $\Phi_d(\omega)$ is when the process model is considered to be adequate, as for example during the commissioning phase. Additionally, as shown in equation* (6.13)*, no setpoint activity will also help in estimating $\Phi_d(\omega)$ using $\Phi_e(\omega)$ even with small modelling errors.*

Remark 6.4.3 *To further simplify the calculation, one can use an upper bound of the power spectrum of the bounded disturbance in equation* (6.26) *instead of $\Phi_d(\omega)$.*

Proposition 6.4.1 can be used for either open-loop or closed-loop conditions. It is interesting that we can test the stability of the closed-loop system without the designed controller implemented. A possible difficulty is that we have to estimate $\Phi_d(\omega)$. To circumvent the need to estimate $\Phi_d(\omega)$, the following proposition is proposed.

Proposition 6.4.2 *A process is considered to have changed significantly and one should reject the identified model if, at any frequency ω*

$$\frac{|Q(jw)||\Phi_{er}(\omega)|}{|\Phi_{ur}(\omega)|} > 1 \tag{6.32}$$

where $Q = C(1 + \hat{G}C)^{-1}$, e is the output error in figure 6.2 *and* 6.3*, r is the process setpoint, d is the disturbance affecting the process, and $\Phi_{er}(\omega)$ is interpreted as the cross power spectrum between signals e and r at frequency ω.*

Derivation. Rewrite equation (6.28) as

$$Qe = Q\Delta_a u + Qd \tag{6.33}$$

It is reasonable to assume that the process setpoint r is independent of the unmeasured disturbance d. Therefore the above equation can be expressed in the frequency domain as

$$|Q(jw)||\Phi_{er}(\omega)| = |Q(jw)||\Delta_a(jw)||\Phi_{ur}(\omega)| \tag{6.34}$$

The robust stability theorem indicates that a sufficient condition for stability is

$$|Q(jw)||\Delta_a(jw)||\Phi_{ur}(\omega)| < |\Phi_{ur}(\omega)| \quad for\ all\ \omega$$

Therefore a necessary condition for instability is

$$|Q(jw)||\Delta_a(jw)||\Phi_{ur}(\omega)| > |\Phi_{ur}(\omega)| \quad for\ one\ or\ some\ \omega$$

equivalently,

$$|Q(jw)||\Phi_{er}(\omega)| > |\Phi_{ur}(\omega)| \quad for\ one\ or\ some\ \omega$$

In other words, the inequality $\frac{|Q(jw)||\Phi_{er}(\omega)|}{|\Phi_{ur}(\omega)|} > 1$ for one or some ω indicates significant process change and gives a warning that the current feedback control system is unable to satisfy the robust stability theorem. □

Compared to proposition 6.4.1, proposition 6.4.2 does not need an estimate of $\Phi_d(\omega)$ and, more importantly, it can be evaluated from the closed-loop system. Both propositions involve the frequency response of $Q(j\omega)$ which may not be available in many cases. The following proposition is given for the cases where $Q(j\omega)$ is not available or difficult to estimate.

Proposition 6.4.3 *A process is considered to have changed significantly and one should reject the identified model if at any frequency* ω

$$\frac{\gamma\Phi_e(\omega) - \frac{\gamma}{1-\gamma}\Phi_d(\omega)}{\Phi_{r-e}(\omega)} > 1 \tag{6.35}$$

where e *is the output error shown in figure* 6.2 *and* 6.3, r *is the process setpoint, and* d *is the disturbance affecting the process.* γ *is a user defined variable which must be chosen within the range* $0 < \gamma < 1$.

Derivation. Rewrite equation (6.18) as

$$Q\Delta_a(r-e) = e - d \tag{6.36}$$

and in the frequency domain

$$|Q(j\omega)|^2|\Delta_a(j\omega)|^2\Phi_{r-e}(\omega) = \Phi_{e-d}(\omega) \tag{6.37}$$

The robust stability theorem indicates that a sufficient condition for stability is

$$|Q(jw)|^2|\Delta_a(jw)|^2\Phi_{r-e}(\omega) < \Phi_{r-e}(\omega) \quad for\ all\ \omega$$

Therefore a necessary condition for instability is

$$|Q(jw)|^2|\Delta_a(jw)|^2\Phi_{r-e}(\omega) > \Phi_{r-e}(\omega) \quad for\ one\ or\ some\ \omega$$

equivalently,

$$\Phi_{e-d}(\omega) > \Phi_{r-e}(\omega) \quad for\ one\ or\ some\ \omega$$

For systems that satisfy the robust stability theorem, the following inequality holds

$$\Phi_{e-d}(\omega) > \gamma\Phi_e(\omega) - \frac{\gamma}{1-\gamma}\Phi_d(\omega) \quad for\ 0 < \gamma < 1$$

So $\gamma\Phi_e(\omega) - \frac{\gamma}{1-\gamma}\Phi_d(\omega) > \Phi_{r-e}(\omega)$ guarantees $\Phi_{e-d}(\omega) > \Phi_{r-e}(\omega)$. In other words, $\frac{\gamma\Phi_e(\omega) - \frac{\gamma}{1-\gamma}\Phi_d(\omega)}{\Phi_{r-e}(\omega)} > 1$ for one or some ω is a signature of significant process changes and gives the signal that the current feedback control system can not satisfy the robust stability theorem. □

Remark 6.4.4 *The robust stability theorem* 6.1 *describes a sufficient condition for stability and violation of such condition does not necessarily indicate instability. Accordingly, propositions* 6.4.1 *to* 6.4.3 *are proposed to indicate model changes, not for testing of instability. A value larger than 1 indicates significant process changes, and does not necessarily indicate that the system is unstable. We now present two detailed examples to illustrate the proposed methodology.*

6.4.1 Simulation Examples

In this sub-section, we show simulation results of the three propositions.

Example 1

In a feedback control loop, the identified model is

$$\hat{G} = \frac{1}{s^2 + s}$$

and the designed controller is

$$C = \frac{0.5}{s+1}$$

Suppose that the true plant model is

$$G = \frac{1}{s^2+s}e^{-\tau s}$$

and the time delay τ may change with time. The time delay change will introduce a phase change equal to $-\omega\tau$, but it will not affect the magnitude of the frequency response of G. The critical stability condition arises when the lag equals the phase margin. The critical value of time delay when the phase margin becomes zero is $\tau = 1.816$ *seconds*.

It is worthwhile to compare this critical value with the one obtained from the robust stability theorem 6.1. The nominal complementary sensitivity is given by

$$\hat{T} = \frac{\hat{G}C}{1+GC} = \frac{0.5}{s^3+2s^2+s+0.5}$$

and the multiplicative modelling error is

$$\Delta_m = e^{-\tau s} - 1 \Longrightarrow |\Delta_m(j\omega)| = 2|sin(\frac{\omega\tau}{2})|$$

A sufficient condition for robust stability is that $|\hat{T}(j\omega)||\Delta_m(j\omega)| < 1, \forall\omega$. Several values of τ were tested in Goodwin *et al.* (2001) and the critical value for time delay is $\tau = 1.5$ *seconds*. In other words, $|\hat{T}(j\omega)||\Delta_m(j\omega)| < 1, \forall\omega$ for $\tau < 1.5$ *seconds*. It can be observed that the critical value obtained by the robust stability theorem is conservative. This is due to the fact that the robust stability theorem only provides a sufficient condition for stability.

We simulate this process for 40000 seconds with a sampling time of 1 second. The initial process has no time delay and after 20000th second the process time delay changes to 1.5 seconds. We introduce a random binary signal (RBS) with magnitude of 2 in setpoint and a normally distributed signal with standard deviation of 0.2 as disturbance. According to previous discussions, the process with $\tau = 1.5$ *seconds* no longer satisfies the robust stability theorem but it is still stable. We would expect proposition 6.4.1 to 6.4.3 to detect the significant process change after 20000th second.

To apply propositions 6.4.1 to 6.4.3, we calculate the test values for a window of 1024 samples (the length of data window can be chosen different, the value chosen here is just for an illustration purpose). The user defined variable γ is chosen as $\gamma = 0.5$. The detection results of propositions 6.4.1 to 6.4.3 are shown in figures 6.6(a) to 6.6(c). The results from all of the three propositions indicate significant process change after the 20000th second.

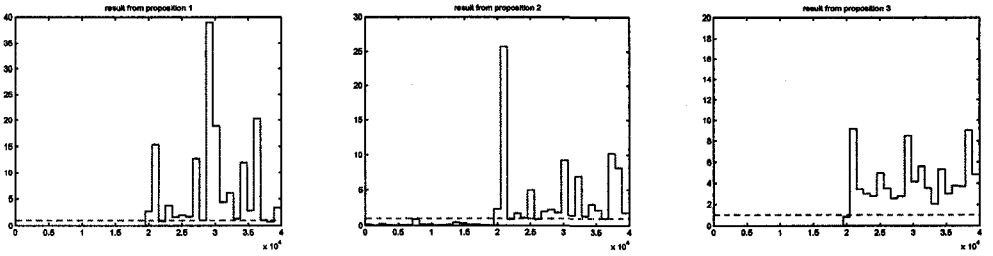

(a) Proposition 6.4.1 (b) Proposition 6.4.2 (c) Proposition 6.4.3

Figure 6.6: Test results for Example 1

Example 2

The plant and controller are adopted from Wan and Huang (2002). The initial true process model is

$$G = \frac{1.28q^{-1} + 1.2q^{-2} + 0.2588q^{-3} + 0.01606q^{-4}}{1 - 0.7932q^{-1} - 0.3698q^{-2} + 0.5184q^{-3} + 0.01298q^{-4}}$$

The sampling time is 1 second. A reduced order model of the true process can be obtained by applying the standard open-loop identification

$$\hat{G} = \frac{1.258q^{-1} + 0.3066q^{-2}}{1 - 1.53q^{-1} + 0.7397q^{-2}}$$

A controller aimed at achieving a good setpoint tracking property is designed based on $\hat{G}$ as

$$C = \frac{q^{-1}}{1 - q^{-1}}\hat{G}^{-1} = \frac{q^{-1}(1 - 1.53q^{-1} + 0.7397q^{-2})}{(1 - q^{-1})(1.258q^{-1} + 0.3066q^{-2})}$$

For this example, we assume that the true process may change with time and the model may become

$$G = k\frac{1.28q^{-1} + 1.2q^{-2} + 0.2588q^{-3} + 0.01606q^{-4}}{1 - 0.7932q^{-1} - 0.3698q^{-2} + 0.5184q^{-3} + 0.01298q^{-4}}$$

A sufficient condition for robust stability is that $|\hat{T}(j\omega)||\Delta_m(j\omega)| < 1, \forall\omega$. Several values of k were tested; a critical value of k is $k = 1.655$. In other words, $|\hat{T}(j\omega)||\Delta_m(j\omega)| < 1, \forall\omega$ for $k < 1.655$.

The process is simulated for 40000 seconds with a sampling time of 1 second. The initial process has $k = 1$, and after the 20000th second the process changes and k is set to 1.655. A random binary signal (RBS) is introduced with magnitude of 2 in setpoint and a normally distributed signal with standard deviation of 0.2 as disturbance. According to the previous discussion, the process with $k = 1.655$ no longer satisfies the robust stability theorem but it is still stable. We would expect propositions 6.4.1 to 6.4.3 to detect the significant process change after the 20000th second.

To apply propositions 6.4.1 to 6.4.3, the test values for a window of 1024 samples are calculated. The user defined variable γ is chosen as $\gamma = 0.5$. The detection results of proposition 6.4.1 to 6.4.3 are shown in figures 6.7(a) to 6.7(c). The results from all three propositions indicate significant process change after 20000th second.

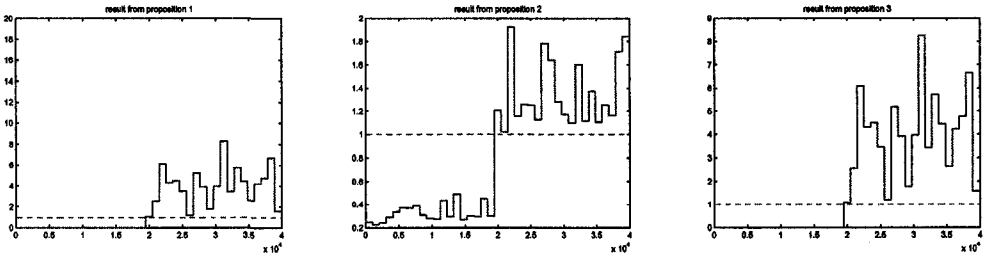

(a) Proposition 6.4.1 (b) Proposition 6.4.2 (c) Proposition 6.4.3

Figure 6.7: Test results for Example 2

6.5 Quantification of Modelling Error in the Frequency Domain

In the previous section, we used the robust stability theorem as a criterion to continuously validate the process model. Model validation gives a "yes" or "no" answer to

the quality of the process model; however it does not try to quantify the modelling error. In this section, we explore the possibility of quantifying the modelling error in the frequency domain.

6.5.1 Ideal SISO Case

In this subsection we assume $N(jw) = 1$, in other words, the white noise sequence a affects the system directly. Then equation (6.13) can be written as:

$$e = \frac{1}{1+\hat{T}\Delta_m} a \triangleq G_\Delta a \tag{6.38}$$

The system is assumed to satisfy the robust stability theorem and $|\hat{T}(j\omega)||\Delta_m(j\omega)| < 1$, $\forall\omega$. Then

$$0 < \left|\frac{1}{G_\Delta(j\omega)}\right| = |1+\hat{T}(j\omega)\Delta_m(j\omega)| < 1 + |\hat{T}(j\omega)||\Delta_m(j\omega)| < 2 \tag{6.39}$$

If there is no modelling error, i.e. $\Delta_m(j\omega) = 0$, $\forall\omega$. Then $G_\Delta(j\omega) = 1$ and $\frac{1}{G_\Delta(j\omega)} = 1$, $\forall\omega$, and $e = a$ for the ideal case. The ideal case is not achievable; therefore using $\frac{1}{G_\Delta(j\omega)} = 1$ as a criterion for model validation or modelling error detection is rather strict. $|\frac{1}{G_\Delta(j\omega)}| = 1$ is a more realistic benchmark. In other words, we want $|\frac{1}{G_\Delta(j\omega)}|$ to be as close as to 1 at any frequency ω. The following expression is proposed as a measure of the modelling error of $\hat{G}$ in the frequency domain:

$$FM = \int_{-\infty}^{\infty} \left| |\frac{1}{G_\Delta(j\omega)}| - 1 \right| d\omega \tag{6.40}$$

FM stands for frequency-domain model mismatch. The bigger the FM value, the larger the modelling error.

Remark 6.5.1 *G_Δ can be directly estimated from routine operating data. $|\frac{1}{G_\Delta(j\omega)}|$ can be calculated from the identified G_Δ.*

Remark 6.5.2 *To calculate FM, we do not need the assumption $|\hat{T}(j\omega)||\Delta_m(j\omega)| < 1$, $\forall\omega$. The purpose of introducing equation (6.39) is to demonstrate that [0 2] is a normal range of $|\frac{1}{G_\Delta(j\omega)}|$.*

6.5.2 SISO Case with Disturbance Model

This section will discuss the situation when the white noise sequence a passes through the disturbance model N to affect the system.

With Known Disturbance Model

N is assumed known as *a priori*, which is usually available from the system identification exercise before the controller is commissioned.

Using routine operating data, there are two ways to identify G_Δ:

(1) Identify $G_\Delta N$ first, and then separate G_Δ with the knowledge of N.

(2) Pass e through a filter N^{-1} and then identify G_Δ using the filtered e.

With Unknown Disturbance Model

If the disturbance model N is unknown, then the situation is different. We can only identify $G_\Delta N$ from routine operating data. In this case, refer to the relative model quality index (RMQI) that will be introduced in the next section to evaluate the modelling error.

6.5.3 Historical Benchmark for General SISO Case

A historical benchmark is the actual FM for the closed-loop system over a specific period when it is considered to have a good performance. A relative model quality index in terms of the historical benchmark can be calculated to measure the current modelling error in comparison with a historical benchmark. A relative model quality index with respect to the historical benchmark can be defined as follows:

$$RMQI = \frac{FM_{benchmark}}{FM_{act}} \tag{6.41}$$

- If the disturbance model N is known, then FM can be calculated using equation (6.40).

- If the disturbance model N is unknown, then only $G_\Delta N$ can be identified from routine operating data. As a result, we can consider N as the un-modelled part

and calculate FM as

$$FM = \int_{-\infty}^{\infty} \left| |\frac{1}{G_\Delta(j\omega)N(j\omega)}| - 1 \right| d\omega \tag{6.42}$$

Such a relative measure of modelling error should usually be between 0 and 1. A value close to 0 implies that current modelling is significantly different from the benchmark; if at the same time the control performance is low, then the reason is probably due to the modelling error. A value near 1 implies that the current modelling error is not significant compared to the benchmark and that the model should be adequate. Theoretically, it is possible to have a RMQI bigger than 1, which means that the modelling error has been reduced.

6.5.4 Simulation Example

Suppose we have an identified model

$$\hat{G} = \frac{Ke^{-ds}}{\tau s + 1} = \frac{1.7021e^{-7.81s}}{70s + 1}$$

and the designed controller based on this model is

$$C = P + \frac{I}{s} = 2.78 + \frac{0.03967}{s}$$

The true process has the following transfer function

$$G = \frac{(K + \Delta K)e^{-(d+\Delta d)s}}{(\tau + \Delta\tau)s + 1}$$

Different sizes of modelling errors are introduced and the FM value is calculated. The results are shown in Table 6.1.

Table 6.1: Simulation result

Size of modelling error	FM value
No modelling error	0.00283
Δd=2	0.0253
ΔK=1.3	0.0263
ΔK=1.3, Δd =2	0.0439
ΔK=1.2, Δd=2, $\Delta\tau$=-20	0.0637

It is clear that as the size of modelling error increases, the FM value increase. The FM values reflect the impact of modelling error on the output error sensitivity function which is defined in equation (6.19).

6.5.5 Experimental Example

For an experimental case study, a continuous stirred tank heater (CSTH) is used for modelling error quantification. The CSTH system is located in the Computer Process Control Laboratory, in the Department of Chemical and Materials Engineering at the University of Alberta, Canada. A simple schematic of the CSTH system in shown in figure 6.8. The CSTH system has two inputs (cold water and steam) and two outputs (water level and outlet water temperature). The water level is controlled by a cold water valve using a PID controller.

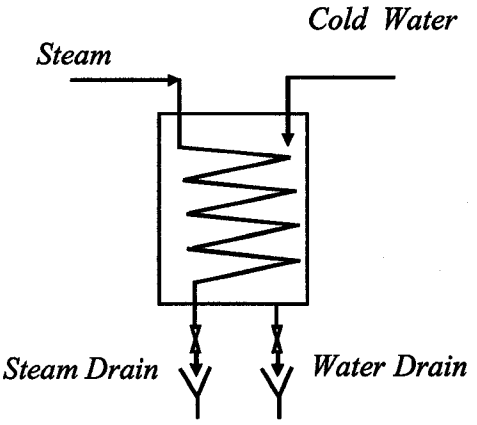

Figure 6.8: Simple schematic of the CSTH system

Suppose that the objective is to design a controller to control the water temperature at 24°C when the water level is 0.2 m. First we identify a model between the water temperature and the steam setpoint. A random binary signal (RBS) is introduced as an excitation at steam setpoint while the water level setpoint is kept constant at 0.2 m. A set of training data of the steam setpoint and the water temperature was collected. Two models with different orders were identified between the water temperature and the steam setpoint:

$$\hat{G}_1 = \frac{1.0278e^{-17.589s}}{20.016s+1}$$
$$\hat{G}_2 = \frac{0.0001423s+0.004817}{s^2+0.01488s+0.004161}e^{-8.77s}$$

A PID controller was designed based on the IMC tuning and then fine tuned based on the real process. The PID controller could maintain the water temperature at 24°C when the water level is 0.2 m.

Then small process changes were introduced to see whether the FM value is able to detect the changes or not. The results are summarized in Table 6.2.

Table 6.2: Summary of experiment result

Different Operation Point	FM value from $\hat{G}_1$	FM value from $\hat{G}_2$
1. Temp. SP at 24°C, level SP at 0.2 m	0.293	0.292
2. Temp. SP at 19°C, level SP at 0.2 m	0.295	0.293
3. Temp. SP at 24°C, level SP at 0.22 m	0.303	0.301

Both FM values calculated from $\hat{G}_1$ and $\hat{G}_2$ indicate that the modelling error is smallest at the nominal operation point (case 1). When the controller is used to control the water temperature at 19°C (case 2), the process change is relatively insignificant. When the water level changes to 0.22 m (case 3), we would expect a more significant process change than only the temperature setpoint change (case 2). Increasing the water level will decrease the gain between steam setpoint and the water temperature, and also increase the time constant of the process. As expected, the FM value for case 3 is highest for both $\hat{G}_1$ and $\hat{G}_2$.

Also, we can see that for the same operating point, the FM value from $\hat{G}_2$ is always smaller than the FM value from $\hat{G}_1$. This means that $\hat{G}_2$ is more accurate than $\hat{G}_1$. This observation is not surprising because $\hat{G}_2$ has higher order than $\hat{G}_1$.

6.6 Concluding Remarks

This chapter focused on the diagnosis of modelling error under closed-loop conditions using output error. The relationship between the output error and modelling error

was first discussed in terms of multiplicative modelling error and additive modelling error. The bounds of the ratio between output error variance and disturbance variance were derived under closed-loop conditions.

Three propositions for on-line model validation were proposed. The propositions used the robust stability theorem as a criterion for model validation. Any process that does not satisfy the robust stability theorem has a small robust margin. The three propositions give a warning of violation of the robust stability theorem typically due to significant model plant mismatch.

How to quantify the modelling error was discussed in the last section of this chapter. A frequency domain measure of the modelling error was proposed. Both simulation and experimental examples demonstrated that the proposed methodology can detect small process changes.

7

Model Analysis and Performance Analysis of Two Industrial MPCs

This chapter presents two case studies on the performance evaluation and model validation of two industrial multivariate model predictive control (MPC) based controllers at Suncor Energy Inc., Fort McMurray, Canada: (1) a 7-output, 3-input kerosene hydrotreating unit (KHU) with three measured disturbance variables that are used for feedforward control; and (2) a 8-output, 4-input naphtha hydrotreating unit (NHU) with 5 measured disturbances. The first case study focuses on potential limits to control performance due to constraints and limits set at the time of controller commissioning. The root causes of sub-optimal performance of KHU are successfully isolated. Data from the NHU unit with MPC on and with MPC off are analyzed to obtain and compare several different measures of multivariate controller performance. Model quality assessment for the two MPCs are performed. A new model index is proposed to have a measure of simulation ability and prediction ability of a model. Open-loop identification of KHU and closed-loop identification of NHU are conducted using the asymptotic method (ASYM) proposed by Zhu (1998). [1]

[1]A condensed version of this chapter has been published as: Hailei Jiang, Sirish Shah, Biao Huang, Bruce Wilson, Rohit Patwardhan and Foon Szeto, "Performance Assessment and Model Validation of Two Industrial MPC Controllers", to appear in the proceedings of the IFAC *World Congress 2008*, Seoul, Korea.

7.1 Introduction

Multivariate model predictive control (MPC) has been widely applied in industry to control increasingly complex processes. At each control interval, an MPC controller attempts to optimize future plant behavior by computing a sequence of future moves of manipulated variables (MVs). Only the first moves of the MVs are sent into the plant and the entire calculation is repeated at the next control interval. This is also known as receding horizon control. There is large volume of publications concerning the theoretical and practical issues associated with MPC technology. Rawlings (2000) had provided an excellent introduction to MPC technology; Qin and Badgwell (2003) have given a good survey of industrial MPC. Several books on MPC have also been published recently (Kouvaritakis and Cannon, 2001; Maciejowski, 2002).

Although there are many publications discussing the design of MPCs and their properties, relatively few of them talk about the performance monitoring of MPC controllers which is also an important issue. MPC control systems usually work well and deliver profit near the period when they are commissioned; however their performance deteriorates with time and the MPC controllers are often turned off eventually if without proper maintenance. There are many reasons for sub-optimal performance: such as process changes, unmeasured disturbances, inappropriate limits setting and poor tuning of lower level PID loops. How to effectively evaluate the performance of the MPC is still an open question.

The kerosene hydrotreating unit (KHU) and the naphtha hydrotreating unit (NHU) at Suncor Energy Inc., Fort McMurray, Canada are controlled by commercial MPC controllers. The KHU MPC controller has 3 manipulated variables (MVs), 7 controlled variables (CVs) and 3 feedforward variables (FFs); while the NHU MPC controller has 4 MVs, 8 CVs and 5 FFs. These two MPC controllers were commissioned in May 2005 and have performed well upto late 2006. Both units have been able to deliver considerable benefit each year. However, since late 2006, both units' MPC controllers have not performed well consistently. Sometimes, the MPC controller could not control the CVs within their limits and therefore could not achieve optimal performance.

In this chapter, we explore the performance issues of the generic MPC controllers

and then apply the developed techniques for studying sub-optimal MPC performance when applied to the KHU and NHU. The objectives of our work are: (1) to validate the models in the MPC controllers; (2) to analyze the data from these two MPC controllers; (3) to diagnose the root cause of the sub-optimal control performance; (4) to provide remedial suggestions; and (5) to re-identify the model using routine operating data. This chapter is organized as follows: Section 7.2 introduces the basic idea of simulation and prediction of a model. We discuss model quality assessment of the KHU MPC and propose a new mode index in Section 7.3. Performance analysis of the KHU MPC will be presented in Section 7.4. In Section 7.5 and Section 7.6, we will discuss model quality assessment and performance assessment of the NHU MPC controller respectively. The chapter will finish with concluding remarks in Section 7.8.

7.2 Model Quality Evaluation

The model of a process to be controlled is a key part of MPC technology. An MPC controller needs fairly accurate model for prediction of future process moves, for computing optimum target settings and in general to deliver overall superior control performance. Most MPC design techniques and MPC properties are proposed on the assumption that an accurate model is available. However, it is commonly known that most real processes are time-variant in nature. Either the process or the disturbance dynamics can change from time to time. The changes can be because of new operating points that are different from the original identification condition, or because of quality changes of the input materials. In other words, model-plant mismatch is always inevitable and usually will increase over time. How to continually evaluate model quality is an important challenge in the diagnosis of sub-optimal MPC performance.

In this section, we first discuss the prediction and simulation properties of a metric of model and introduce a model fit that has been widely used in academia. Most of the materials of this section can be found in Ljung (1998).

7.2.1 Simulation and Prediction

Assume that a system description is given in the following form

$$y(t) = G(q)u(t) + N(q)e(t) \tag{7.1}$$

where $G(q)$ is the process transfer function, $N(q)$ is the disturbance transfer function, $\{u(t)\}$ is an input sequence, $\{y(t)\}$ is an output sequence and $\{e(t)\}$ is a sequence of independent random variables with zero mean and variance λ.

Simulation

A basic use of a system description is to simulate the system's response based on different input signals. For instance, if an input sequence $u(t), t = 1, 2, ...$ is given, then we can simulate the system output as

$$\hat{y}(t) = G(q)u(t), \qquad t = 1, 2, ... \tag{7.2}$$

$\hat{y}(t)$ is called the *simulation output* which is the output that the system would produce if there is no disturbance. In industry, $\hat{y}(t)$ is defined as *unbiased prediction* because no real measurement of y is used in its calculation.

Prediction

With the assumption that the disturbance model $N(q)$ is invertible, then $\hat{y}(t+1|t)$

$$\hat{y}(t+1|t) = N^{-1}(q)G(q)u(t) + [1 - N^{-1}(q)]y(t) \tag{7.3}$$

is defined as the 1-step-ahead prediction which is an optimal prediction of $y(t+1)$ given the data up to time t (i.e. $y(t), u(t), y(t-1), u(t-1), ...$). Here 'optimal' is in the sense that the prediction error $\{y(t+1) - \hat{y}(t+1|t)\}$ has minimum variance. In industry, $\hat{y}(t+1|t)$ is called *biased prediction* because its calculation involves real measurements of y.

k-step-ahead Prediction

Having the definition of 1-step-ahead perdition, it is easy to generalize the prediction computation as follows: if we have data up to time t (i.e. $y(t), u(t), y(t-1), u(t-1), ...$), what is the optimal prediction of $y(t+k)$?

We first rewrite the disturbance model $N(q)$ as

$$N(q) = \sum_{\ell=0}^{\infty} h(\ell)q^{-\ell} = \sum_{\ell=0}^{k-1} h(\ell)q^{-\ell} + \sum_{\ell=k}^{\infty} h(\ell)q^{-\ell} \tag{7.4}$$

and define

$$\bar{N}_k(q) = \sum_{\ell=0}^{k-1} h(\ell)q^{-\ell}, \quad \tilde{N}_k(q) = \sum_{\ell=k}^{\infty} h(\ell)q^{-\ell} \tag{7.5}$$

Then the optimal prediction of $y(t+k)$ is given as (Ljung, 1998)

$$\hat{y}(t+k|t) = W_k(q)G(q)u(t) + [1 - W_k(q)]y(t) \tag{7.6}$$

where $W_k(q) = \bar{N}_k(q)N^{-1}(q)$.

7.2.2 Why Should We Consider Simulation and Prediction Properties of a Model?

MPC needs to predict future CV trajectory based on the current MV and CV information. Using the predicted CV trajectory, the MPC controller is able to optimize the designed control objective and calculate a sequence of MV moves. Therefore, it is natural that MPC controllers need models with good prediction ability to achieve good performance.

After the prediction stage, the next step in MPC controller is the optimization stage for calculating the MV moves. The effectiveness and accuracy of the MV moves depend greatly on the simulation ability of the model. A naive yet clear way to explain this point is by using the following equation $u_{future} = G^{-1}y_{desired}$ to convey the concept of future MV move calculation, where $y_{desired}$ is the desired trajectory of y is typically the desired target or setpoint trajectory and u_{future} is the MV moves that we want to calculate. This is simplistic way of illustrating the importance of a model in calculating the MV moves.

Therefore, we know that prediction ability and simulation ability of a model are both important for a successful implementation of an MPC controller. In the next sub-section we introduce a concept of model fit which can be used to evaluate the prediction and simulation ability of a model.

7.2.3 Model Fit

A model fit was proposed by Ljung (1998)

$$model\ fit = 1 - \sqrt{\frac{\sum_{t=1}^{n}[y(t+k) - \hat{y}(t+k|t)]^2}{\sum_{t=1}^{n}[y(t) - \bar{y}]^2}} \tag{7.7}$$

where $y(t)$ is the measured output, $\hat{y}(t+k|t)$ is k-step-ahead prediction and $\bar{y}(t)$ is the mean value of the measured output. This model fit measures the percentage of variation that is explained by the model in terms of k-step-ahead prediction. If we choose $k = 1$ and substitute $\hat{y}(t+1|t)$ into the equation, then we have a 1-step-ahead prediction fit (for short, we call it prediction fit) which evaluates the 1-step-ahead prediction ability of a model. If we choose $k = \infty$ and substitute $\hat{y}(t)$ into the equation, then we have a simulation fit which evaluates the simulation ability of a model. The highest value of the model fit is 1 which indicates a perfect model when $\hat{y}(t+k|t)) = y(t+k)$. A zero value of model fit means the model doesn't explain any variation in the data and it has similar performance as using $\bar{y}$ as a model. If the model fit is negative, then it indicates a bad model. Therefore, we would want a model with high model fit.

The data from the two industrial MPCs provides a good opportunity to test this model fit based on real data. In the next section, we discuss whether the prediction fit or simulation fit is more reasonable to reflect the quality of a model in an industrial MPC controller. Also we will propose a new model index, a metric for model quality, based on the prediction fit and simulation fit.

7.3 Model Quality Assessment of the KHU MPC

The kerosene hydrotreating unit (KHU) at Suncor Energy Inc. is a standard hydrotreating unit that desulphurizes the coker intermediate kerosene streams through a catalytic reaction with hydrogen. The KHU is controlled by an MPC controller which has 3 manipulated variables (MVs), 7 controlled variables (CVs) and 3 feedforward variables (FFs). The MPC controller recalculates and executes MV moves every 1 minute. The detailed information of the CVs, MVs and FFs are listed in Table 7.1 - 7.4. A simplified schematic of the KHU is shown in figure 7.1 where MV1-MV3 and

CV1-CV6 are marked by circles. The FFs are not shown in the schematic because of the confidentiality of the process. CV7 is not shown in the schematic because it is an inferential which is calculated on-line in the process computer.

Table 7.1: CVs of the KHU MPC controllers

CV tags	Description
CV1 - LIC17.OP	Position of the feed valve (of the kero stripper)
CV2 - PIC36.OP	Position of the pressure valve (of the kero stripper)
CV3 - TI67.PV	Condenser outlet temperature
CV4 - LIC19.OPT*	Position of the accumulator level valve
CV5 - PIC117.PV	Pressure of the fuel gas to roboiler
CV6 - TI58.PV	Bottom temperature of the kero stripper
CV7 - KUKEROFL	Kero product flash (which is an inferential)

* The 'OPT' indicates that the controller is using a transformation of the OP to linearize the valve response.

Table 7.2: Ranking and control objective of CVs for KHU MPC

CV tags	Control Objective	Rank*
CV1 - LIC17.OP	Between limits	medium
CV2 - PIC36.OP	Between limits	medium
CV3 - TI67.PV	Between limits	low
CV4 - LIC19.OPT*	Low limit	medium
CV5 - PIC117.PV	Between limits	high
CV6 - TI58.PV	Between limits	low
CV7 - KUKEROFL	Low limit	low

* 'Rank' indicates the importance of each CV. 'High' means most important and 'Low' means least important. When there is no feasible solution and one or some of the CV limits has or have to be violated, then the lower rank CV should be sacrificed first.

7.3.1 Initial Model Quality Assessment

The initial step test data of the KHU was provided by the process engineer at Suncor Energy Inc. The step test was completed in May 2005 and lasted over 9 days. The MVs trajectories are shown in figure 7.2 for a sampling interval of 1 minute. Between

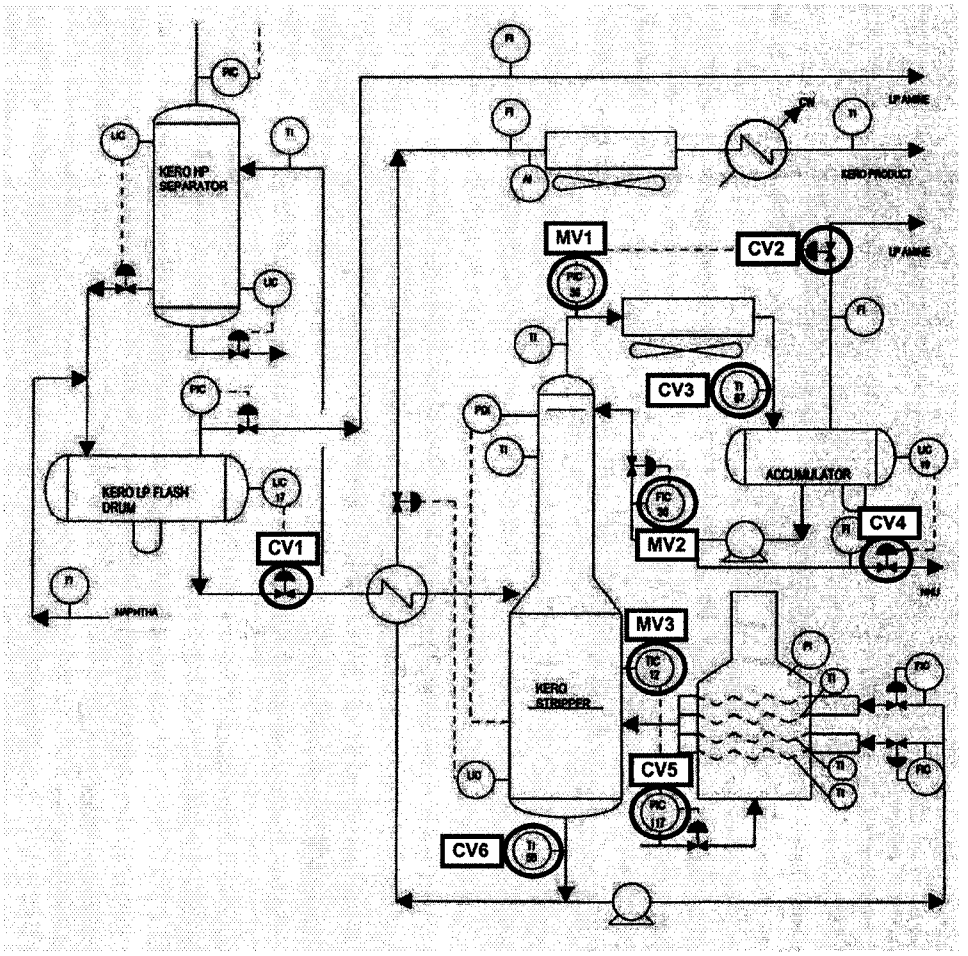

Figure 7.1: Schematic of the kerosene hydrotreating unit (KHU)

Table 7.3: MVs of the KHU MPC controllers

MV tags	Description	Cost Action*
MV1 - PIC36.SP	Pressure of the kero striper	maximize
MV2 - FIC30.SP	Reflux flow of the kero striper	minimize
MV3 - TIC12.SP	Reboiler outlet temperature	minimize

* 'Cost Action' indicates movement direction of MVs in order to achieve the control objective. 'maximize' means it is desired to maximize the SP of the corresponding MV and 'minimize' means it it desirable to minimize the SP of the corresponding MV. More discussion is in Section 7.4.1.

Table 7.4: FFs of the KHU MPC controllers

FF tags	Description
FF1 - FIC20.SP	Reactor charge
FF2 - PIC30.SP	Pressure of kero LP separator
FF3 - TI999.PV	Ambient temperature

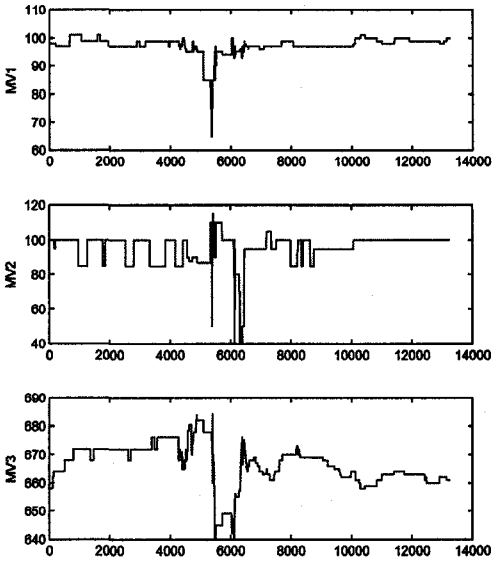

Figure 7.2: KHU MV trajectories in the step test

4001st and 7000th data point, the process was under abnormal condition and these data points are not used in identification.

The identified model from this step test is also provided. In order to evaluate the initial model quality, we first calculate the simulation and prediction fits using the model and the step test data. To get rid of the bad data (4001st-7000th data points), we divide the step test data into two sets: the first set contains the first 4000 data points and the second set contains data from 7001st data point to the last data point. The results from the two sets of data are shown in Tables 7.5 and 7.6. Figure 7.3 shows a comparison of the prediction fit and simulation fit.

Table 7.5: Initial prediction fit of the KHU model

Tags	Based on 1st data set	Based on 2nd data set	Averaged prediction fit
CV1	92.13%	89.19%	90.66%
CV2	78.84%	87.27%	83.055%
CV3	91.66%	91.89%	91.775%
CV4	81.35%	83.87%	82.61%
CV5	81.35%	85.3%	83.325%
CV6	92.27%	91.17%	91.72%
CV7	86.26%	91%	88.63%

Table 7.6: Initial simulation fit of the KHU model

Tags	Based on 1st data set	Based on 2nd data set	Averaged simulation fit
CV1	49.09%	45.43%	47.26%
CV2	18.14%	23.29%	20.715%
CV3	13.13%	17.15%	15.14%
CV4	17.43%	27.53%	22.48%
CV5	26.2%	25.5%	25.85%
CV6	74.79%	73.84%	74.315%
CV7	43.03%	16.36%	29.695%

It is can be observed in figure 7.3 that the prediction fits of the CVs are around 80% to 90% and the difference is less than 10%; however the simulation fits of the CVs are relatively low and are quite different from each other. The average prediction fit of the 7 CVs is 87.4% while the average simulation fit of the 7 CVs is 33.64%. It

is clear that the simulation fit is much lower than the prediction fit.

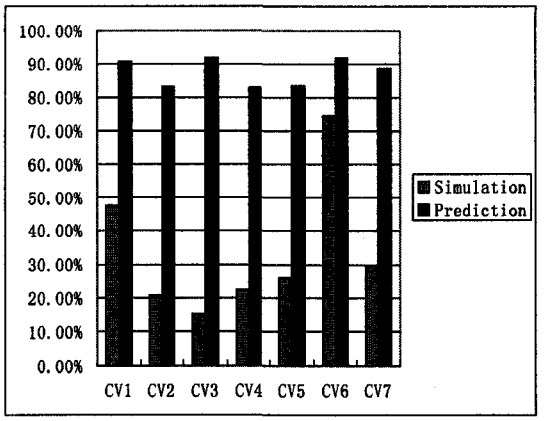

Figure 7.3: Initial model fit of KHU model

7.3.2 Recent Model Quality Assessment

Since late 2006, the KHU MPC has not performed as well as possible. 9 weeks of data were collected between October 2006 to January 2007. We calculated the prediction and simulation fit based on weekly data. The model fits of the CVs are shown in figure 7.4 where the blue lines represent prediction fits and the red lines represent simulation fits. For individual CV, we can see that the prediction fit is always higher than the simulation fit and close to 90%; while the simulation fit is relatively low and fluctuates significantly from week to week. Figure 7.4(h) shows the average model fit of the 7 CVs for each week which can be thought of as the overall plant model fit.

The average model fit of each CV over the 9 weeks are shown side by side with their initial model fit in figure 7.5. Figure 7.5(a) shows the comparison of prediction fit and we can see that the recent prediction fits of some CVs are even better than their initial values. The recent average prediction fit of the 7 CVs is 90.12% while the initial value is 87.4%. The plot shows that the 1-step prediction ability of the model is very good and even better than before. Figure 7.5(b) shows the comparison of simulation fit. It is clear that the recent simulation fits are worse than initial simulation fits. The recent average simulation fit of the 7 CVs is 14.06% while the initial value is 33.64%. This is more than 50% drop from the initial average simulation fit. We should pay

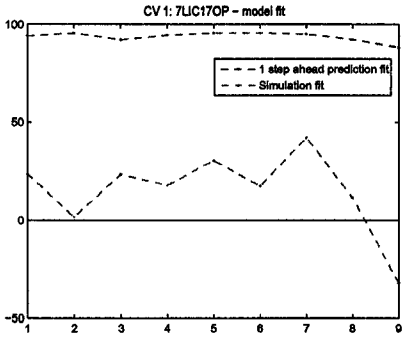

(a) Weekly model fit of CV1

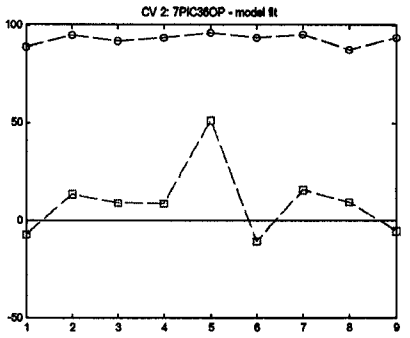

(b) Weekly model fit of CV2

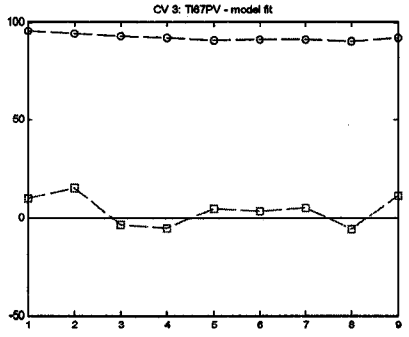

(c) Weekly model fit of CV3

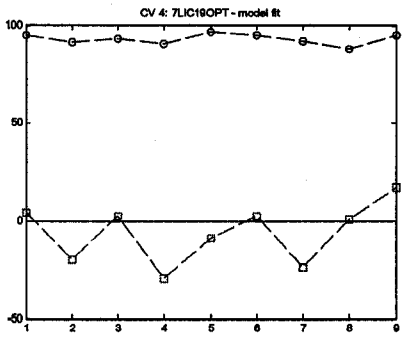

(d) Weekly model fit of CV4

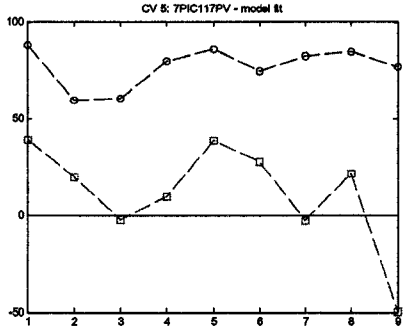

(e) Weekly model fit of CV5

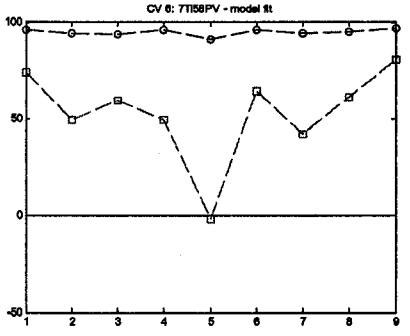

(f) Weekly model fit of CV6

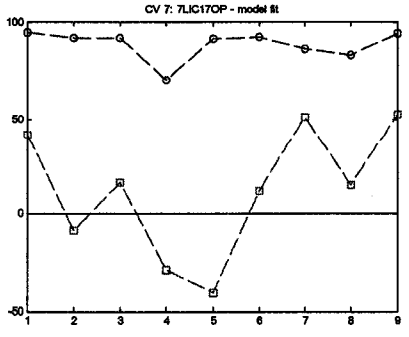

(g) Weekly model fit of CV7

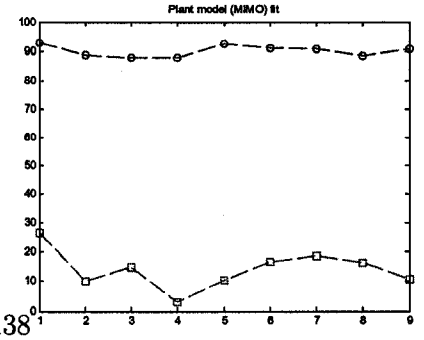

(h) Averaged weekly model fit of CVs

Figure 7.4: Recent model fit of KHU model (the y-axis is in unit of %)

138

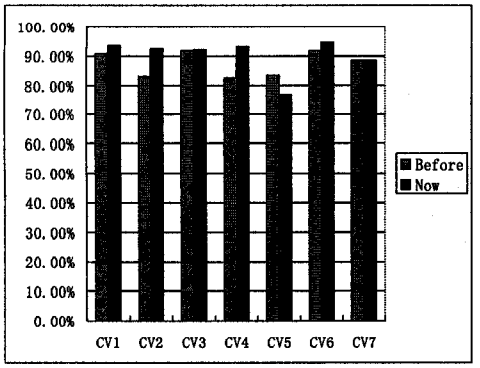

(a) Comparison of prediction fit

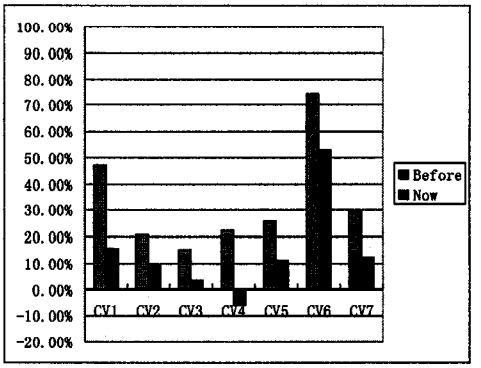

(b) Comparison of simulation fit

Figure 7.5: Model fit comparison of KHU model

special attention to CV4 (LIC19.OP) whose simulation fit is now negative. It is an indication of bad model and this particular simulation fit contributes a lot to the drop of the average simulation fit. We will see more diagnosis of this CV in Section 7.4. In summary, this analysis shows that prediction fits are good, irrespective of the model quality, as they simply are a 1-step ahead extrapolation of the data. A better picture of the model quality is obtained from the simulation fit.

7.3.3 Summary of Model Fit

Through the comparison of prediction fit and simulation fit, we can see that even a bad model (e.g. with a negative simulation fit) could have good 1-step-ahead prediction ability. The average prediction fit of the KHU model even increased compared to its initial value. We should be careful when we use prediction fit as an measure of model quality. It may always indicate good model even when the reality is not the case.

Compared to the prediction fit, simulation fit is a better measure of model quality. It does not use any real measurement of the CVs and is the toughest test for assessing model quality. In the case of KHU, the simulation model fit does indicate model degradation which concurs with experiences of Suncor engineers and also is the likely cause of sub-optimal MPC performance as evident from its low service factors. Specifically our analysis indicates a bad model for CV4 (LIC19.OP) which will be diagnosed as a major root cause of the sub-optimal MPC performance in Section 7.4. This leads us to the conclusion that a simulation fit is a better measure of model

quality compared to the prediction fit. However, a drawback of simulation fit is that it is sensitive to disturbance and as such the presence of disturbances can easily confound the model discrepancies. This is because a simulation fit does not use any feedback of the real CVs and any mismatch between the simulated value and real measurement would be confounded as a deficient model. In particular, figure 7.4(b) for CV2 shows that the simulation fit of week 2 is close to 50% but drops to a negative value in the subsequent week. However, over the same period, the prediction fit is fairly consistent in the plots because it uses feedback of the CV measurement within which is captured the effect of disturbances present in the process. In the presence of (unmeasured) disturbances the simulation fit would give false alarms of poor model quality.

7.3.4 A New Model Index for Assessment of Model Quality

As discussed in the last section, the use of prediction or simulation fit alone to evaluate model quality has its pros and cons. In this sub-section, we would explore issues of k-step-ahead predictions and propose a new model index which considers both prediction and simulation ability of a model at the same time.

An important concept in MPC control is the *prediction horizon* which defines how far in the future that the algorithm has to predict at each control execution. The prediction horizon is an integer number of sampling interval and the MPC controller will predict future CV trajectory within the prediction horizon. For example, if the sampling interval is 1 minutes and the prediction horizon is 15 minutes, then at each control execution, the MPC controller needs to predict the CV trajectory over the next 15 minutes. Therefore for this example, the MPC controller has to do k-step-ahead prediction with $k = 1, 2, 3, ..., 15$ that is from 1 upto the prediction horizon. The accuracy of future CV trajectory not only depends on the prediction fit (1-step-ahead prediction), but also depends on the k-step-ahead prediction fit. Therefore it is meaningful to compute the k-step-ahead prediction fit (Huang *et al.*, 2003) and compare it with the (1-step ahead) prediction fit and the (infinite-horizon) simulation fit.

The KHU MPC uses a prediction horizon of 15 minutes. So we calculated k-step-ahead prediction fit ($k = 2, 3, ..., 15$) for each week over a 9 week period. In figure

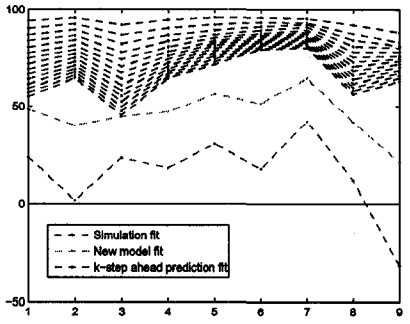

(a) Weekly model fit of CV1

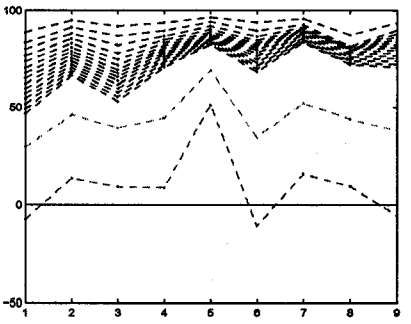

(b) Weekly model fit of CV2

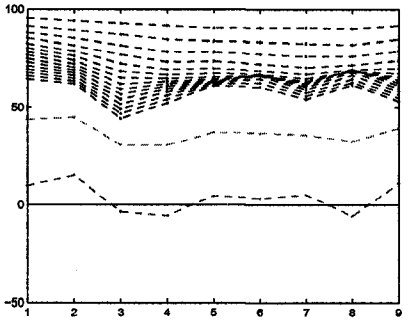

(c) Weekly model fit of CV3

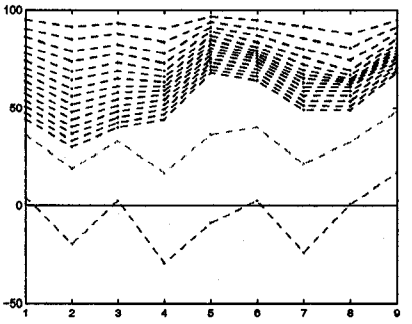

(d) Weekly model fit of CV4

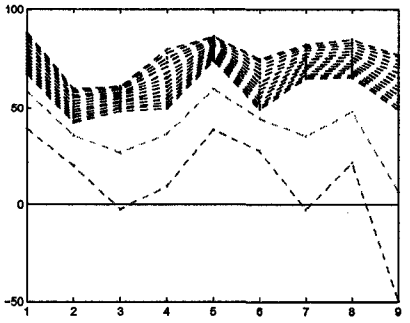

(e) Weekly model fit of CV5

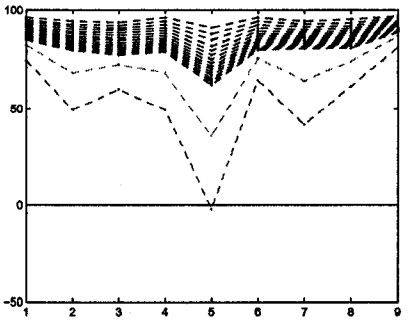

(f) Weekly model fit of CV6

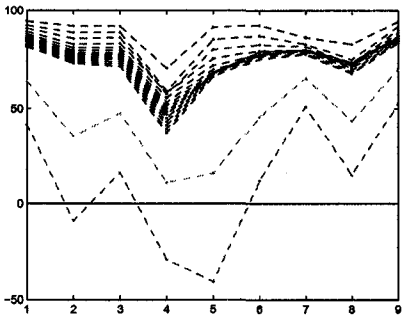

(g) Weekly model fit of CV7

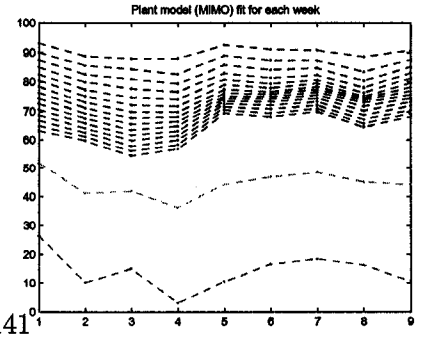

(h) Averaged weekly model fit of CVs

Figure 7.6: k-step-ahead prediction fit of KHU model (the y-axis is in unit of %)

7.6, we show the prediction fit, the k-step-ahead prediction fit ($k = 2, 3, ..., 15$), the simulation fit and a new model index (to be discussed soon). From the plots of model fit, we arrive at the following observations based on the KHU process data:

- better simulation fit does NOT always indicate better 1-step ahead prediction. For example, in figure 7.6(a) for CV1, the simulation fit of week 3 is better than week 2, but the prediction fit of week 3 is worse than week 2.
- better 1-step ahead prediction (or simulation fit) does NOT always indicate better k-step ahead prediction. For example, in figure 7.6(d) for CV4, the prediction fit (and the simulation fit) of week 3 is better than week 4, but the 15-step-ahead prediction of week 3 is worse than week 4.
- The variance of model fits form 1-step-ahead prediction to 15-step-ahead prediction is different from week to week.
- Even though (1-step-ahead) prediction fit looks good and can be close to 90%, the k-step ahead prediction fit can be very different and especially the 15-step-ahead prediction fit can be as low as 40% (see week 4 fit in figure 7.6(g)). In figure 7.6(d) for CV4, the prediction fits (and the simulation fits) of week 2 and week 5 are close to each other, but the 15-step-ahead prediction of the same two weeks are quite different from each other.

Also, our experience with (1-step-ahead) prediction fit and simulation fit of industrial data leads us to the following remarks:

- 1-step-ahead prediction is very easy to achieve even with a bad model.
- Good simulation fit is only achieved by a good model. However, even a good simulation model will give poor fit in the presence of disturbances.
- Even when MPC performance is satisfactory, simulation fits are often relatively poor in multivariate industrial data sets because of the presence of disturbances.
- A good model will have good 1-step-ahead prediction and its k-step-ahead prediction will degrade slowly, such as the case in figures 7.13(g) and 7.13(h). But

a bad model with good 1-step-ahead prediction will not have good k-step-ahead prediction. The fit will drop quickly as k increases, such as the case in figures 7.6(d) and 7.13(b)

- If the k-step-ahead fits of a model drops quickly and its simulation is also low, then it is a signature of bad model.

- If the k-step-ahead fits of a model are good, but the simulation is low, we probably still do not need to worry about it because it is quite possible that the low simulation fit is due to the effect of disturbance.

Therefore, we can see that the prediction ability of a model may not be as good as the (1-step-ahead) prediction fit shows. We should also take the k-step-ahead prediction fit into account to have a complete evaluation of the prediction ability. Our new idea of model index is to include information of prediction fit, k-step-ahead prediction fit and simulation fit. The new model index we propose is defined as

$$model\ index = \frac{averaged\ prediction\ fit\ +\ simulation\ fit}{2} \tag{7.8}$$

where the 'averaged prediction fit' means the average value of k-step-ahead prediction fits ($k = 1, 2, ..., p, where\ p\ is\ the\ prediction\ horizon\ value$).

This model index serves as a measure of both prediction ability and simulation ability of a model. It not only has the advantage of the prediction fit that reduces the effect of disturbance by using the feedback of CV measurement, but also has the advantage of simulation fit which is sensitive to the model change. The green lines in plots of figure 7.6 are the values of this new model index.

The initial model index value of the KHU model and the recent model index value (average value of the 9 weeks for each CV) is shown in figure 7.7. The new model index of KHU model shows model degradation, but is not as significant as the simulation shows. Among all the CVs, CV4 has the lowest model index which will be diagnosed as the root cause of sub-optimal performance in Section 7.4.

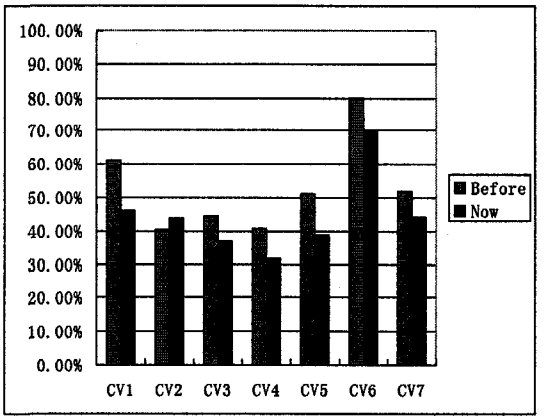

Figure 7.7: New model index value of KHU model

7.4 Performance Analysis of the KHU MPC

During the 9 week period that the Suncor engineers collected the data, the service factor of the KHU MPC was only 11.16% which means that for only 11.16% of the 9 weeks time period the MPC was on. The longest consecutive period that the MPC was on is 3183 minutes (just over 2 days). Our analysis is based on these 3183 data points.

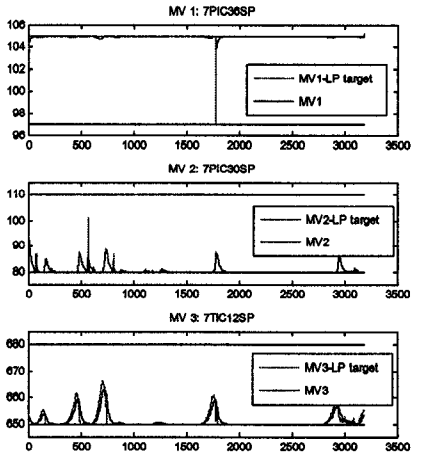

Figure 7.8: MVs moves when the MPC was on. The black lines are the limits.

The MV moves of the 2 days that the MPC was on are shown in figure 7.8. The corresponding CVs trajectories are shown in figure 7.9. In both figures, the blue lines are the real measurement, the red lines are the LP-targets and the black lines are the limits. The 'LP-target' is short for 'linear programming target' which is calculated by the MPC every minutes as the setpoint for CV. Looking at the MVs and CVs, we can notice that:

- The MVs are at their limits most of the time.
- There is limit violation in CV3(low rank), CV4(medium rank) and CV7(low rank). Especially CV4, which has median rank, has large excursions from its limits.
- There are some wave pattern fluctuations in MV2 and MV3. Very similar pattern of fluctuation also exist in CVs, such as CV2-CV7.
- The MVs and CVs follow their LP-targets very well.

To understand and diagnose these observations, we perform limits and constraints analysis, PID loop diagnosis and cause & effect analysis in the following sub-sections.

7.4.1 Analysis of Limits and Constraints

An important feature of MPC technique is its ability to handle multiple constraints and limits. During each control execution, MPC controller will carry out LP or QP optimization to find the feasible solution for CV and MV moves. During the time period when there is no feasible solution to satisfy all the limits and constraints, the MPC controller will choose to violate some of the constraints and limits according to the weights of different CVs and MVs. Usually MVs' limits are 'hard constraints' which means that they should be respected all the time and not violated. CVs' limits can be 'soft constraint' meaning they can be violated to some extent if there is no feasible solution to satisfy all the limits and constraints. For a well designed MPC application, one expects the CVs to be at their designed limits to achieve maximum profit and MVs to be between their limits to have enough freedom for control. As such the analysis of limits and constraints of a MPC controller can provide valuable information about control performance.

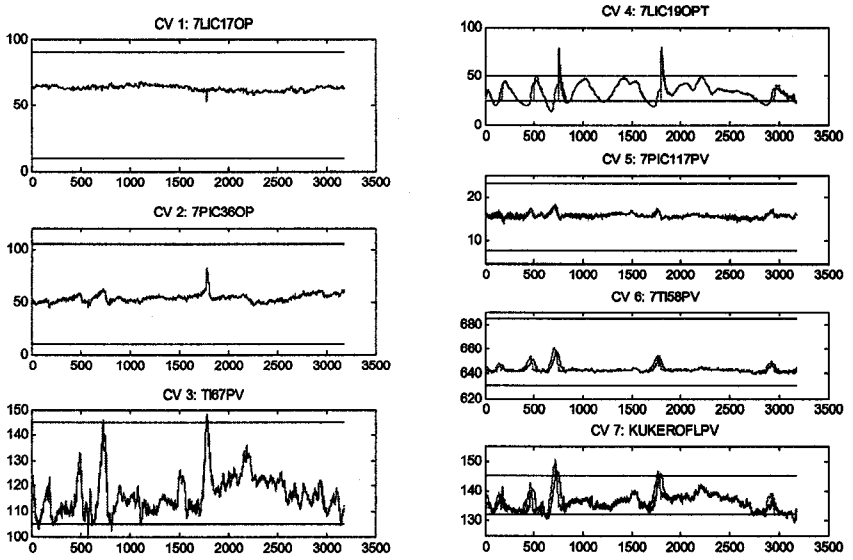

(a) CV1 - CV3

(b) CV4 - CV7

Figure 7.9: CVs trajectories when the MPC was on. The blue lines are the real measurement, the red lines are the LP-targets and the black lines are the limits.

Table 7.7: Constraints analysis of the MVs LP-targets

Tags	Cost Action	High limit activation	Low limits activation
MV1	Maximize	99.76%	0.14%
MV2	Minimize	0%	98.16%
MV3	Minimize	0%	74.95%

Table 7.8: Limits activation analysis of the CVs LP-targets

Tags	Control objective	High limit activation	Low limit activation
CV1	Between limits	0%	0%
CV2	Between limits	0%	0%
CV3	Between limits	0.07%	2.85%
CV4	Low limit	0.31%	30.08 %
CV5	Between limits	0%	0%
CV6	Between limits	0%	0%
CV7	Low limit	0.28%	1.11%

Limits and constraints analysis of 2 days' period of data from the KHU MPC controller was performed using the Controller Performance Monitor software from Matrikon Inc. Table 7.7 shows the limit activation of the MVs. Here 'limit activation' measures the percentage of time one MV LP-target is at its high or low limit. As explained in Table 7.3, the 'cost action' of a MV indicates the desired move direction of that MV in order to achieve the control objectives of the CVs. An ideal scenario is that the MVs move in the desired move directions until the CVs achieve their control objective and some of the CVs stay at their desired limits. We can see in Table 7.7 that the MVs do move in the desirable direction, but they hit their constraints most of the time and are therefore unable to move anymore. At the same time, we can see from Table 7.8 that the CVs actually have not achieved their control objectives, especially CV4 and CV7 whose control objective is to operate at the low limit settings. Therefore, we can say that the MVs are moving in the right direction to achieve the control objectives; but they hit their constraints before they can fully achieve the control objectives. Consulting with Suncor engineers, we know that the limits may be overly restrictive; however they may be set for safety or other considerations and cannot be extended. This situation is not rare in practice where people try to maximize production and always tend to hit the process or equipment related MV limits.

Another obvious problem with the current system is that the MVs stay at their limits for long periods and therefore do not have enough freedom for control. In this situation, any unmeasured disturbance can easily affect the system and the MPC controller may not be able to do much about such disturbances. This could explain why the operators sometimes see unsatisfactory control performance and decide to turn the MPC off.

7.4.2 Diagnosis of the Limit Violation

As we have seen in figure 7.9 that CV3(low rank), CV4(medium rank) and CV7(low rank) encounter limit violations. Table 7.9 shows the average violation and peak violation of each CV. Peak violation of a CV is a ratio between the maximum violation and the CV's operation range. Average violation of a CV is a ratio between its averaged violation magnitude and the CV's operation range. It is clear that CV4

has significant amount of limit violations. A detailed diagnosis of CV4 is apparently needed.

Table 7.9: Constraints violation analysis of the CVs

Tags	Average violation	Peak violation
CV1	0%	0%
CV2	0%	0%
CV3	4.6%	14.53%
CV4	20.88%	116.64%
CV5	0%	0%
CV6	0%	0%
CV7	5.08%	12.92%

CV4 is the position of an accumulator level valve which is directly controlled by a PID level controller (denoted as LIC1). This level controller regulates the level in the accumulator by manipulating the valve opening. Therefore the performance of this PID loop has great effect on CV4. A plot of SP and PV of the level is shown in figure 7.10(a). Before we judge whether this PID controller is performing well or not, two important issues should be taken into account:

1. This is a level controller for an accumulator. It is quite often that a level controller is tuned loosely to have buffer effect to absorb or filter upstream disturbances in the process.

2. The level is not only affected by the valve opening. The MVs of the MPC controller also have an effect on the level.

To clarify whether LIC19 actually is tuned to be sluggish as shown in figure 7.10(a), we compare it with PID controller LIC17. PID LIC17 controls the level of flash drum and the valve opening LIC17.OP is also a CV in KHU MPC controller. Consulting with the Suncor engineers, we know that PID LIC17 and LIC19 have very similar control strategy and control objectives. Figure 7.10(b) shows the SP and PV of PID controller LIC17 which is very different from figure 7.10(a). Apparently, LIC17 is performing very well but LIC19 is not.

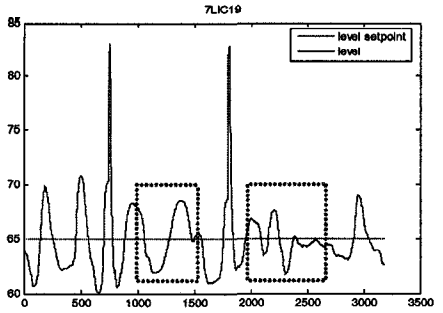

(a) SP and PV of PID loop LIC19

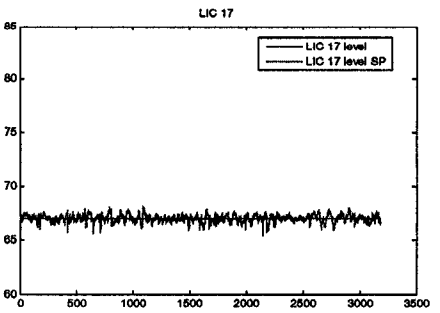

(b) SP and PV of PID loop LIC17

Figure 7.10: PID loop LIC19 and LIC17

An additional point to clarify is how can we be sure the sub-optimal performance was not because of the effect of the MV moves of the MPC controller? To answer this question, examine the two highlighted areas with red dashed box in figure 7.10(a). During these two highlighted periods (1000th-1500th & 2000th-2700th data points), there are almost no MV moves as can be seen in figure 7.8. Therefore, during these two periods, only the PID controller LIC19 controlled the level and the performance is not good.

From the above analysis and experience from Suncor engineers, we have confirmed that this level PID loop was not performing well. There is a severe known nonlinearity/backlash in the LIC1 control valve that causes the poor level control. Suncor engineers try to control this valve output at a very low opening. Then some obvious questions arise: how does the limit violation occur? Why are there similar wave pattern fluctuations in MV2-MV3 and CV2-CV7? What is the root cause?

A simple way to answer these questions is to plot all the MV and CV Lp-targets in one figure and to see which LP-target changes first just before a limit violation occurs. Our cause & effect analysis has shown that

- The sub-optimal performance of the PID controller LIC19 is the root cause of limit violation.
- Every time, when CV4 (LIC19.OP) hits its lower limit, the MPC makes MVs move and tries to bring CV4 back to its limits. These MV moves make the other CVs to move, such as CV2, CV3, CV6, CV7 and CV8 (see figure 7.9).

- The limit violation of CV3 and CV7 is due to the MV moves which is used for bringing CV4 back to its limits. This is because CV3 and CV7 have lower rank than CV4 and the MPC will try to bring CV4 back to limits even at the cost of sacrificing performance of CV3 and CV7.

- Once CV4 goes back to its limits, MVs will be optimized to move to their desired directions which is towards their limits in this MPC. The MVs will not move until CV4 touches its limit again next time.

- The above procedure explains why we see the wave pattern in MV2-MV3 and CV2-CV7.

- The sub-optimal performance of CV4 matches our analysis in Section 7.3.2 where we detected a poor model for CV4.

7.4.3 Summary of KHU MPC Performance

As we can see in figures 7.8 and 7.9, MVs and CVs follow their LP-targets very well. This is an indication of good performance of the lower layer of the MPC system, such as sensors, valves and actuators. Valve stiction analysis did not show any valve problem in the KHU.

Limits and constraints analysis in Section 7.4.1 reveals that the limits setting for CV and MV have limited the optimal performance of the MPC controller. The MPC controller did try to move the MVs to achieve the control objectives for CVs. However, the MVs hit their limits before they can achieve the optimal performance. This makes the MVs stay at their limits and lose certain degree of freedom for control.

The limits violation analysis in Section 7.4.2 shows that the PID loop LIC19 is the root cause of limit violation. The PID controller could not control the accumulator level well and made CV4 (LIC19.OP) out of its limit from time to time. In order to bring CV4 back to its limits, the MPC controller moved the MVs and even sacrificed the performance of two lower rank CVs (CV3 and CV7). The main reason of the sub-optimal performance of PID controller LIC19 is because of the process changes that may have taken place over two years of operation since commissioning. The PID controller loses its control performance gradually. This also reflected as a poor model

for CV4 as we have discussed in Section 7.3.2. Therefore, we have not only detected the bad model in the MPC controller, but also isolated the root cause of the poor model.

7.5 Model Quality Assessment of the NHU MPC

The naphtha hydrotreating unit (NHU) at Suncor Energy Inc. is a standard hydrotreating unit that desulphurizes the coker intermediate naphtha streams through a catalytic reaction with hydrogen. The NHU is controlled by a MPC controller which has 4 manipulated variables (MVs), 8 controlled variables (CVs) and 5 feedforward variables (FFs). The MPC controller recalculates and executes MV moves every 1 minute. The detailed information of the CVs, MVs and FFs are listed in Table 7.10 - 7.13. A simplified schematic of the KHU is shown in figure 7.11 where the MV1-MV4 and CV1-CV7 are marked by circles. The FFs are not shown in the schematic because of the confidentiality of the whole process. CV8 is not shown in the schematic because it is an inferential which is calculated on-line in computer.

Table 7.10: CVs of the NHU MPC controllers

CV tags	Description
CV1 - FC173.OP	Position of the feed valve (of naphtha depropanizer)
CV2 - PIC17.OP	Position of the pressure valve (of naphtha depropanizer)
CV3 - TI210.PV	Condenser outlet temperature
CV4 - FI11.PV	Reflux of the naphtha depropanizer
CV5 - LIC8.OPT	Position of the accumulator level valve
CV6 - PC115.PV	Pressure of the fuel gas to roboiler
CV7 - TI25.PV	Bottom temperature of the naphtha depropanizer
CV8 - NUNAPRVP	Naphtha product RVP (which is an inferential)

7.5.1 Initial Model Quality Assessment

The step test data and the identified model were provided by Suncor engineers. The initial prediction fit and simulation fit of the NHU model based on the step test data were calculated. The results are shown in Table 7.14. A comparison of prediction fit and simulation fit is shown in figure 7.12.

Table 7.11: Ranking and control objective of CVs for KHU MPC

CV tags	Rank	Control objective
CV1 - FC173.OP	medium	High limit
CV2 - PIC17.OP	medium	High limit
CV3 - TI210.PV	low	Between limits
CV4 - FI11.PV	medium	Between limits
CV5 - LIC8.OPT	medium	Between limits
CV6 - PC115.PV	high	High limit
CV7 - TI25.PV	low	Between limits
CV8 - NUNAPRVP	low	Between limits

Table 7.12: MVs of the NHU MPC controllers

MV tags	Description	Cost Action
MV1 - TIC232.SP	Feed temperature (to the naphtha depropanizer)	minimize
MV2 - PIC17.SP	Pressure of the naphtha depropanizer	maximize
MV3 - TIC234.OP	Condenser louvers	maximize
MV4 - TIC231.SP	Reboiler outlet temperature	minimize

Table 7.13: FFs of the NHU MPC controllers

FF tags	Description
FF1 - FIC100.PV	Butane flow rate
FF2 - FIC3.SP	Reactor charge
FF3 - TIC1.SP	Reactor inlet temperature
FF4 - PIC11.SP	Pressure of the LP seperator
FF5 - TI999.PV	Ambient temperature

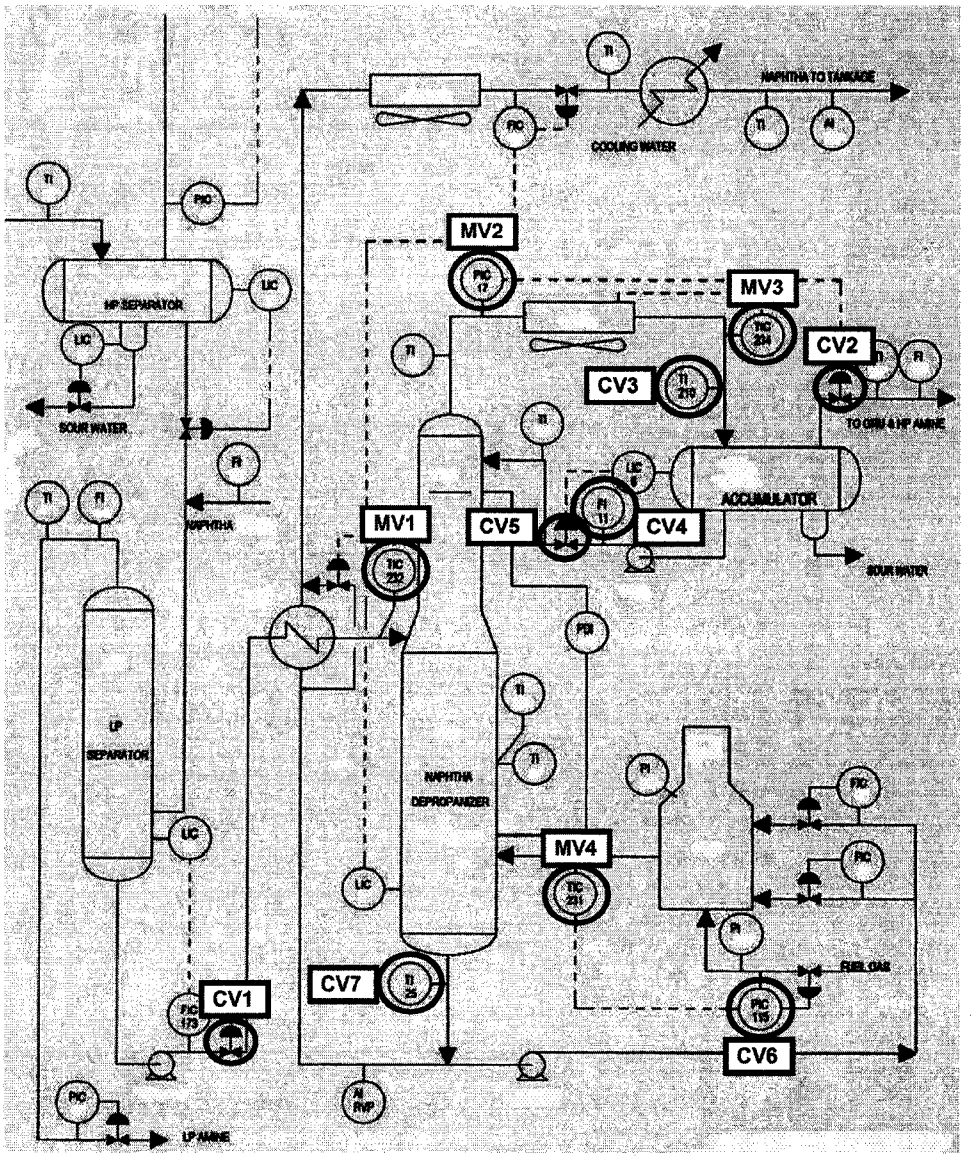

Figure 7.11: Schematic of NHU

Table 7.14: Initial prediction and simulation fit of the NHU model

Tags	Prediction fit	Simulation fit
CV1	91.54%	63.51%
CV2	77.57%	12.22%
CV3	94.45%	17.98%
CV4	92.72%	10.69%
CV5	94.48%	3.882%
CV6	77.11%	25.23%
CV7	93.48%	75.64%
CV8	95.31%	82.89%

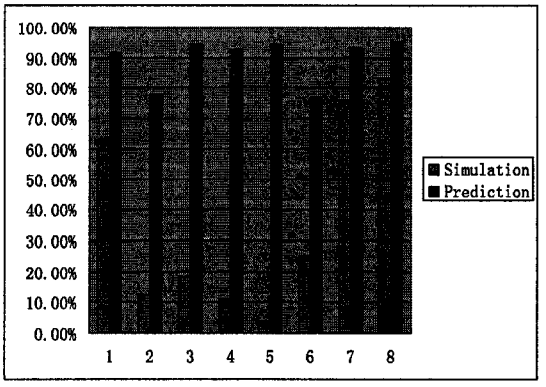

Figure 7.12: Comparison of prediction fit and simulation fit

It is clear that the simulation fits of the NHU model are much lower than the prediction fits. Especially the simulation fits of CV2-CV5, they are all less than 20%.

7.5.2 Recent Model Quality Assessment

5 weeks' data was collected between May 2007 to June 2007. We calculated the prediction and simulation fit based on weekly data. The model fits of the CVs are shown in the plots in figure 7.13 where the blue lines represent k-step-ahead prediction fits and the red lines represent simulation fits. Here $k = 1, 2, ..., 15$ because the prediction horizon of the NHU MPC is 15 minutes. One interesting observation from figure 7.13(a) and figure 7.13(b) is that the k-step-ahead prediction fits of some weeks are even lower than the simulation fit. The k-step ahead prediction fit of CV1 in week 3 (figure 7.13(a)) is as low as 7.3% while its 1-step-ahead prediction fit is 72.58% and the simulation fit is 17.62%. This observation once again supports our claim that the prediction ability of a model should not be measured only by 1-step-ahead prediction fit. A comparison of prediction fit and simulation fit is shown in figure 7.14. The prediction fits do not show any significant problem. The simulation fit of CV4 indicates a bad model. However, our experience with simulation fit and prediction fit does not indicate a bad model for CV4. This is because the k-step-ahead predictions of CV4 are consistently good over the weeks and are the best among all 8 CVs. While its simulation fits fluctuates from close to 20% to close to -60%. It is quite possible that the low simulation fit is because of the effect of disturbances. If CV4 had a bad model, we would expect its k-step-ahead predictions to deteriorates quickly as k increases which is not the case here.

Our new model quality index for NHU MPC controller is calculated based on initial step test data and recent process data. The comparison between the initial model quality and recent model quality is shown in figure 7.15.

The new model index values show that most of the models have degraded except the model for CV5. The worst model is the one for CV2. This makes sense because the model for CV2 not only has low prediction fit (around 70%) and low simulation fit, its k-step-ahead prediction fits also deteriorate quickly as k increases. The new index does not indicate any problem for CV4 which matches our expectation. Overall, we did not find any particular model that has a significant problem.

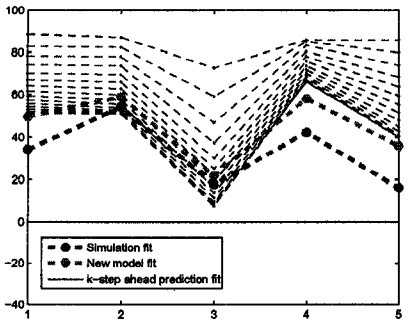

(a) Weekly model fit of CV1

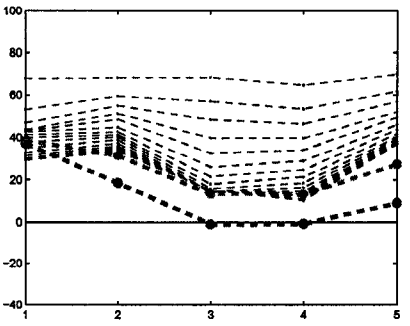

(b) Weekly model fit of CV2

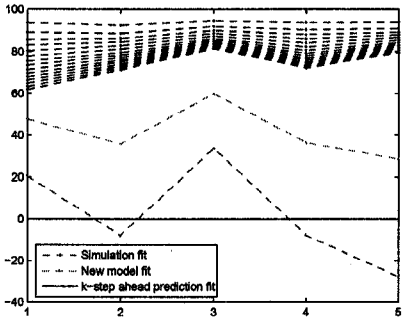

(c) Weekly model fit of CV3

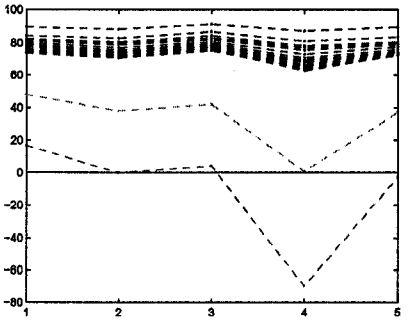

(d) Weekly model fit of CV4

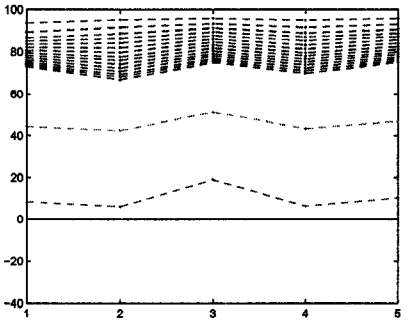

(e) Weekly model fit of CV5

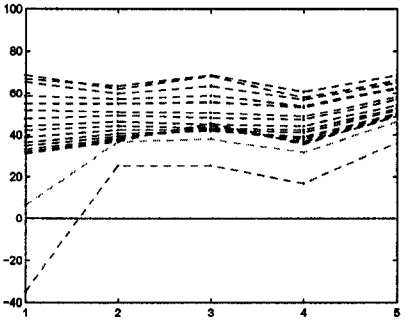

(f) Weekly model fit of CV6

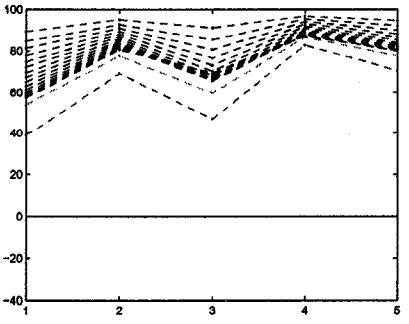

(g) Weekly model fit of CV7

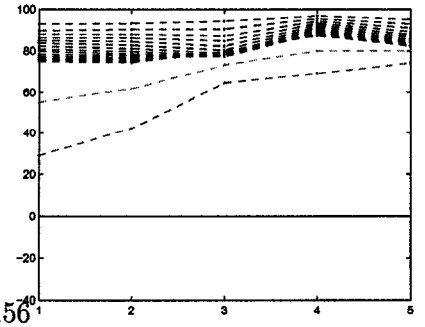

(h) Weekly model fit of CV8

Figure 7.13: Recent model fit of NHU model (the y-axis is in unit of %)

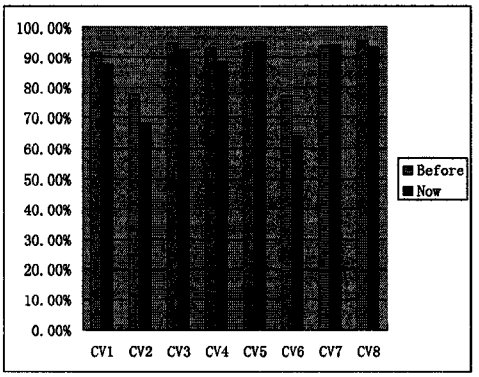

(a) Comparison of prediction fit

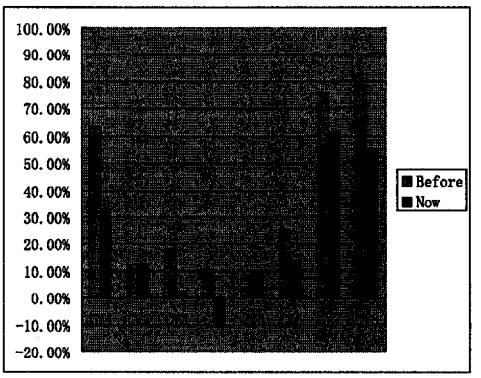

(b) Comparison of simulation fit

Figure 7.14: Model fit comparison of KHU model

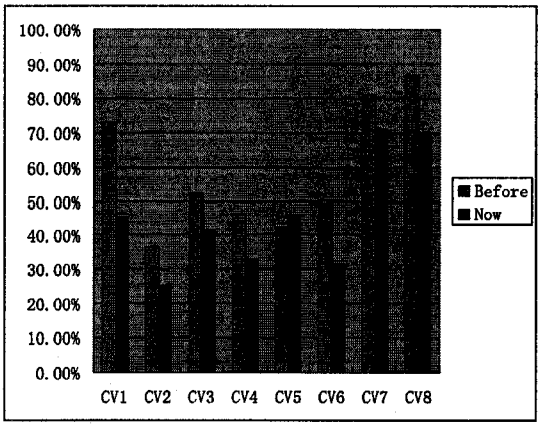

Figure 7.15: New model index value of NHU model

7.6 Performance Analysis of the NHU MPC

During 5 weeks of data collection, the service factor of the NHU MPC controller was 41.48%, much higher than the service factor for the KHU MPC controller. Within the 5 weeks' data set, we selected 15 days' data where for the first 8 days the MPC was off and over the last 7 days the MPC was on. Our purpose is to assess the performance of MPC controller and compare the plant performance when MPC was on and off. Figures 7.16 and 7.17 show the MV and CV activities during the selected 15 days' period. The portion that is highlighted by dashed line box in each figure is corresponding to the period that the MPC was on.

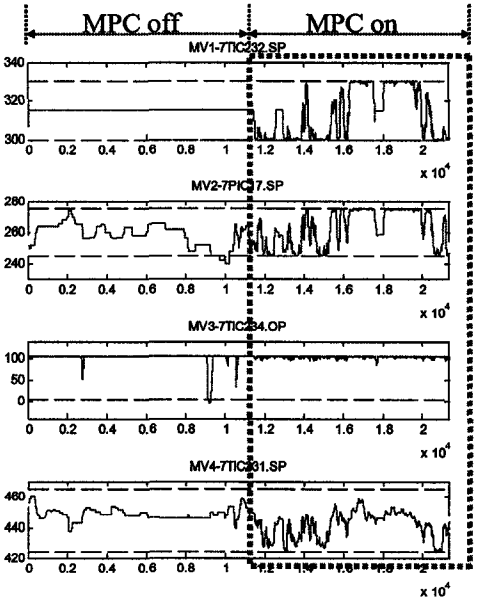

Figure 7.16: MVs moves for the selected 15 days. The black lines are the limits.

In figure 7.17, it is quite clear that most of the CVs are better regulated with reduced variance after the MPC was turned on. Variances of each CV when MPC was on and when MPC was off are calculated and compared. For each CV, the percentage of variance reduced after the MPC turned on is shown in Table 7.15. It is obvious that most of the CVs have reduced variance after MPC was turned on. The only variable with increased variance is CV7 (TI25.PV). This CV is the bottom

temperature of the naphtha depropanizer which has a low rank (weight) in the MPC. The temperature loop is often designed to have sluggish control because of its slow dynamic. In other words, it is usually affordable to have some extent of variance in temperature loop. This is why CV7 in NHU MPC is designed to have a low rank. In reality, the MPC controller transferred the variability of other CVs to CV7 where the process can afford to have increased variance. This is an indication of good performance of the NHU MPC.

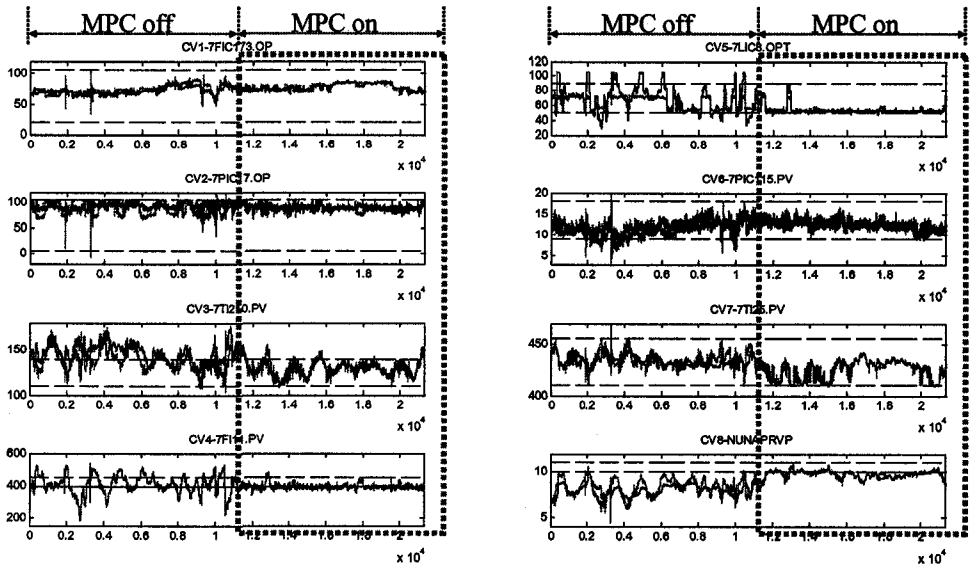

(a) CV1 - CV4

(b) CV5 - CV8

Figure 7.17: CVs moves when the MPC was on. The blue lines are the real measurement, the red lines are the LP-targets and the black lines are the limits.

Table 7.15: Percentage of variance reduced after MPC turned on

Tags	CV1	CV2	CV3	CV4
Variance reduced	6.12%	61.11%	47.88%	94.11%
Tags	CV5	CV6	CV7	CV8
Variance reduced	90.55%	64.40%	-199.89%	59.20%

Table 7.16: Constraints analysis of the MVs LP-targets

Tags	Cost Action	High limit activation	Low limits activation
MV1	Minimize	39.05%	41.05%
MV2	Maximize	55.75%	20.23%
MV3	Maximize	99.21%	0%
MV4	Minimize	3.08%	0%

7.6.1 Analysis of Limits and Constraints

Within the selected 15 days' period, the NHU MPC was on over the last 7 days. Limits and constraints analysis of the last 7 days' data was performed using the Controller Performance Monitor software from Matrikon Inc. Table 7.16 shows the limit activation of the MVs. Among 4 MVs, only MV3 stays at its limit most of the time. This means that the MPC controller has at least the remaining 3 MVs with room to move most of the time. At the same time, we can see in figure 7.17 that CV4, CV5 and CV8 are very close to their limit while other CVs are within their limits. Such CVs' activities indicate that the MPC controller was performing well to push some CVs to their limits and control other CVs to remain within their limits.

7.6.2 Summary of NHU MPC Performance

Considering the variance reduction and the limit tracking of some CVs, we would consider the NHU MPC controller performance was acceptable during the 7 days' period. However, it is not the most optimal performance that the MPC controller can achieve and there still appears to have some room for improvement, such as

- Ideally, we want MVs to stay within their limits and not activate any limits. This could provide maximum degree of freedom for the MPC controller to handle disturbances and operating condition changes. However, this is not case for NHU. One of the MVs stayed at its limit most of the time. Therefore the MPC controller lost one degree of freedom for control.

- Limits violation existed in CV8(see figure 7.17(b)). Calculations show that 56.01% of the time, its LP-target is out of limit. This indicates that the MPC

controller has to sacrifice this low rank CV to ensure performance of other CVs.

- Table 7.11 shows the control objective of each CV. Actually the plant is designed to operate CV1, CV2 and CV6 at their upper limits. But in reality, these three CVs are not at limits while some other CVs are at limits.
- The MPC controller could not perform well consistently.

There are many sources that can cause the problems mentioned above, such as a deficient model, lower layer PID tuning, operating condition changes and so on. This MPC has been running over 2 years, but the service factor could be improved.

7.7 Model Identification Using Routine Operating data

Zhu (1998) has introduced the asymptotic method (ASYM) for identification of multivariable process. The ASYM method is especially efficient in identifying models for MPC controllers. Besides identification, the ASYM method also validate models. The identified models are graded in A (very good), B (good), C (marginal) and D (poor, or, no model exists). In this section, we use the ASYM method to re-identify the models of KHU and NHU using routine operating data. The software used is the Tai-Ji Module of the CPM product from Matrikon Inc. (Matrikon, 2007)

The KHU MPC controller was turned off for 1 week period in November 2006. During that period, operators at Suncor manually changed the MVs from time to time in order to keep the process within the safe operating range. This week's data was used to identify the model of KHU using the ASYM method. The results are shown in figure 7.18. The blue lines represent the original model used in the MPC and the red lines represent the newly identified model with A or B grade. The models with C or D grade are not shown. If there is no model between a CV and a MV, we omit that plot. In figure 7.18, we observe significant changes in the models for CV2 & MV3, and CV4 & MV2 where the model gain has changed from negative to positive. Gain mismatch is also observed in models for CV1 & MV1, CV3 & MV3 and CV5 & MV2. Overall, the model of KHU has changed considerably and re-identification of the process is recommended.

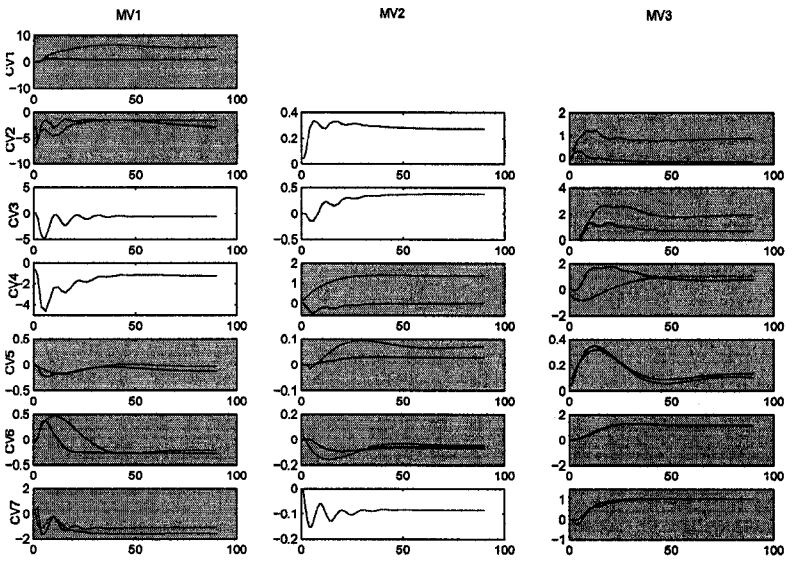

Figure 7.18: KHU model

For NHU, we performed closed-loop identification using the routine operating data with MPC on. The results are shown in figure 7.19. In figure 7.19, we see some gain mismatches, but the overall dynamics of the models are close to their original ones. We do not see significant mismatches for the NHU models. Especially for CV4, the newly identified models are close to the original ones. This again indicate that the negative simulation fit of CV4 in figure 7.14(b) is a false alarm.

7.8 Concluding Remarks

This chapter has analyzed the model quality and assessed the performance of two industrial MPC controllers. A new model index based on prediction fit and simulation fit was proposed to evaluate model quality for MPC controllers.

Analysis shows that the performance of the KHU MPC controller was less than optimal. There are two main reasons why the KHU MPC controller could not perform as well as possible. The first reason is because the limit settings for the MVs and CVs are overly restrictive, but possibly for valid reasons. The MPC computations have the MVs reach the limits set by the designers before it can achieve the control

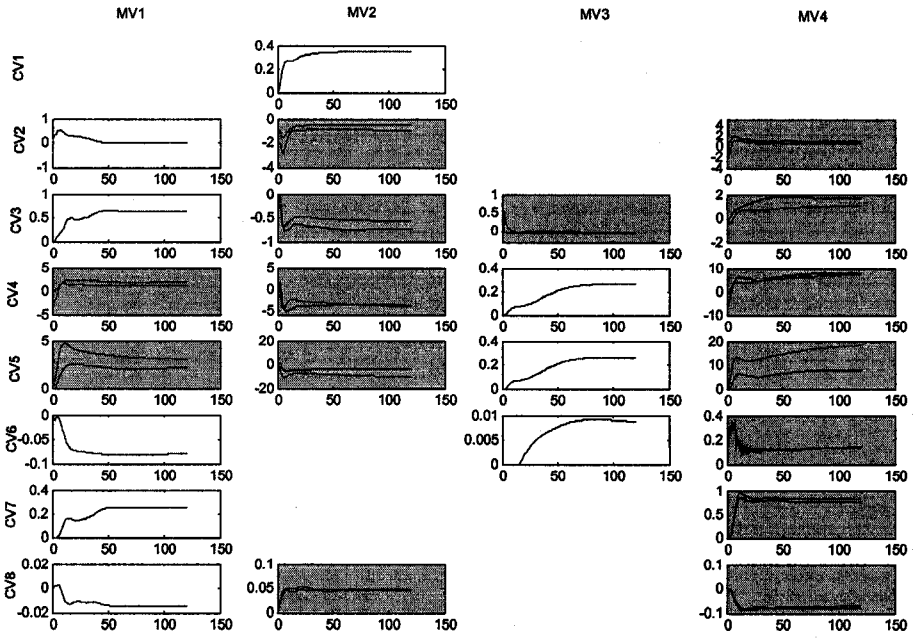

Figure 7.19: NHU model

objective for each CV. The second reason is that one of the PID controllers in the unit could not perform well. Because of this the CV related to this PID controller was out of limit from time to time.

The performance of the NHU MPC controller was acceptable. Compared to manual control, the MPC greatly reduced the variance in most of the CVs and transferred the variability to a temperature loop where the plant can afford to have it. During the period that MPC was on, the MVs and CVs were within their limits most of the time. Some of the CVs were operating at their limits and this indicates that the MPC controller was performing optimization to achieve the performance it could. There is also some room for improvement and we have suggestions for improving this level of control.

Identification of KHU and NHU using routine operation data were performed using the ASYM method.

8

Concluding Remarks and Future Work

8.1 Concluding Remarks

The main objectives of the work reported in this thesis is to develop diagnostic strategies for poor controller performance. In particular, the work has focused on detection and diagnosis of plant-wide oscillations and detection and analysis of model-plant mismatch. The main contributions of this thesis are:

- Extension and application of the spectral envelope method for oscillation detection and root cause diagnosis. The three tasks (1) oscillation detection, (2) variable categorization and (3) root cause diagnosis can be successfully accomplished using the methods proposed in this thesis.

- A non-data based method for root cause diagnosis of plant-wide oscillations has been proposed based on the concept of the adjacency matrix. A novel feature of the new method is that it utilizes the information in the process flowsheet. This method complements the data-based methods very well and it is best used in combination with other data-based methods to provide powerful and complementary diagnosis of plant-wide oscillations.

- Model-plant mismatch of state space model is formulated and discussed. Three

MPM detection indices (MDIs) are proposed based on the concept of primary residual vector (PRV) to detect model-plant mismatch. A logic framework is proposed to isolate the system matrices that have MPM.

- Two algorithms for control relevant model validation under closed-loop conditions have been proposed. For the situation where the changes in plant dynamics are not a concern, both algorithms can also be applied to detect process faults, e.g. sensor decalibration and valve stiction.

- The effect of (additive and multiplicative) modelling error on process output error (which is the process output minus the simulated output) is analyzed. We also relate the process output error with robust stability conditions and introduce three propositions for on-line model validation. Any process change (or modelling error) that makes the system no longer satisfy the condition specified by the robust stability theorem can be detected.

- Constraints and limits analysis for industrial MPC controller have been performed. A new model index based on simulation and k-step-ahead prediction is proposed for model quality assessment of industrial MPC controllers.

The newly proposed techniques and tools have been evaluated on a variety of simulation, experimental and industrial examples.

- The spectral envelope based method (in Chapter 2 and 3)for oscillation detection and diagnosis has been successfully applied on two industrial plants: (1) a plant at Eastman Chemical Company , USA; and (2) a plant at Mitsubishi Chemical Corporation, Mizushima, Japan.

- The adjacency matrix based method (in Chapter 3) for root cause diagnosis has also been applied on to both of the afore mentioned industrial plants. The spectral envelope based method and the adjacency matrix based method give consistent results.

- The two algorithms (in Chapter 5) for control relevant model validation under closed-loop condition were implemented on a two-tank system in the Process Control Laboratory at the University of Alberta.

- The index for quantification of frequency model mismatch (in Chapter 6) was evaluated on a continuous stirred tank heater (CSTH) at the Process Control Lab, University of Alberta.

- In Chapter 7, constraints & limits analysis and model quality assessment was successfully performed on two industrial MPC controllers at Suncor Energy Inc., Fort McMurray, Canada.

8.2 Recommendations for Future Work

A number of challenges remain in the area of performance diagnosis.

- *Analysis of the effect of MPM on MPC performance.* It is known that the MPM will degrade the performance of MPC controllers. However, few studies been done to analyze how MPM affects the performance of MPC controllers. For example, how does the gain mismatch affect the optimization (linear programming or quadratic programming) calculations for MPC controllers. More analysis of the effect of MPM on MPC control needs to be explored. Of particular interest is the economic impact of MPM on MPC performance.

- *Isolation of poor models that affect process performance.* For a multivariate process, the whole process model matrix consists of several SISO models for specific input-and-output channels. Most of current model validation and MPM detection methods aim at validating the entire multivariate process model. However, it is often the case that only few of the elements of the multivariate transfer matrix models cause poor process performance while the rest of the models (or transfer matrix elements) are still good. Effective isolation of poor models in a model matrix could save significant time and effort in performance diagnosis. It also helps model re-identification. With such a tool, engineers or practitioners can focus on re-identifying only a few poor models instead of re-identifying the entire multivariate process.

- Model validation or MPM detection for state space model is still an open question. The isolation logic we proposed in Chapter 4 does not provide a complete isolation of MPM. Further research is required to achieve a complete isolation.

- Chapter 6 presented the analysis of modelling error. Most of the analysis has been performed for the SISO case. It will be useful to extend these ideas to MIMO case.

Bibliography

Basseville, M., A. Benveniste and G. Moustakides (1987). The asymptotic local approach to change detection and model validation. *IEEE Transactions on Automatic Control* **32**, 583–592. 77, 99

Basseville, M. and A. Benveniste (1983). Sequential segmentation of nonstationary digital signals using spectral analysis. *Information Science* **29**, 57–73. 70, 71, 72

Basseville, M. and I. Nikiforov (1993). *Detection of abrupt Changes.* Prentice Hall,Englewood Cliffs, NJ. 70, 72

Bauer, M., J. W. Cox, M. H. Caveness, J. J. Downs and N. F. Thornhill (2007). Finding the direction of disturbance propagation in a chemical process using transfer entropy. *IEEE transactions on control systems technology* **15**, 12–20. 41

Bialkowski, W. L. (1992). Dreams vs. reality: A view from both sides of the gap. *Control Systems* pp. 283–294. 86

Brillinger, D. R. (1981). *Time series: Data analysis and theory (2nd ed., 1981).* San Francisco: Holden-Day. 13

Chatfield, C. and A. J. Collins (1980). *Introduction ot multivariate analysis.* Chapman and Hall, London, UK. 17

Choudhury, M. A. A. S. (2004). Detection and diagnosis of control loop nonlinearities, valve stiction and data compression. Phd thesis. Department of Chemical and Materials Engineering, University of Alberta, Canada. 36, 37

Choudhury, M. A. A. S., N. F. Thornhill and S. L. Shah (2005*a*). Modelling valve stiction. *Control Engineering Practice* **13**, 641–658. 36, 86, 93

Choudhury, M. A. A. S., S. L. Shah and N. F. Thornhill (2004*a*). Detection and quantification of control valve stiction. In: *The proceedings of DYCOPS 2004, July 5-7, 2004.* Cambridge, USA. 37

Choudhury, M. A. A. S., S. L. Shah and N. F. Thornhill (2004*b*). Diagnosis of poor control loop performance using higher order statistics. *Automatica* **40**(10), 1719–1728. 36, 37, 48, 52, 85, 86

Choudhury, M. A. A. S., S. L. Shah, N. F. Thornhill and D. S. Shook (2006). Automatic detection and quantification of stiction in control valves. *Control Engineering Practice* **14**, 1395–1412. 37, 38, 48, 52

Choudhury, M. A. A. S., V. Kariwala, S. L. Shah, H. Douke, H. Takada and N. F. Thornhill (2005*b*). A simple test to confirm control valve stiction. In: *The 16th IFAC World Congress.* Prague, Czech Republic. 39

Chow, E. and A. Willsky (1984). Analytical redundancy and the design of robust failure detection system. *IEEE Transactions on Automatic Control* **AC-29**, 603–614. 58

Desborough, L. and R. Miller (2001). Increasing customer value of industrial control performance monitoring - honeywell's experience. In: *Proc. of CPC VI.* Tuscon, Arizona. pp. 172–192. 8, 86

Ding, X., L. Guo and T. Jeinsch (1999). A characterization of parity space and its application to robust fault detection. *IEEE Transactions on Automatic Control* **44**, 337–343. 58

Doyle, J. C., B. A. Francis and A. R. Tannenbaum (1992). *Feedback Control Theory.* Macmillan, New York. 99

Gertler, J. (1988). Survey of model-based failure detection and isolation in complex plants. *IEEE Control system Magazine* **12**, 3–11. 55

Gertler, J. J. (1998). *Fault Detection and Diagnosis in Engineering Systems.* Marcel Dekker, Inc., New York. 85

Gevers, M. and L. Ljung (1986). Optimal experiment designs with respect to the intended model application. *Automatica* **22**, 543–554. 69

Gevers, M., X. Bombois, B. Codrons, G. Scorletti and B. Anderson (2003). Model validation for control and controller validation in a prediction error identification framework-part i: theory. *Automatica* pp. 417–427. 99

Goodwin, G. C. and M. Salgado (1989). A stochastic embedding approach for quantifying uncertainty in estimation of restricted complexity models. *Int. J. Adaptive Control Signal Processing* **3**, 333–356. 99

Goodwin, G. C., M. Gevers and B. Ninness (1992). Quantifying the error in estimated transfer functions with applications to model order selection. *IEEE Trans Automatica Control* **37**, 913–929. 99

Goodwin, G. C., S. F. Graebe and M. E. Salgado (2001). *Control System Design.* Prentice Hall. 99, 101, 103, 105, 111, 118

Hägglund, T. (1995). A control-loop performance monitor. *Control Engng. Prac.* **3**, 1543–1551. 36

Hannan, E. J. (1970). *Multiple time series.* Wiley. New York. 13

Harris, T. (1989). Assessment of closed loop performance. *The Canadian Journal of Chemical Engineering* **67**, 856–861. 1, 54

Huang, B. (2000). Multivariable model validation in the presence of time-variant disturbance dynamics. *Chemical Engineering Science* **55**, 4583–4595. 99

Huang, B. (2001). On-line closed loop model validation and detection of abrupt parameter changes. *Journal of Process Control* **11**, 699–715. 70, 71, 79, 80

Huang, B., A. Malhotra and E. Tamayo (2003). Model predictive control relevant identification and validation. *Chemical Engineering Science* **58**, 2389–2401. 140

Huang, B. and E. Tamayo (2000). Model validation for industrial model predictive control systems. *Chemical Engineering Science* **55**, 2315–2327. 55, 70, 71, 74

Huang, B. and S. L. Shah (1997). Closed-loop identification: a two step approach. *Journal of Process Control* **7**, 425–438. 76

Huang, B. and S. L. Shah (1999). *Performance assessment of control loops: theory and applications.* Springer-Verlag Ltd. 1, 55

Jenkins, G. M. and D. G. Watts (1968). *Spectral Analysis and Its Applications.* Holden Day. 11

Johnson, R. and D. Wichern (1998). *Applied Multivariate Statistical Analysis (4th Editon).* Prentice-Hall Inc. 17, 59

Kosut, R. L., G. C. Goodwin and M. P. Polis (1992*a*). Special issue on system identification for robust control design. *IEEE Trans Automatica Control.* 99

Kosut, R. L., M. K. Lau and S. P. Boyd (1992*b*). A set-membership identification of systems with parametric and nonparametric uncertainty. *IEEE Trans Automatica Control* **37**, 929–942. 99

Kouvaritakis, B. and M. Cannon (2001). *Nonlinear predictive control, theory and practice.* London: The IEE. 128

Lai, T. L. and J. Z. Shan (1999). Efficient recursive algorithms for detection of abrupt changes in signals and control systems. *IEEE Trans Automatic Control* **44**(5), 952–966. 99

Li, W. and J. Jiang (2004). Isolation of parametric faults in continuous-time multivariate systems: a sampled data-based approach. *International journal of process control* **77**, 173–187. 55

Li, W. and S. L. Shah (2002). Structured residual vector-based approach to sensor fault detection and isolation. *Journal of Porcess control* **12**, 429–443. 55, 58

Ljung, L. (1998). *System Identification (2nd ed.).* Prentice Hall,Englewood Cliffs, NJ. 69, 75, 77, 99, 101, 112, 129, 131, 132

Ljung, L. and L. Guo (1997). The role of model validation for assessing the size of the unmodeled dynamics. *IEEE Transactions on Automatic Control* **42**, 3894–3899. 69

Maciejowski, J. M. (2002). *Predictive control with constraints.* Englewood Cliffs, NJ: Prentice Hall. 128

Mah, R. (1989). *Chemical Process Structures and Information Flows.* Butterworth Publishes. 41, 42, 43

Malhotra, A. and B. Huang (2002). Detection of abrupt change and applications in sensor decalibration monitoring. *ISA transactions* **41**, 155–166. 87

Matrikon (2007). Tai-ji multivariable identification package. *CPM Product User Manual.* 161

Maurya, M. R., R. Rengaswamy and V. Venkatasubramanian (2003*a*). A system framework for the development and analysis of signed digraphs for chemical processes. 1. algorithms and analysis. *Ind. Eng. Chem. Res.* **42**, 4789–4810. 40

Maurya, M. R., R. Rengaswamy and V. Venkatasubramanian (2003*b*). A system framework for the development and analysis of signed digraphs for chemical processes. 2. control loops and flowsheet analysis. *Ind. Eng. Chem. Res.* **42**, 4811–4827. 40

McDougall, A. J., D. S. Stoffer and D. E. Tyler (1997). Optimal transformations and the spectral envelop for real-valued time series. *Journal of Statistical Planning and Inference* **57**, 195–214. 9, 21

Miao, T. and D. E. Seborg (1999). Automatic detection of excessive oscillatory feedback control loops. In: *Proc. of IEEE international Conference on Control Applications*. Kohala Coast, Hawai'i. 4, 9, 34

Montgomery, D. G. and G. C. Runger (1994). *Applied Statistics and Probability for Engineers*. John Wiley & Sons, Inc, New York. 89

Morari, M. and E. Zafiriou (1989). *Robust Process Control*. Prentice Hall. 102

O'Reilly, P. G. (1998). Detection of sensor decalibration using the asympotic local approach. *Electronics Letters* pp. 2022–2023. 87

Patwardhan, R. and S. L. Shah (2002). Issues in performance diagnostics of model-based controllers. *Journal of Process Control* **12**, 413–427. 104

Qin, J. and T. A. Badgwell (2003). A survey of industrial model predictive control technology. *Control Engineering Practice* **11**, 733 – 764. 128

Qin, S. (1998). Control performance monitoring - a review and assessment. *Computer and Chemical Engineering* **23**, 173–186. 1, 8, 112

Rawlings, J. B. (2000). Tutorial overview of model predictive control. *IEEE Control System Magazine* **20**, 38–52. 128

Rengaswamy, R., T. Hägglund and V. Venkatasubramanian (2001). A qualitative shape analysis formalism for monitoring control loop performance.. *Engng. Appl. Artificial Intell.* **14**, 23–33. 36

Shumway, R. H. (1988). *Applied Statistical Time Series Analysis*. New Jersey: Prentice Hall. 13

Skogestad, S. and I. Postlethwaite (1996). *Multivariable Feedback Control*. John Wiley & Sons. 101, 104, 111

Söderström, T. and P. Stoica (1989). *System Identification*. UK: Prentice-Hall International. 69, 99, 112

Stoffer, D. S. (1999). Detecting common signals in multiple time series using the spectral envelope. *Journal of the American Statistical Association* **94**, 1341–1356. 12

Stoffer, D. S., D. E. Tyler and A. J. McDougall (1993). Spectral analysis for categorical time series: Scaling and spectral envelope. *Biometrika* **80**, 611–622. 9, 21

Stoffer, D. S., D. E. Tyler and D. A. Wendt (2000). The spectral envelope and its applications. *Statistical Science* **15**, 224–253. 14

Stoustrup, J. and H. Niemann (1999). Fault detection and isolation systems with parametric faults. *Proceedings of the 14th IFAC Triennial World Congress* **7E**, 139–144. 55

Tangirala, A. K., J. Kanodia and S. L. Shah (2007). Non-negative matrix factorization for detection and diagnosis of plantwide oscillations. *Industrial and Engineering Chemistry Research* **46**, 801–817. 18

Thornhill, N. F., B. Huang and H. Zhang (2003*a*). Detection of multiple oscillations in control loops. *Journal of Process Control* **13**, 91–100. 4, 9, 19, 34

Thornhill, N. F., J. W. Cox and M. A. Paulonis (2003*b*). Diagnosis of plant-wide oscillation through data-driven analysis and process understanding. *Control Engineering Practice* **11**, 1481–1490. 23, 34, 38, 40

Thornhill, N. F., S. L. Shah and B. Huang (2001). Detection of distributed oscillations and root-cause diagnosis. In: *Proc. of CHEMFAS 4*. Jejudo Island, Korea. pp. 167–172. 34, 40

Thornhill, N. F., S. L. Shah, B. Huang and A. Vishnubhotla (2002). Spectral principal component analysis of dynamic process data. *Control Engineering Practice* **10**, 833–846. 9, 17, 34

Thornhill, N.F. and T. Hägglund (1997). Detection and diagnosis of oscillation in control loops. *Control Engineering Practice* **5**, 1343–1354. 4, 9, 34

Van den Hof, P. and R. Schrama (1995). Identification and control–closed-loop issues. *Automatica* **31**, 1751–1770. 69

Wahlberg, B. and L. Ljung (1992). Hard frequency-domain model error bounds from least-squares like identification techniques. *IEEE Trans Automatica Control* **37**, 900–912. 99

Wan, S. and B. Huang (2002). Robust performance assessment of feedback control systems. *Automatica* pp. 33–46. 119

Yim, S. Y., H. G. Ananthankumar, L. Benabbs, A. Horch, R. Drath and N. F. Thornhill (2006). Using process topology in plant-wide control loop performance assessment. *Computers & Chemical Engineering* **31**, 89–99. 41

Zames, G. (1966). On the input-output stability of time-varying nonlinear feedback systems. part i: conditions using concepts of loop gain, conicity and positivity. *IEEE Tans. Autom. Control* **AC-11**, 228–238. 99

Zhang, Q., M. Basseville and A Benveniste (1994). Early warning of slight changes in systems. *Automatica* **30**(1), 95–113. 70, 99

Zhu, Y. (1998). Multivariable process identification for MPC The asymptotic method and its applications. *Journal of Process Control* **8**, 101–115. 127, 161